Rep. Prog. Phys. **59** (1996) 29–90. Printed in the UK

Physics of solids under strong compression

W B Holzapfel

Universität-GH Paderborn, Fachbereich Physik, Warburger Strasse 100, D-33095 Paderborn, Germany

Abstract

Progress in high pressure physics is reviewed with special emphasis on recent developments in experimental techniques, pressure calibration, equations of state for simple substances and structural systematics of the elements. Short sections are also devoted to hydrogen under strong compression and general questions concerning new electronic ground states.

This review was received in February 1995

0034-4885/96/010029+62$59.50

Contents

1. Introduction

The continuous development of the diamond anvil cell (DAC) technology over the last thirty years has opened a wide field of high pressure science not only to large national laboratories but especially to many university research groups due to the simplicity of this new technique. With small commercial devices pressures in excess of 50 GPa are now produced routinely in many laboratories and the upper limits of this technique are still increasing steadily to always higher records. At the present time primary limitations seem to arise thereby not yet from the diamond material but rather from the measuring techniques which require special developments to obtain well characterized informations from the miniature samples under pressure.

One leading goal for these developments arises from the challenge to produce metallic hydrogen under static conditions in the laboratory and this field was just the subject of a recent review [1]. However, similar phenomena like strong compression, phase transitions, metallization and other changes in crystal structure, lattice dynamics and electronic structure including superconductivity and magnetism have been investigated also in many other materials where the experimental tools often provide better access and the theoretical understanding seems to be more advanced.

Since the pioneering work of P W Bridgman [2, 3], this field expanded rapidly, and various recent monographs can be consulted as excellent introductions into the fields of high pressure techniques [4–8], of equations of states [9–11], and on the systematics and physical understanding of *Phase Diagrams of the Elements* [12]. In addition, two specialized journals, *High Pressure–High Temperature* and *High Pressure Research*, as well as the regular series of AIRAPT conference proceedings on *High Pressure Science and Technology* [13–21] together with additional proceedings from various topical conferences [22–34] and recent reviews [35–43] document the rapid growth of this field.

With this perspective in mind, the present review must be limited to a small section of the wide field of high pressure research. Chemistry, biology and food science will be discarded and also the wide field of linear pressure coefficients for a wide variety of solid state properties must be excluded to provide sufficient space for nonlinear dependences under strong compressions and discontinuities in various physical properties, occurring under strong compression. Obviously these are the phenomena, which are more difficult to predict and where new rules challenge also new theoretical developments.

2. Experimental techniques

2.1. Overview

The foundation of modern high pressure technologies was established by P W Bridgman with the development of piston cylinder devices and strongly supported Large Anvil Cells (LAC) with the use of sintered tungsten carbide as ultimate construction material.

Further developments using multi-anvil systems [44], belts [45], girdles [46, 47], supported anvils [48, 49], and special toroidal gaskets [50] widened either the range of pressure up to 30 GPa or the range of temperatures up to 5000 K or just the size of the sample chamber to accept more complex sample devices. These developments are documented in the monographs mentioned in the introduction and recent reviews [51] illustrated also further

progress. Therefore, only a short section (2.2) will be devoted to some special developments of these LAC techniques. Typical ranges in pressure and temperature accessible by these LAC techniques are illustrated in figure 1 together with ranges also for the other techniques.

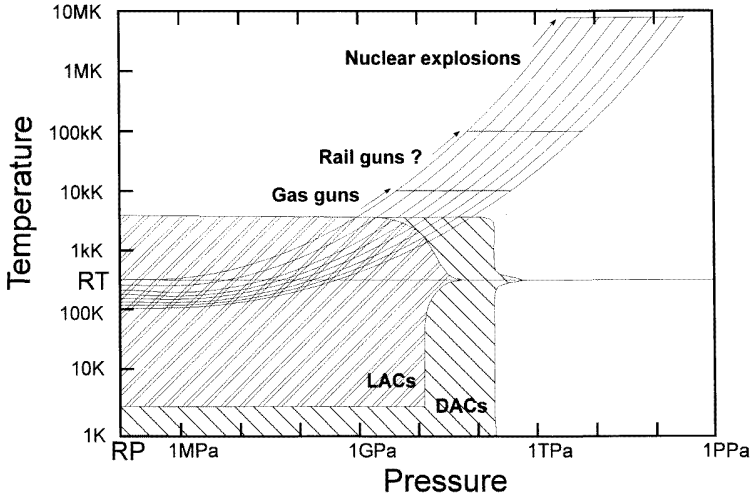

Figure 1. Pressure and temperature ranges for different high pressure techniques.

With the DAC technique on the other hand, pressures beyond 500 GPa have been obtained at ambient temperature [52] and by the use of well controlled laser heating temperatures up to about 5000 K at 60 GPa [53] or 4000 K at 200 GPa [54] have been maintained simultaneously for short periods in time to provide information on melting or structural transitions under conditions which simulate almost the Earth's core, where temperatures around 7000 K and pressures of 360 GPa are expected according to standard geophysical models [55, 56]. Besides these developments, section 2.3 will be devoted primarily to a review of new diagnostic techniques which have been adapted to DACs.

At a first glance, figure 1 might give the impression, that the strongest compressions may be obtained in solids under shock conditions, however, due to the adiabatic heating melting occurs under shock conditions in most solids much before a compression of 50% is achieved. Thus, higher energy depositions in shock waves open up the field for studies on strongly compressed fluids and highly ionized plasmas, but both the LAC and DAC techniques provide usually much stronger compressions for many materials like rare gas solids, molecular crystals and the sp-bonded metals, especially at low temperatures, where the range accessible to the shock wave techniques is very limited (figure 1).

Also much of the heat produced by internal friction in shock fronts can be avoided by magnetically driven isentropic compression [57], costs and technical problems have limited the application of this technique in recent years. Similarly, well tailored laser pulses could also be used for isentropic compression. However, also this technique seems to need much more development before it could possibly find a wide spread application.

Due to the fact, that all the pressure determinations in DACs depend more or less directly on equation of state (EOS) data, which have been derived to a large extent from shock wave experiments, a short section 2.4, will be devoted to some details of these techniques, to serve for the discussion of precision and accuracy in static EOS measurements and for some questions concerning pressure calibrations.

2.2. Large anvil cells (LACs)

Large Anvil Cells (LACs) are usually applied in cases where the sample space of Diamond Anvil Cells (DACs) is just too small and where the pressures must exceed nevertheless the 5 GPa limit typical for piston cylinder devices based on sintered tungsten carbide parts. While figure 2 illustrates the differences between simple Bridgman anvil devices and the later developments of supported taper anvils, girdles, belts and toroidal gasket arrangements, one may note that neutron diffraction is most conveniently adapted to the toroidal gasket technique which has been used up to 15 GPa and a doubling of this pressure range is expected when diamond compacts are applied also with this technique [58], while 13 GPa seems to be the ultimate pressure limit for neutron diffraction with large sapphire anvil cells [59]. Girdle type LACs were primarily used for Mössbauer spectroscopy with isotopes like ^{67}Zn, ^{119}Sn, ^{125}Te, ^{133}Cs, ^{197}Au, ^{151}Eu, ^{153}Eu, ^{170}Yb and ^{237}Np [60–71], where γ-ray energies exceeding 20 keV (see figure 3) allow for a transmission measurements through a pair of sintered boron carbide anvils with a total thickness of typically 20 mm, and the relatively low specific activities of the sources required mostly the use of large area absorbers. Other applications of LAC techniques include electrical measurements, TDPAC measurements of nuclear γ-ray cascades [72–74], and recent tests of compton profile studies [75]. When ever possible, these diagnostic techniques had been adapted also to measurements with DACs, which are discussed in more detail in the next section.

A different compromise in sample size, maximum pressure and accessibility with x-rays and electrical contracts was obtained by the use of Multi Anvil Cells (MACs), where 6 or 8 identical anvils compress a small cubic or octahedral sample spaces. Typically, 25 GPa were obtained with sintered tungsten carbide anvils and samples of 1.5 mm length of the edges [76] and 15 GPa were typical for larger sample spaces with internal heaters reaching 1600 °C [77]. The use of sintered diamond compacts resulted also here in an enlargement of either the sample size or the combined pressure–temperature region with typical values of 14 GPa and 1400 °C, 20 GPa and 800 °C or even 41 GPa at ambient temperature with samples of only 500 μm length of the edges but quite sufficient for *in situ* x-ray diffraction with synchrotron radiation [78]. It should be noted, however, that these devices are not only very useful for x-ray diffraction but also for x-ray absorption studies, EXAFS and XANES, as indicated recently [79].

2.3. Diamond anvil cells (DACs)

Since the first application of DACs in a high pressure study up to 3 GPa [80] enormous progress has been made not only with respect to widening the accessible range in pressure and temperature but also with respect to developments of new diagnostic techniques. Many earlier reviews on this field discussed the different designs [81–83] and how to operate the DACs [84–86] as well as many applications. A complete monograph presented the early applications of DACs in high pressure single crystal x-ray diffraction [87]. For other applications, which are more widely scattered in the literature, a few references can be given here for optical studies with measurements of optical absorption [88–92], reflectance [93], FTIR [94–97], fluorescence [98], Raman [99–103], Brillouin [104–114], x-ray absorption [115–118] and Mössbauer spectroscopy [119–130], for powder x-ray diffraction [131–137], neutron diffraction [138–140], NMR [141, 142], positron annihilation [143], and electrical measurements [144–151]. In fact, many further references are also easily found in the

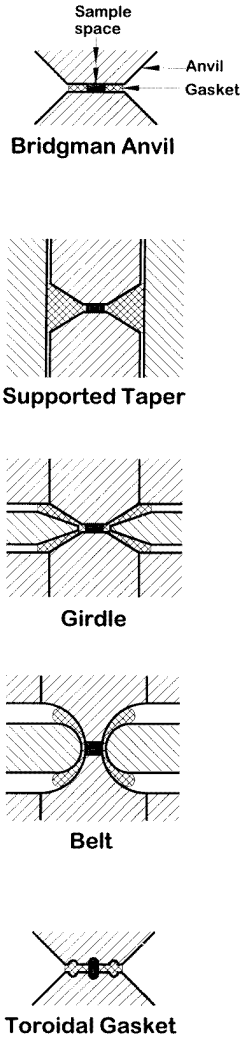

Figure 2. Static high pressure techniques.

proceedings of the biannual AIRAPT conferences. Therefore, only a few very specific recent developments deserve some extra discussion here.

In addition to internal heating of miniature wires in the sample space of the DAC much higher *p*-*T*-conditions were provided more recently with well controlled laser heating with thermal insulation of the sample from the anvils either by a layer of solid or fluid argon reaching 120 GPa and 3000 K or 62.5 GPa and 5000 K. With transparent solid insulation, as illustrated in figure 4, the accessible *p*-*T*-range was further extended to 200 GPa and 4000 K [54].

The dispute on the possible errors of the pyrometric temperature measurements in these studies [152–154] and recent shock temperature measurements [155] seem to lend more support to the previously determined lower values for the melting curve of iron [156], however, an estimated uncertainty of only 8% in temperature under these extreme conditions

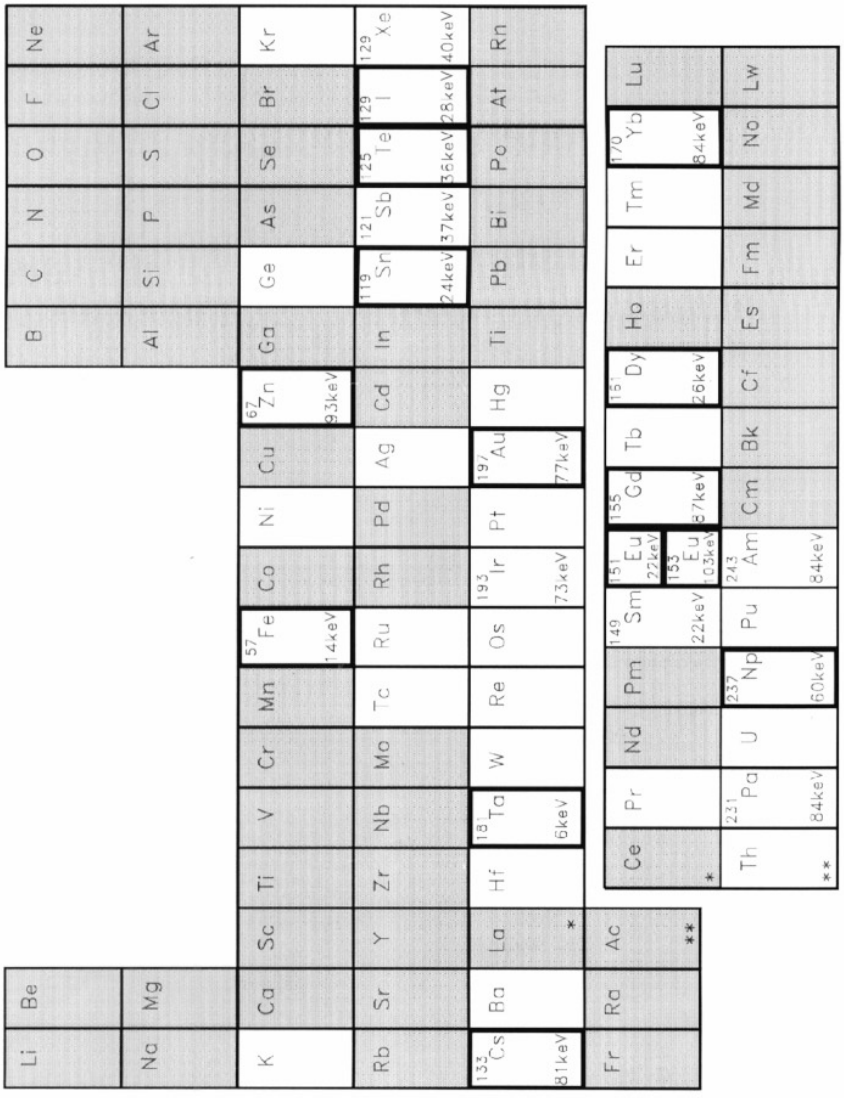

Figure 3. Table of elements with isotopes for Mössbauer spectroscopy shown on white background. Isotopes suitable for high pressure studies are given with their transition energies. Heavy frames mark isotopes which have been used in high pressure studies (with modifications from reference 23).

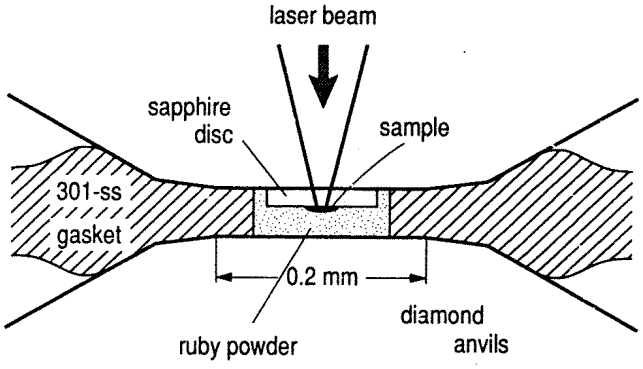

Figure 4. Sample space of laser heated DAC. (Reproduced with permission from the author [54].)

is obviously not yet accepted [157–162].

Other extremes concern simultaneous x-ray diffraction high pressure and high temperature measurements, where external heaters gave good results up to 1500 K at 10 GPa [163, 164], or 608 K at 22.4 GPa [165], however, much higher values in the range of 2000 K at 20 GPa were recently sustained with internal laser heating also together with x-ray diffraction.

The earliest powder x-ray diffraction measurements with DACs reviewed by Jayaraman (1983, 1986) used mostly the conventional angular dispersive technique (ADXD) with films. Later it was recognized that the energy dispersive technique (EDXD) has many specific advantages, especially if one uses a conical slit system [166] which collects all the intensity from one fixed diffraction cone simultaneously. This idea was adopted by various groups at first for conventional x-ray sources [167–173] and later also to synchrotron radiation sources [174, 175] whereby the use of the specially designed fourfold detector system illustrated in figure 5 maintained the high resolution typical for small area detectors. The separate development of a special ring detector sacrificed some of the high resolution obtainable with the highly collimated synchrotron radiation, but maintained the full intensity of the larger area detector.

Already from the early considerations it was clear, that the graininess of the powder diffraction rings from small stationary samples is efficiently averaged out by the ring detector system, and also the search for single crystal reflections from tiny and weakly scattering samples especially with the restrictions of the DACs is speeded up extremely by the use of EDXD techniques [176], when ring shaped or large area detectors are used.

Another advantage of the EDXD technique was demonstrated recently [177] with a DAC using a boron carbide backing plate for EDXD with large diffraction angles ($2\Theta > 15^\circ$) and hard synchrotron radiation to obtained diffraction pattern from simple substances with very highly indexed lines usually not obtained with any other technique. A first study with gold in this modified DAC using a scattering angle of 20° resulted in a diffraction pattern with 20 diffraction lines up to (khl)= (641) and a standard deviation in the lattice parameter determination of $\Delta a/a < 2 \cdot 10^{-4}$ in comparison with $\Delta a/a < 5 \cdot 10^{-4}$ for a pattern taken with $2\Theta = 9.2^\circ$. Thus, this new technique results in a precision which opens the route for measurements of pressure dependences for the thermal expansion coefficients when highly sensitive and temperature independent pressure sensors [178, 179] are used.

Since complete structural studies need not only accurate line positions for the

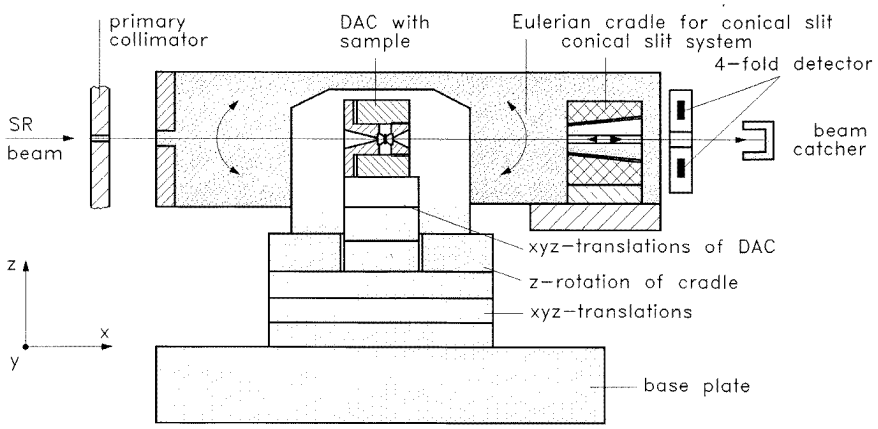

Figure 5. Conical slit system with fourfold detector for energy dispersive x-ray diffraction with DAC from reference 74.

determination of lattice parameters but also reliable intensity data for the evaluation of atomic position parameters, much care had been devoted to this last problem in recent years. Since texture, preferred orientation, and graininess effect the diffraction pattern from the tiny polycrystalline samples in DACs very commonly [137, 180], one can use sample spinners which provide an efficient averaging of the intensities usually distributed unequally over the diffraction rings as illustrated in figure 6 for the EDXD technique, where the first four spectra A–D, were taken on $NdMn_2$ in a DAC with the spinner at rest in different orientations. Large differences in the intensities are noticed in these four cases due to preferred orientations of the grains while the last spectrum E with the rotating spinner gives good average intensities and good resolution of the higher indexed reflections. On the other hand, similar progress has been made also by the adaptation of x-ray image plates to angular dispersive x-ray diffraction (ADXD) with synchrotron radiation [182] and even the use of conventional laboratory x-ray sources for ADXD with DACs has been improved considerably in recent years by digitizing and averaging of film pattern. As an example for the special advantages of the x-ray image plate technique, figure 7 illustrates that pattern from mixed phases close to a phase transition under pressure can reveal special preferred orientation relations in the new phase which can be useful also to distinguish lines from different (intermediate) phases.

In addition, single crystal x-ray diffraction methods have also been applied in many studies on solids under pressure, but strong compressions were obtained thereby only on solidified gases like δ-N_2 [183], β-O_2 [184–186], CO [187], and finally on H_2 and D_2 [188–191] whereby the highest pressure reached so far in single crystal x-ray diffraction was 42 GPa.

Especially for hydrogen and hydrogen bonded systems, also neutron diffraction with DACs had been developed, but recently also LACs with toroidal gaskets contribute much to the progress in this field [192–195].

In studies of local structure and local distortions around impurities with information on the number of nearest neighbours and nearest neighbour distances, extended x-ray absorption fine structure (EXAFS) from solids under pressure resulted also in recent years in very valuable complementary information in comparison with x-ray diffraction [196–200] and the potential of this method is largely increasing with the present developments with

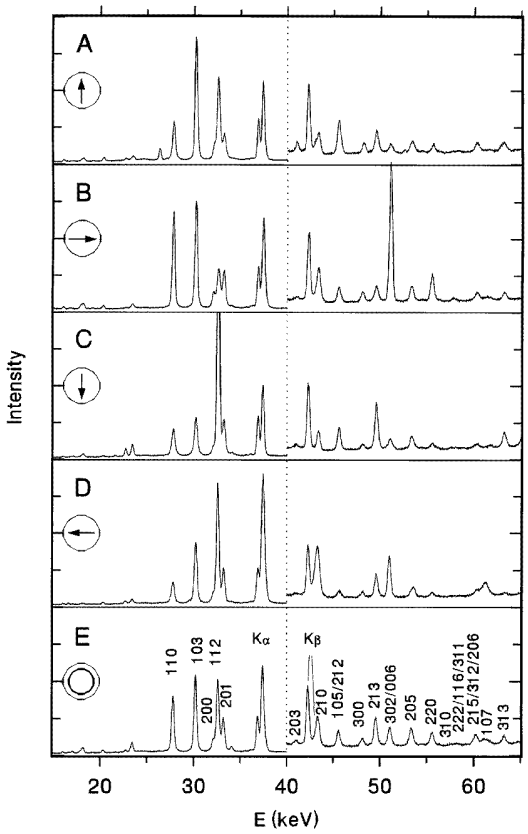

Figure 6. EDXD pattern for $NdMn_2$ under pressure taken with a sample spinner at four different orientations (A to D) and with continuous rotation (E) to illustrate effects from preferred orientations of the crystallites in the sample. Reliable intensity data with corresponding indexing of the diffraction peaks are only obtained in pattern E from reference 181.

synchrotron radiation. In addition, the near edge structure (XANES) in these studies gives valuable information on bonding properties and, especially, on changes in valencies under pressure.

From the technical point of view, much progress has also been made with Mössbauer spectroscopy on samples under pressure especially with DACs [201–203] mostly with isotopes like ^{57}Fe, ^{119}Sn, ^{125}I and ^{151}Eu, where the transition energies are rather low as shown in figure 3. Very recently, the first high pressure studies were performed in a new type of Mössbauer spectroscopy, whereby synchrotron radiation replaces the conventional radioactive source. Due to the especially good collimation and unique time structure of the synchrotron radiation much progress can be expected in the near future in this new field. Another technique using nuclear transitions to obtain information on the local hyperfine fields is the Time Differential Perturbed Angular Correlation (TDPAC), where the early high pressure measurements used various types of LACs in limited pressure ranges [204] but promising results have been obtained recently also with DACs [205].

In Raman spectroscopy with DACs much progress was made in recent years by the use of modern triple monochromators with linear (CCD) detectors not only on hydrogen

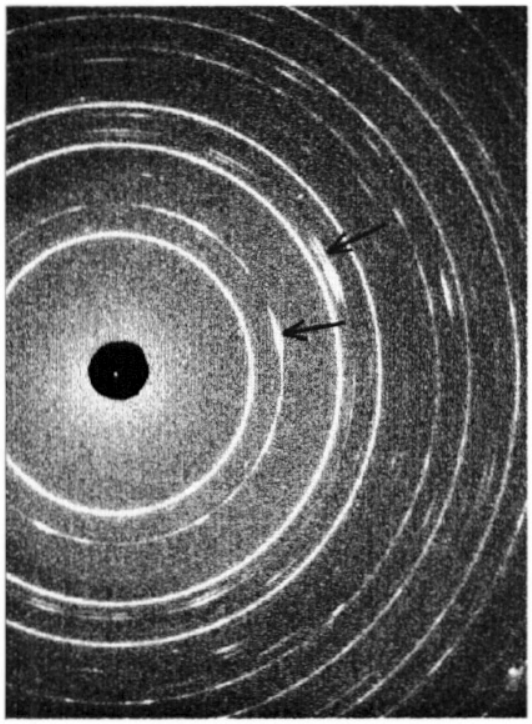

Figure 7. ADXD pattern of CdTe at the phase transition from zincblende to cinnabar structure around 3.5 GPa showing continuous rings for the zincblende phase and preferred orientations for the cinnabar phase. (Reproduced with permission from the authors [136].)

[206], but also on metals [207–210] with strong impact on the respective fields. A complete mapping of the sound velocities in the various crystal directions was finally obtained by the development of Brillouin spectrometry with suitable DACs and a rotational stage providing all the necessary degrees of freedom [111–113]. Interesting prospects are offered also by the recent construction of a DAC for optical measurements on samples under pressure in high pulsed magnetic fields whereby all parts of the DAC were made from nonmetallic materials [211].

2.4. Shock wave techniques

For the later comparison of results from static and dynamic measurements, a very short introduction into the field of shock wave techniques seems to be necessary also here, and further detailed information can be found easily in many specialized books which give excellent introductions into the wide field of high pressure studies with shock wave techniques [212]. Basically, when a flat projectile hits the surface of a flat sample with sufficiently high speed to overcome the elastic limits in the sample, a planar shock wave is generated and travels into the sample with the shock wave velocity u_s.The mass or average particle velocity u_p directly behind the steep shock front is usually measured together with u_s as primary data. Conservation laws for mass, momentum, and energy are used

to determine the density ρ_H or the specific volume $v_H = 1/\rho_H$, the pressure p_H, and the specific internal energy e_H (per mass unit) in the shocked material. With the initial sample at rest ($u_{s_0} = u_{p_0} = 0$) at ambient pressure ($p_0 \approx 0$), one obtains:

$$\rho_H = \rho_0 \cdot u_p/(u_p - u_s)$$
$$p_H = \rho_0 \cdot u_p \cdot u_s \qquad \text{and} \qquad e_H - e_0 = u_s^2/2 = p \cdot (v_H - v_0)/2. \tag{1}$$

Thereby, one should keep in mind that the so-called Hugoniot pressure, p_H, represents the hydrostatic pressure behind the shock front only, when the nonhydrostatic deviatoric stresses are so small that their effects can be neglected.

Series of experiments with many samples from the same material and starting from the same initial state result at first in a relation between the measured quantities u_s and u_p, and linear relations of the form

$$u_s = c_0 + s \cdot u_p \tag{2}$$

are commonly observed for simple solids, when phase transitions or electronic anomalies are not encountered in the experimental region. With the conservation laws, one obtains then also continuous curves for v_H versus p_H or ρ_H versus p_H, which represent the 'Hugoniot curves' for the given material. For linear u_s–u_p relations one finds immediately:

$$p_H = K_{H_0} \cdot \left(1 - \frac{v_H}{v_0}\right) \Big/ \left(1 - s \cdot \left(1 - \frac{v_H}{v_0}\right)\right)^2 \tag{3}$$

where by $K_{H_0} = c_0^2/v_0$ represents the limiting value ($p_H \to$ zero) of the 'shock bulk modulus' $K_H = \mathrm{d}\, p_H/\mathrm{d} \ln v_H$, and $s = (1 + K'_{H_0}/4)$ determines the corresponding derivative $K'_H = \mathrm{d} \ln K_H/\mathrm{d} \ln v_H$ at $p_H = 0$. In fact, in terms of the scaled variables $p^* = s \cdot p_H/K_{H_0}$ and $\Delta^* = s \cdot (1 - (v_H/v_0))$ one obtains a 'universal' Hugoniot relation

$$p^* = \Delta^*/(1 - \Delta^*)^2 \tag{4}$$

which is of some interest for considerations on 'corresponding states' in shock compressions [213]. According to this simple relation, p^* is expected to diverge, when $\Delta^* = 1$ or in other words, when v_H approaches the critical value $v_c = v_0 \cdot (s - 1)/s$.

One problem encountered typically in the evaluation of such u_s–u_p data is illustrated in figure 8 and figure 9 where figure 8 shows data for Al up to extremely high velocities and figure 9 similar data for Cu under more moderate conditions. While all the data appear to follow closely a linear relation, the solid dashed line represents the extrapolation of low pressure static data into this shock wave region to illustrate, that just at the beginning, the slope s_0 and the intercept c_0 both deviate slightly from the static data. In addition to the special stress state in the shock front, also transitions into the liquid state may partly account for these variations in slopes and initial values, which have to be taken into account in later comparisons between shock wave and static data, where the results for K'_0 from the initial slopes of shock wave data appear to be systematically lower than the data from static measurements.

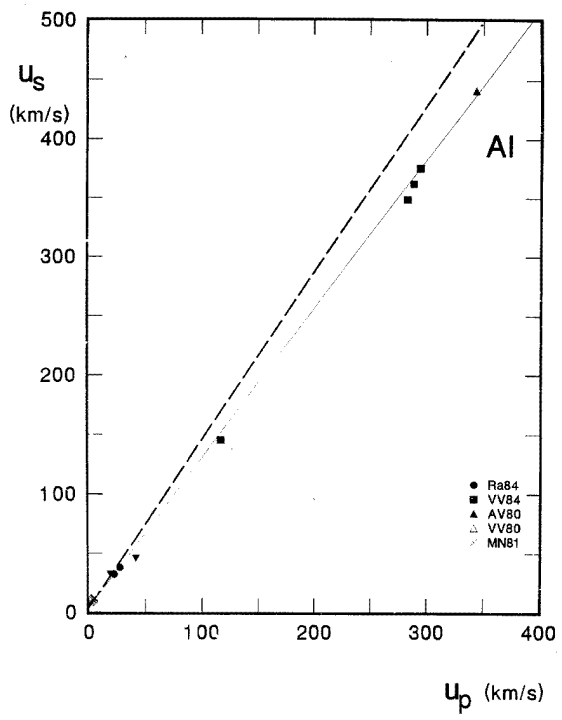

Figure 8. Comparison of experimental u_s–u_p data for Al under strong shock conditions with low pressures static results represented by the extrapolated heavy dashed line. The shock wave data Ra84, VV84, AV80, VV80 and MN81 are given in references 214–216, 218 respectively.

More detailed evaluations of room temperature (isothermal) *p*-*v*-data from shock wave measurements require additional information on the thermal behaviour of the material, including thermal excitations of the lattice vibrations, as well as excitations of electrons in the conduction band, and under strong compression also core level excitations. Additional information on stress homogeneity, defect concentration, and possibility also on structural changes and melting are mostly considered as minor corrections. Some of these problems can be handled by theoretical models, but it is also desirable to check these models by additional diagnostics like temperature measurements in the shocked state, measurements of sound wave velocities, flash x-ray diffraction, electrical conductivity, and optical properties like refractive index and reflectivity or Raman and Brillouin scattering. Direct determinations of the Grüneisen parameters γ_G for samples in the shocked state have also been made for more direct evaluations of *p*-*v*-isotherms from the Hugoniot data.

Here, all the ambiguities in the evaluation of simple u_s–u_p relations or Hugoniot curves may serve just as a warning for later comparisons of shock wave data with the results of static measurements.

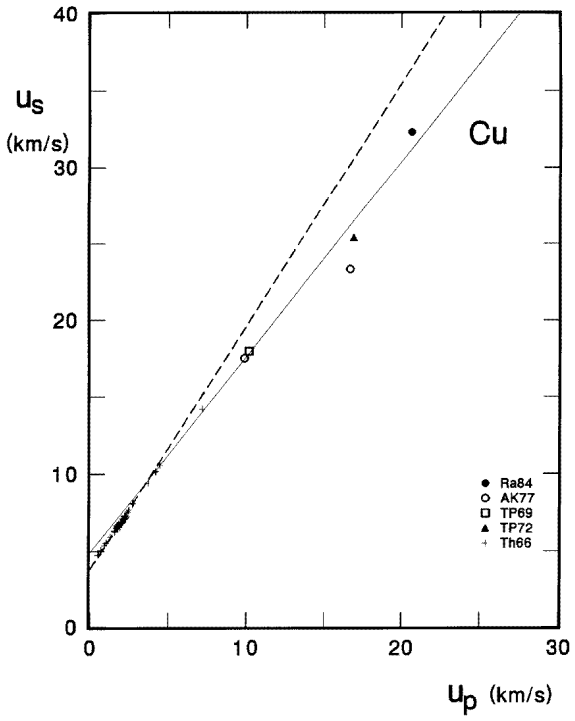

Figure 9. Comparison of experimental u_s–u_p data for Cu under strong shock conditions with low pressures static results represented by the extrapolated heavy dashed line. The shock wave data Ra84, AK77, TP69, TP72, Th66 are given in references 214, 219–222, respectively.

3. Pressure sensors and scales

Since piston cylinder devices work at the best up to 10 GPa and require large corrections for friction and deformation in this range, direct determinations of pressure by force per unit area measurements have not exceeded 10 GPa, and their accuracy was limited in this upper range to 1% at the best [223]. On the other hand, simultaneous measurements of the specific volume v and the bulk modulus K_T would allow by an integration of the form

$$p = \int_{v_0}^{v_p} (K_T/v)\ \mathrm{d}\, v \tag{5}$$

an absolute determination of pressure [224], however, problems with thermal corrections of adiabatic compressibility measurements and other limitations have still prevented extended applications of this method [225, 226]. Therefore, up to now all pressure determinations in the range above 10 GPa are ultimately based on shock wave measurements with the use of corresponding EOS data for simple 'calibrants'. By comparison of these shock waves data with accurate experimental data (for K_0) at low pressures and with first principle or semiempirical EOS data for high pressures, room temperature p-v-isotherms for several calibrants have been established for the pressure range up to 500 GPa with an accuracy in pressure of probably better than 5% [227, 228] for Al, Cu, Ni, Ag, and Pt, and with a somewhat larger uncertainty also for Au [229]. An intercomparison of accurate powder

x-ray measurements with other common standards like NaCl [230–233], KCl, CsCl, CsI [234–236], Pd [237], Mo [238–240], Re [241] or W may further improve the (absolute) accuracy of this pressure scale in the near future. At the present time, however, a recent study points out that the scales for Cu, Ag and Au [242] may show discrepancies with respect to each other by more than 10%. With a precision in high pressure x-ray diffraction measurements of $\Delta a/a \leqslant 2 \cdot 10^{-4}$ and typical bulk moduli of 1 TPa at 200 GPa, one should be able to obtain a precision of the corresponding pressure determinations of $\Delta p/p \leqslant 0.3\%$, which is in fact an order of magnitude smaller than the present uncertainty in any of these scales.

Due to the ease of luminescence studies with DACs, measurements and calibrations of the ruby R line shifts under pressure with respect to different EOS calibrants [243–245] were indeed very instrumental for the development at the whole field of high pressure studies with DACs. Under truly or nearly hydrostatic conditions, where the line width of the ruby R lines remains constant or decreases even slightly with increasing pressure, one can obtain a precision of 20 MPa in the pressure determination with the ruby luminescence line shift, however, the (absolute) accuracy remains still much more limited to 3% up to 10 GPa and a value of 10% may be typical for 100 GPa due to the uncertainty in the EOS data used in the primary ruby calibrations. A comparison of the specific EOS data used in these calibrations [246] with more recent estimates indicates in this case that the original form

$$p = 1\,904\,\mathrm{GPa}/B \cdot ((1 + \Delta\lambda/\lambda_0)^B - 1) \tag{6}$$

with $B = 5$ for quasihydrostatic and $B = 7.665$ for hydrostatic [247] conditions may underestimate the pressure by 3 to 10% below 100 GPa, and it is not clear whether an increase of the prefactor by about 3% or only an increase of the B values by up to 30% would be more appropriate.

Besides these (minor) problems with the absolute calibration at ambient temperature, there exist also some additional uncertainties for measurements at elevated temperatures. By the use of ultrasonic data for the adiabatic bulk modulus at ambient pressure, $K_{s_0}(T)$, and semiempirical forms for the EOS of simple solids, best estimates for Cu, Ag, Au and Al were recently derived also for these applications, and it will be interesting to see, whether a calibration of the ruby line shift at elevated temperatures would show differences with respect to the temperature dependent offset well known from ambient pressure conditions [248]. With respect to this question and from the point of view to find some other luminescence sensors with weaker temperature dependences, as well as higher intensities at elevated temperatures, and possibly even still higher resolution in the pressure measurements, various sensor materials with divalent and trivalent lanthanide ions in different host materials have been compared with ruby and chromium doped YAG as shown in table 1.

Since Sm^{2+}:SrFCl shows (i) the highest 'resolution' $\mathrm{d}\ln\lambda/\mathrm{d}\,p$, (ii) a much weaker temperature sensitivity $(\mathrm{d}\,\lambda/\mathrm{d}\,T)/(\mathrm{d}\,\lambda/\mathrm{d}p)$ than ruby, (iii) a simple (singlet) line shape, and (iv) strong luminescence intensity up to at least 600 K, a detailed calibration study was performed on this material [249], but only up to 20 GPa, where pressure induced luminescence quenching reduced the intensity significantly, similar to the situation in Sm^{2+}:BaFCl at lower pressures [250]. For the $Y_{1,2}$ lines of Sm^{3+}:YAG (included in table 1) similar quenching was not observed but on the contrary the intensity increased by an order of magnitude up to 100 GPa [251–254]. Even though the resolution of this sensor is much poorer than for Sm^{2+}:SrFCl the weaker temperature sensitivity and the wider pressure range for the $Y_{1,2}$, luminescence of Sm^{3+}:YAG make this sensor especially useful

Table 1. Comparison of different luminescence pressure sensors [178] with estimated values in parenthesis.

Material	λ (nm)	$\frac{d\lambda}{dp}$ (nm/GPa)	$\frac{d\lambda}{dT}$ (nm/10^3 K)	$\frac{d\lambda}{\lambda dp}$ (GPa^{-1})	$\frac{d\lambda}{dT} / \frac{d\lambda}{dp}$ (GPa/10^3 K)	Transition
Cr^{3+} : Al_2O_3	694.2	0.365	+6.8	0.49	18.6	$^2E \rightarrow 4_2^A$ doublet
Cr^{3+} : $YAlO_3$	722.8	0.70	+7.6	0.7	10.9	$^2E \rightarrow ^4 A_2$ doublet
Eu^{3+} : LaOCl	578.7	0.25	(−0.5)	(1)	(−2)	$^5D_0 \rightarrow ^7 F_0$ singlet
Eu^{3+} : LaOBr	(578)	(0.3)	(−0.5)	(1)	(−1.7)	$^5D_0 \rightarrow ^7 F_0$ singlet
Eu^{3+} : YAG	590.6	0.197	−0.5	(0.7)	−2.5	$^5D_0 \rightarrow ^7 F_1$ doublet
Sm^{3+} : YAG	617.8	0.298	+0.2	0.23	0.7	? $\rightarrow ^6$ H multiplet
	616.1	0.228	+0.1	0.20	0.4	
Sm^{2+} : SrB_4O_4	685.4	0.225	−0.1	1.7	−0.4	$^5D_0 \rightarrow ^7 F_0$ singlet
Sm^{2+} : BaFCl	687.6	1.10	−1.6	4.8	−1.5	$^5D_0 \rightarrow ^7 F_0$ singlet
Sm^{2+} : SrFCl	690.3	1.10	−2.3	5.8	−2.1	$^5D_0 \rightarrow ^7 F_0$ singlet

for applications involving both high pressure and high temperature. A comparison of ruby and alexandrite *R* lines at pressures up to 50 GPa and temperatures up to 250 °C [255] specified, on the one hand, the limited range in temperature for both of these sensors, but gave, on the other hand, additional experimental evidence at higher pressures complementing the previous low pressure measurements [256] to support the assumption, that the pressure–temperature cross derivatives of the luminescence line shifts are negligible for both ruby and alexandrite. It may be worth noting, that also the ruby luminescence becomes too weak for useful measurements above 250 GPa [257] and Sm:YAG transforms irreversibly into a different disordered structure above 100 GPa. Thus, the ideal luminescence sensor has not yet been found, but significant progress may be expected also in this field just in the near future. Finally, it should be mentioned, that the calibration of the superconducting transition temperature $T_c(p)$ for lead [258, 259], with respect to the ruby scale provides also a manometer for use in LACs at low temperatures with a precision of better than 1%, which is better than the accuracy of the ruby scale.

4. Equations of state (EOS)

4.1. General considerations

Equations of state for condensed matter under strong compression represent a central link between various fields of science [260, 261]. In geo, planetary, solar and stellar physics, pressure, temperature and density in the interior of these objects are coupled to each other by equations of state, and adiabatic compressions with corresponding temperature gradients give certain bounds for the convective models of all the different layers not only in the Earth but also in the giant planets with their completely different constituent materials and similarly also for the stellar internal convections.

The interpretation of shock wave experiments and models on fusion by inertial confinement depend both strongly on EOS data for many different materials under strong compression and, finally, EOS data represent also an excellent link between macroscopic thermodynamic descriptions of the materials and microscopic quantum mechanical models.

Basically, one considers a system with a fixed number of identical particles N confined to a volume V in thermal equilibrium characterized by the temperature T. When the total energy of this system in all its individual quantum states is given by a function $E\{n\}$, whereby $\{n\}$ represents the complete set of quantum numbers, all static thermodynamic equilibrium properties of the system are then incorporated in the partition function

$$Z(V, T, N) = \sum_{\{n\}} \exp(-E\{n\}/kT) \tag{7}$$

as shown for instance by the well known relations for

$$\begin{aligned} &\text{the free energy} && F(V, T, N) = -kT \ln Z(V, T, N) \\ &\text{the entropy} && S = -\partial F/\partial T|_{V,N} \\ &\text{the pressure} && p = -\partial F/\partial V|_{T,N} \end{aligned} \tag{8}$$

and the common interrelations between internal energy $U = F + TS$, enthalpy $H = U + pV$ and (Gibbs) free enthalpy $G = F + pV$.

Since $F(V, T, N)$ determines all the other quantities, it is often considered as 'thermodynamic potential' of this system. Similarly, with respect to their different variables $U(V, S, N)$, $H(p, S, N)$ and $G(p, T, N)$ are thermodynamical potentials, which determine by their partial derivatives also all the other (canonically conjugated) thermodynamic variables.

However, it should be noted that $p(V, T, N)$ alone gives only an incomplete description of the system, since partial integration of pdV does not determine the missing part $\Delta F(T)$ which is involved in the integration for the entropy. Similarly $U(V, T, N)$ would also give only an incomplete characterization of the system, missing the term $\partial S/\partial V|_{T,N}$, which could be determined only, when

$$p(V, T, N) = -\partial U/\partial V|_{T,N} + \partial S/\partial V|_{T,N} \tag{9}$$

would be known in addition.

Such incomplete characterizations of a thermodynamic system represent in a general sense 'equations of state' and, historically [262], there was a distinction between thermal (TEOS) and caloric (CEOS) equations of state referring to $p = p(V, T, N)$ and $U = U(V, T, N)$, respectively, whereas in recent years the term EOS has been restricted in its meaning mostly to the *p-V-T*-relations.

With respect to solids under strong compression, one may separate first the ground state energy $E_{\mathrm{sl}}(V, N)$ of the static lattice from all the other excitations $\epsilon\{n\}$ which can be splitted further by the Born–Oppenheimer approximation into electronic ϵ_{el} and phononic ϵ_{ph} contributions. Usually, anharmonicities, electron phonon coupling, defects, and nonequilibrium stresses are neglected, and then one arrives at the Mie–Grüneisen EOS:

$$p = p_{\mathrm{sl}}(V, N) + p_{\mathrm{ph}}(V, T, N) + p_{\mathrm{el}}(V, T, N) \tag{10}$$

where the term p_{sl} stands for the static lattice (electronic ground state) contribution, p_{ph} represents the phonon pressure, and p_{el} gives the pressure from electronic excitations.

Thereby, theoretical calculations consider mostly just the static lattice part and a comparison with static measurements needs then additional (small) corrections for zero point motion of the lattice and for the thermal pressure from the phonons, which contribute typically about 0.3 GPa at ambient temperature. However, in shock wave measurements, the thermal pressure rises to a significant contribution and even electronic excitations, not only in metals but also in semiconductors and insulators, can often not be neglected.

For a quasiharmonic lattice, where anharmonicities are taken into account only through mode Grüneisen parameters $\gamma_i = \mathrm{d}\ln\nu_i/\mathrm{d}\ln V$ for the volume dependence of the lattice mode frequencies ν_i without any (isochoric) temperature dependences of these modes, the general form for the phonon contribution to the free energy is given by

$$F_{\mathrm{ph}} = \sum_i ((h\nu_i/2) + kT\,\ln(1 - \exp(-h\nu_i/kT))) \tag{11}$$

where the sum counts all the eigenmodes [263]. For most explicit calculations the Grüneisen approximation [264] is commonly used which implies that all the mode Grüneisen parameters γ_i are replaced by one common average value γ related to the characteristic temperature $\theta(V)$ of this model by $\gamma\theta = -\mathrm{d}\ln\theta/\mathrm{d}\ln V$. Within this approximation this parameter $\gamma\theta$ becomes identical to the 'thermodynamic' Grüneisen parameter $\gamma = \alpha_v\, K_T\, V/C_v$, whereby α_v represents the volume expansion coefficient, K_T stands for the isothermal bulk modulus, V is the volume of the solid and C_v is the isochoric heat capacity. Explicit forms for $F_{\mathrm{ph}}(V, T, N)$ depend then only on N, $\theta(V)$, and the scaled temperature $\tau = T/\theta$ through a model dependent functional form. For many applications it is convenient to use a pseudo Debye approximation which results in the following forms for the phonon contributions to the free energy

$$F_{\mathrm{ph}} = 3Nk\theta \cdot \left(\frac{3}{8} + \tau^2 \cdot \frac{3}{2} \cdot \frac{\tau + 2a/3}{(\tau + a)^2} - \tau\ln(1 + \tau/a)\right) \tag{12}$$

with $a \approx 0.2$, and for the pressure

$$p_{\mathrm{ph}} = (\gamma/V) \cdot 3Nk\theta \cdot \left(\frac{3}{8} + \frac{\tau^4}{(\tau + a)^3}\right) \tag{13}$$

In the classical limit ($T \geqslant \theta$), which is obtained at room temperature for most solids, except for diamond and for the light gas solids (H_2, He and Ne) under pressure, the much simpler approximation $p_{\mathrm{ph}} \Rightarrow (\gamma/V) \cdot 3NkT$ shows immediately, that the common assumption $\gamma/V = \gamma_0/V_0$ with $\gamma \approx 2$ results in a useful estimate of the phonon pressure with the additional observation, that this contribution is almost pressure independent for such 'regular' solids. Since further discussions of these effects are only needed for the light gas solids or for other solids at very low temperatures, the special literature should be consulted for these cases. For heavier elements, their compounds, and alloys, the phonon pressure is usually noticed only in the thermal expansion and in the detailed balance of structural stabilities at elevated temperatures. The static lattice part, which represents the changes in

the electronic ground state energy, is then the dominant contribution for the comparison with theoretical results.

Before one enters into a detailed discussion of modern total energy calculations and their results on static pressures and structural stabilities, it appears to be useful to look at the historical path, where interactions of 'free atoms' were studied by atomic beam collisions, virial expansions, and in measurements of transport coefficients to determine quantitatively the detailed forms of two- and three-body interactions for atomic and molecular species [265–270]. When these forms were applied to calculate EOS data also for the solid state at strong compressions, special damping terms in the two-body potentials as well as special contributions from changes of the crystal atomic wave functions [271] had to be taken into account to reconcile the semi-theoretical and experimental data for instance for solid argon in the region from 40 to 80 GPa.

Therefore, it seems to be more appropriate to modify the empirical potentials directly in such a way, that most of the many body interactions are already absorbed in 'effective' two-body interactions for the solid state, and there appear to be slightly different approaches to derive either effective two-body potentials for the total ground state energy [272–276] or separate out the volume dependent part of the total energy to describe the remaining much weaker structural energy term (at constant volume) by a more rapidly converging expansion of effective (fixed volume) two- and multi-body interactions [277].

Since these calculations have to be performed individually for each substance, there exists still the need to use also simple empirical analytic forms to describe all the experimental EOS data now available for solids under strong compression, and one can ask, whether there are specific forms, which describe best the behaviour of 'regular' solids, which would be materials without any drastic changes in their electronic structure, typically also with close packed structures without any changes in the structure type. These attempts go naturally much beyond the classical 'theory of finite strains' [278, 279], which was planned as a series expansion for finite 'small' strains only with obvious divergencies at strong compressions.

Without entering into a detailed discussion of the historical developments at this point [280], it can be noted that the second order Murnaghan equation, MU2 in table 2, offers a definite advantage only, when the range of the data is limited to small compressions, and when one is interested in a form, which can be analytically inverted from $p = p(v)$ to $v = v(p)$.

The theories of finite strain using a general strain $f = (x^{-n} - 1)/n$ with $x = (v/v_0)^{1/3}$ and $n = 2$ for Eulerian strain or $n = -2$ for Lagrangian strain lead then in second order to the generalized strain expansion for the pressure given with the label GS2 in table 2. The case with $n = 2$ is commonly referred to as Birch Equation and will be labelled here as BE2 in second order or BEL for any order L. Thereby, the 'order' L stands for the number of independent elasticity parameters used in the given form. In first order, only the isothermal bulk modulus at zero pressure, K_0, enters into the form and the corresponding first and higher order derivatives (with respect to pressure), K_0', K_0'', K_0''', ..., enter successively as free parameters into the higher order forms.

The common use of Birch's form (BEL) is certainly related to the fact, that its first order form BE1, with $c = 0$ in table 2 and the resulting implicit assumption $K_0' = 4$, represents almost the best 'average' form for any first order finite strain expansion and only $n = 3$ would also lead, in first order with $K_0' = 5$, to similarly reasonable results. However, one should note, that extrapolations of finite strain expansions beyond the range, where data had been fitted, diverge quite rapidly from reasonable values as indicated also in table 2 in the column under K_∞', which represents the ultimate value for the pressure derivative of the

Table 2. Common EOS forms with their parameter relations. The fit parameters are usually K_0 and K_0' with prefixed values for v_0, the (atomic) volume at ambient conditions. $x = (v/v_0)^{1/3}$ represents a reduced length and the Fermi-gas pressure $p_{\mathrm{FG}_0} = a_{\mathrm{FG}} \cdot (Z/v_0)^{5/3}$ is discussed further in the text.

Name	EOS	K_0'	K_x'	K_0V_0/E_0
MU2	$p = \frac{3}{c}K_0 \cdot x^{-c} \cdot (1-x^c)$	$\frac{c}{3}$	$\frac{c}{3}$	0
GS2	$p = \frac{3}{n}K_0 \cdot x^{-2n-3} \cdot (1-x^n) \cdot (1+c(x^{-n}-1))$	$n+2+\frac{2n}{3}c$	$1+n$	< 0 if $K_0' > 2(n+1)$
BE2	$p = \frac{3}{2}K_0 \cdot x^{-7} \cdot (1-x^2) \cdot (1+c(x^{-2}-1))$	$4+\frac{4}{3}c$	3	< 0 if $K_0' > 6$
MS2	$p = K_0 \cdot (1-x^3) \cdot (1+c(1-x^3))$	$4c-1$		0
MG3	$p = \frac{3}{n}K_0 \cdot x^{-m} \cdot (1-x^n)$	$\frac{2m-n}{3}$	$\frac{m}{3}$	$(K_0'-K_\infty'-1)(K_\infty'-1)$
GBM	$p = \frac{3K_0}{c-n-1} \cdot x^{-2} \cdot (1-x^{-n-1} \cdot \mathrm{e}^{-c(1-x)}) \cdot \mathrm{e}^{c(1-x)}$	$\frac{4}{3}+\frac{c^2-c-(n+1)^2}{3(c-n-1)}$	$\frac{2}{3}$	complex
EMo EM2	$p = \frac{6}{c}K_0 \cdot x^{-2} \cdot (1-\mathrm{e}^{-(c/2)(1-x)}) \cdot \mathrm{e}^{c(1-x)}$	$1+\frac{1}{2}c$	$\frac{2}{3}$	$\frac{2}{3}(K_0'-1)^2$
ERy MV2	$p = 3K_0 \cdot x^{-2} \cdot (1-x) \cdot \mathrm{e}^{c(1-x)}$	$1+\frac{2}{3}c$	$\frac{2}{3}$	$\frac{1}{4}(K_0'-1)^2$
HO2	$p = 3K_0 \cdot x^{-5} \cdot (1-x) \cdot \mathrm{e}^{c(1-x)}$	$3+\frac{2}{3}c$	$\frac{5}{3}$	$\approx \frac{1}{4}(K_0'-1)^2 - \frac{2}{5}$
H12	$p = 3K_0 \cdot x^{-5} \cdot (1-x) \cdot \mathrm{e}^{cx(1-x)} \cdot \mathrm{e}^{c_0(1-x)}$	$3+\frac{2}{3}(c_0+c)$	$\frac{5}{3}$	$c_0 = -\ln(3K_0/p_{\mathrm{FG}_0})$
H22	$p = 3K_0 \cdot x^{-5} \cdot (1-x) \cdot (1+cx(1-x)) \cdot \mathrm{e}^{c_0(1-x)}$	$3+\frac{2}{3}(c_0+c)$	$\frac{5}{3}$	$\approx \frac{1}{4}(K_1'-1)^2\left(1+\frac{3c}{2c_0}\right) - \frac{2}{5}$

bulk modulus at very strong compression, and which should approach the limit of a free electron Fermi gas, $K_{\mathrm{FG}}' = 5/3$. On the other hand, also the value for the corresponding cohesive energy, $E_0 = -3V_0 \int_1^\infty p(x)x^2 \mathrm{d}\,x$, remains positive for BE2 only, when $K_0' < 6$, which is not always the case.

The situation is even worse for the second order form MS2, which represents the Hugoniot curves related to linear u_s–u_p relations [281], and diverges rapidly from reasonable values, when it is used for isotherms. This observation applies not only to the second order form MS2 but also to its higher order expansions MSL, which have been used also for 'convenient' representations of EOS data.

For safer extrapolations of experimental data into the range of strong compression, the use of effective two-body potentials appears to be most appropriate, especially, if these potentials are modelled in such a way that they approach reasonably the Thomas–Fermi limit, which can be described also within a good approximation by the free electron Fermi-gas limit $p_{\mathrm{FG}} = a_{\mathrm{FG}}(Z/v)^{5/3}$ with additional screening of the form $\exp(-\beta_{\mathrm{TF}}\sigma)$, where Z stands for the electron number, v for the atomic volume, $\sigma = (3/4\pi \cdot Zv)^{1/3}$ for a scaled atomic radius and both $a_{\mathrm{FG}} = (3\pi^2)/5 \cdot \hbar^2/m_e = 23.369\,05\ (2)\ \mathrm{nm}^5$ MPa and $\beta_{\mathrm{TF}} = 2/3 \cdot (3/2\pi)^{2/3}/a_0 = 7.696\,061\ (1)\ \mathrm{nm}^{-1}$ are (universal) constants.

With this consideration in mind, one can notice, that the effective Lennard–Jones potential, already used by Grüneisen (1912) [282] and labelled MG3 in table 2, could be adapted with $m = 5$ to match the Fermi-gas limit $K_\infty' = 5/3$) to avoid a divergence at ultimate compression, however, the corresponding value for K_0' would then be restricted to unusually small values ($\leqslant 3$). All the other commonly used effective potentials, either of a Generalized Born–Mayer type (GBM in table 2), or of the Effective Morse (EMo) or Rydberg (ERy) type, lead also at ultimate compression to strong divergences due to their values for $K_\infty' = 2/3$. Since the repulsive term in these potentials has just a simple exponential form, its integration for the determination of the cohesive energy, E_0, is trivial and simple relations are derived for correlations between K_0V_0/E_0 and the parameter K_0' as shown in table 2. The relation $K_0V_0/E_0 = (K_0'+1)/8$ has been discussed as Rodean's rule just recently [283, 284], in a comparison of shock wave data for K_0V_0 and K_0' with

literature data for E_0. With data for E_0 covering two decades for the metallic elements, a scatter of only 10% was noticed with respect to Rodean's rule and for the alkali halides the deviations were even smaller when heats of sublimation were used in these later cases for E_0. However, it can be noted that the effective potentials EMo and ERy result in almost the same correlations for the restricted range of $4 < K_0' < 8$ as illustrated in figure 10, where experimental data for the ratio K_0V_0/E_0 are plotted for all the metallic elements and noble gas solids together with some 'theoretical' curves, which represent the correlations implied by various second order EOS forms. An inspection of figure 10 illustrates first of all, that none of the second order forms can be considered as 'universal' EOS [291] or 'universal bond energy relation' [292], and any proposal of 'universal' second order forms represents just a lack of knowledge or an intention to discard the experimental facts.

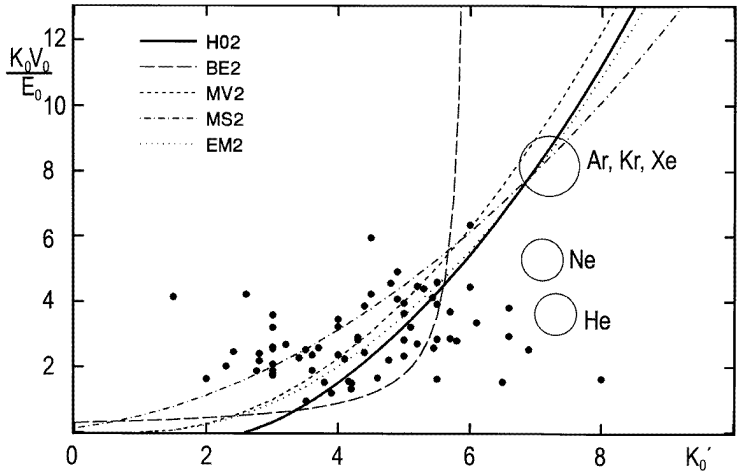

Figure 10. Correlations of K_0V_0/E_0 with K_0' incorporated in different second order EOS forms. Rodean's correlation is marked as MS2. Experimental data for metallic elements at ambient temperature [12, 284–286] are shown by small dots and data for the noble gas solids at 0 K [287–289] by open rings, respectively.

The superior correlation observed by Rodean [293] for restricted data sets, where only the metallic elements with linear u_s–u_p relations were taken into account, may be traced back just to a special selection of 'regular' or 'simple' elements.

Besides this restriction, typical for any second order form, all the effective potentials discussed so far suffer from the fact, that they do not approach the Thomas–Fermi limit under strong compression.

However, this deficiency is easily removed, if one replaces the Born type exponential repulsion by an effective Thomas–Fermi type potential of the form $\phi_{\mathrm{TF}} = (A/R^2)\exp(-R/R_s)$ with corresponding values for the nearest neighbour distances R, and adapted values for the strength A and screening length R_s. With these considerations in mind, the Effective Rydberg potential ERy can be modified into the form HO2. The other label MV2 for the form ERy in table 2 indicates thereby that the 'universal' EOS strongly promoted by Vinet *et al* is just the second order form of a more general expansion [294]. A perfect match with the Fermi-gas limit is finally obtained with the form H12, which couples in its first order form H11 by $c = 0$ and $K_0' = 3 + \frac{2}{3}c_0$ through the parameter $c_0 = -\ln(3K_0/p_{\mathrm{FG}_0})$ with $p_{\mathrm{FG}_0} = a_{\mathrm{FG}} \cdot (Z/v_0)^{5/3}$ the value of K_0' to both K_0 and v_0.

This first order variation of K_0' for H11 can be compared in figure 11 with the constant value $K_0' = 4$ of BE1 and with the experimental values for the elements C, Si, Ge (in their covalent diamond structures), for the noble gas solids with their van der Waals bonding, and with the data for the cubic elemental metals, which are represented just by dots. While both the covalent elements and the heavier noble gas solids fit much better to the correlation implied by H11 than to the fixed value $K_0' = 4$, the differences for the lighter noble gases Ne and He are easily traced back to effects from zero point motion, and special 'anomalies' are noticed for many of the 'pretransition metals' as shown by larger deviations from the H11 correlation and these effects will be discussed in detail later.

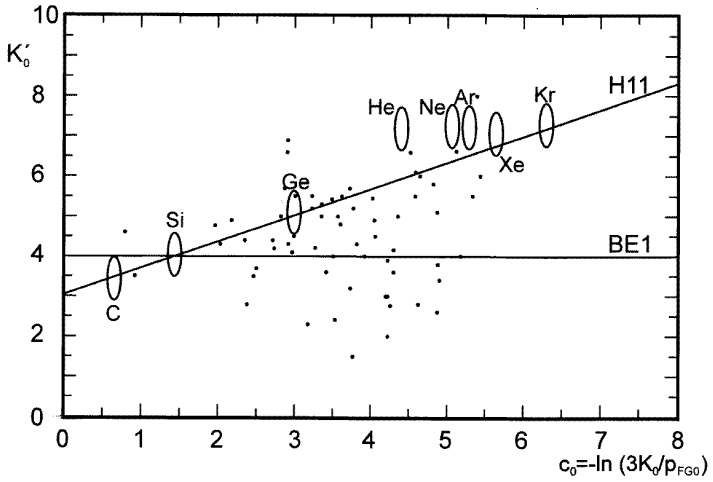

Figure 11. Plot of K_0' versus $c_0 = -\ln(3K_0/p_{\mathrm{FG}_0})$ for the covalent carbon group IV elements in their diamond structures and for the noble gas solids (at 0 K) showing close agreement with the correlation implied by the first order EOS form H11. Large deviations from the constant value $K_0' = 4$ corresponding to the first order finite strain form BE1 can be noticed. Small dots represent data for the cubic metallic elements and their deviations are discussed in the text. Literature data for V_0, K_0, K_0' are taken from various references [12, 285–290].

At this point, it should be noted, however, that the finite strain expansions GSL and BEL may find some reasonable applications, when EOS data for a high pressure phase should just be fitted around a given reference point p_r, v_r. In this case, just p_r has to be added to the right hand side of GSL or BEL and all the zero pressure parameters v_0, K_0, K_0', are then replaced by the respective values V_r, K_r, K_r' the reference point. Corresponding zero pressure values for such high pressure phases may then be determined by extrapolation, however, with rather large uncertainties due to the correlations in the errors of these parameters. For EOS forms related to effective potentials like H0L, H1L or H2L, extrapolated values for v_0 enter as additional free parameter and a lower order L may be sufficient in this more involved fitting procedure.

For these procedures as well as for the comparison of different EOS forms and EOS data, various 'linearization schemes' had been proposed. In fact, not only the EOS forms presented in table 2 but any second order form, which contains the 'second order parameter' c only in one place, can be inverted in such a way, that one obtains a conjugated linearization scheme as shown in table 3, where the resulting 'generalized strain coefficients' $\eta(p, x)$ are represented in the form of series expansions with respect to the generalized finite strains

$f(x)$ and the letters L in the names of the different forms indicate, that the parameter c of the earlier second order forms has been replaced by a series expansion $c = \Sigma_{k=0}^{L-2} c_{2+k} \cdot f^k$ to obtain the corresponding L-th order form. Since the parameter c_2 determines the slopes of these linearizations, one can see that typical values of $K_0' \approx 4$ give rather small slopes for BEL, GSL, H0L, H1L and H2L but larger slopes for MVL and MSL which can then mask more perfectly additional nonlinear contributions.

Table 3. Linearization schemes with their parameter relations. x, c_0 and p_{FG_0} are defined in table 2. Note that large slope parameters c_2 hide nonlinearities of MSL and MVL.

Name	η	$= C_1$	$+C_2 \cdot f(x)$	$+C_3 \cdot f^2(x)$	c_2
GSL	$\frac{p \cdot n \cdot x^{2 \cdot n+3}}{3 \cdot (1-x^n)}$	$= K_0$	$+K_0 \cdot c_2 \cdot (x^{-n}-1)$	$+\ldots$	$\frac{3}{2n}(K_0' - n - 2)$
BEL	$\frac{p \cdot 2 \cdot x^7}{3 \cdot (1-x^2)}$	$= K_0$	$+K_0 \cdot c_2 \cdot (x^{-2}-1)$	$+\ldots$	$\frac{3}{4}(K_0' - 4)$
MSL	$\sqrt{\frac{1-x^3}{p}}$	$= \frac{1}{\sqrt{K_0}}$	$-\frac{c_2}{\sqrt{K_0}} \cdot (1-x^3)$	$-\ldots$	$\frac{1}{4}(K' + 1)$
MVL	$\ln\left(\frac{p \cdot x^2}{3 \cdot (1-x)}\right)$	$= \ln(K_0)$	$+c_2 \cdot (1-x)$	$+\ldots$	$\frac{3}{2}(K_0' - 1)$
HOL	$\ln\left(\frac{p \cdot x^5}{3 \cdot (1-x)}\right)$	$= \ln(K_0)$	$+c_2 \cdot (1-x)$	$+\ldots$	$\frac{3}{2}(K_0' - 3)$
H1L H2L	$\ln\left(\frac{p \cdot x^5}{p_{\mathrm{FG}_0} \cdot (1-x)}\right)$	$= -c_0$	$+(c_0 + c_2) \cdot (1-x)$	$+\ldots$	$\frac{3}{2}(K_0' - 3) - c_0$

In passing, it can be noted that the use of series expansions for the second order parameter c has also been proposed for bond energy relations [295], however, even if these effective potentials may appear to be simpler, the corresponding EOS forms are rather complicated with the series expansions appearing also with their derivatives and with no possibility to find some conjugated linearization scheme, and therefore, with no obvious practical advantage.

On the other hand, Thomas–Fermi scaling with $\sigma = \sigma_0 \cdot x = ((3/4\pi)Zv)^{1/3}$, with the electron number Z and the atomic volume v, leads to the observation that η-σ-plots of the H1L linearization result in common limiting behaviour at ultimate compression with almost the same slope not only for the elements but also for any solid near (σ, $\eta \to 0$), when appropriate 'effective' values for the average atomic volume v_{eff} and the electron number Z_{eff} are used for alloys and compounds as discussed at the end of section 4. This common behaviour is illustrated at first just for metallic elements in figure 12, where many 'normal' metals approach just by straight lines the common average behaviour of 'ideal' solids. Unusual deviations with special breaks and smaller or larger slopes as in the case of Cs reflect thereby some special 'softening' or 'hardening', which will be discussed in detail in the next section, when this scheme is applied to specific groups of solids.

4.2. Equations of state for specific substances

First of all, one can expect that the metallic elements with broad and partly filled sp-bands and with no specific contributions from the more localized d or f shells may exhibit specially 'simple' behaviour under strong compression with smooth and simple variations in their EOS. Hybridization of outer shells with inner shells introduces at very strong compression only minor modulations in the EOS since one can safely assume that the structural energies

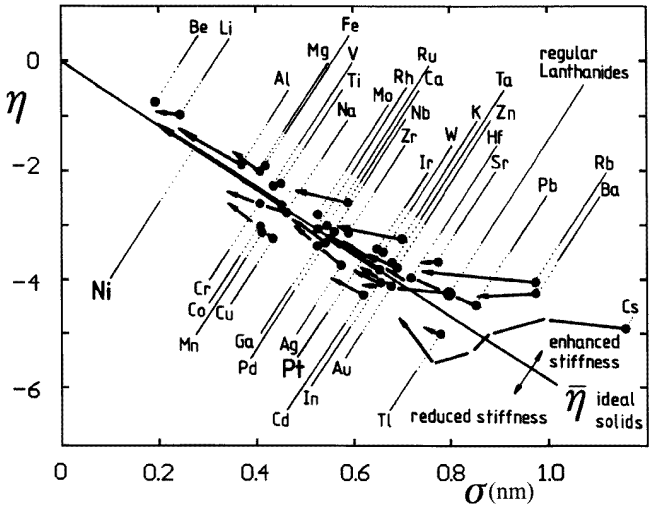

Figure 12. Variation of the generalized stress coefficient η(H1L) defined in table 3 with respect to the Thomas–Fermi radius $\sigma = Z^{1/3} \cdot R_{WS}$ where Z stands for the atomic number and R_{WS} for the pressure dependent Wigner–Seitz radius. Data are given for the low pressure phases of all the metallic elements, and only for Cs data for different high pressure phases are also included [280].

per atom may remain of the order of 10 mRy/atom corresponding to a structural pressure of about 5 GPa /$(R_{WS}/100\ \text{pm})^3$ which means that the relative contribution of the structural pressure to the total pressure is expected to decrease very rapidly under strong compressions corresponding to a rapid approach towards a structure independent EOS for each solid.

Before entering into a detailed discussion of EOS data and structural phase transitions of the elements under pressure, a few words seem to be necessary to promote the use of a systematic nomenclature for high pressure phases of the elements. In fact, IUPAC [296] recommends strongly the use of Pearson's nomenclature for structures of the elements due to its systematic nature and its minimum number of letters to identify the Bravais lattice type with c, t, o, m, a, and h for cubic, tetragonal, orthorhombic, monoclinic, anorthic, and hexagonal cells, and, respectively, P, I, F, S, and R for Primitive, (Inside) body, (fourfold) Face, and (onefold) Surface centering or for the Rhombohedral lattices. Together with the number of atoms in the conventional (centred) unit cell, using the larger hexagonal cell for rhombohedral lattices, this nomenclature gives unambiguous identifications for most of the presently worked out structures and phases of the elements with the only exceptions of cP8, oS8, hP3, and hP4, where the names of the elements or elemental groups, like Ln for the lanthanide metals, may be added to distinguish for instance between cP8-H for cubic H_2 with space group $Pa\bar{3}$ and H on the 8c positions in contrast to cP8-W for β-W with space group $Pm\bar{3}n$ and W on the 2a and 6c positions.

4.3. EOS data for simple metals

To judge on the quality of EOS data from different sources also with respect to different EOS forms, a look at the η-x plots figures 13–16 for some of the most regular solids

under strong compression can be instructive. For clarity, these figures include only ambient temperature data and theoretical values for static lattice calculations were shifted by the use of the appropriate values for v_0. Perfect straight line interpolations from ambient conditions to ultimate compression corresponding to the one parameter form H11 are noticed for Al (figure 13) and for Ni (figure 14) within the experimental and theoretical uncertainties of the data. The label 'simple solids' has been introduced [305] to characterize those solids which fit perfectly to the straight line interpolations H11. In fact, the straight line interpolations find very strong support in many cases where theoretical data extend far beyond the range of the experimental results. While the smooth data which are derived from shock wave measurements (SW) by the use of appropriate thermal corrections, show almost perfect agreement with the theoretical data (TH) and with the initial value from ultrasonic measurements (US) in the case of Ni in figure 14, much larger discrepancies are noticed in the case of Al in figure 13 with respect to the earlier shock wave results [286] at moderate compressions, where these deviations correspond to about 10%. In many cases, these deviations can be traced back to uncertainties in the estimates of Grüneisen parameters and, at the highest pressures, also to shock melting. To illustrate the effects of thermal contributions in the original shock wave data, curves with the label MS2 are calculated from the best values of K_0 and K_0' just as reference Hugoniot curves. The same values of K_0 and K_0' are then also used in the extrapolations of isotherms with different second order EOS forms. Obviously, the EOS form MU2 diverges most rapidly in these 'regular' cases, BE2 shows strong positive deviations, and MV2 shows similar deviations to the opposite side.

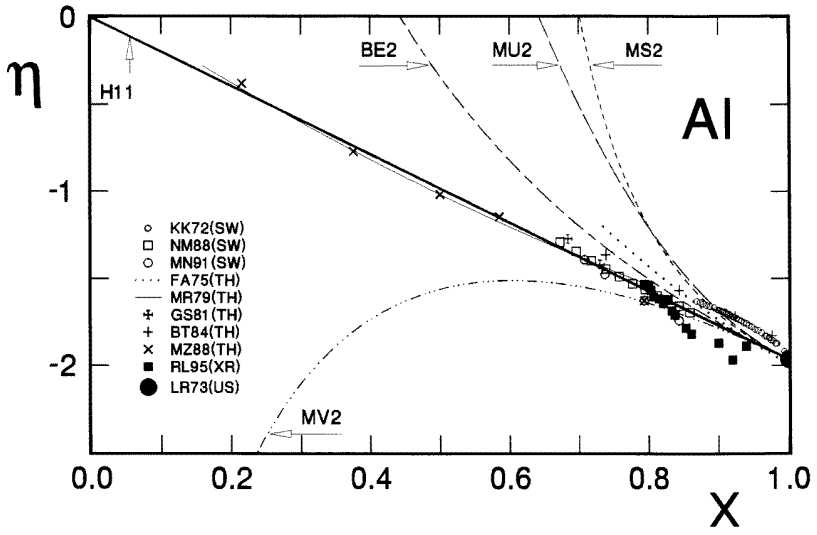

Figure 13. η-x plot for Al with different shock wave (SW) [286, 297–299], theoretical (TH) [260, 297, 300–302], x-ray (XR) [303], and ultrasonic (US) [304] data from the literature. Fixed best values for K_0 and K_0' are used for the extrapolation of different first and second order EOS forms defined in table 2. MS2 represents the Hugoniot curve to illustrate the magnitude of the thermal corrections used in the evaluation of isothermal data from shock wave results.

A slightly different behaviour is illustrated in figure 15 with the data for Pt, where the expanded view shows just a marginal superiority of the second order fits H02 and H12 at

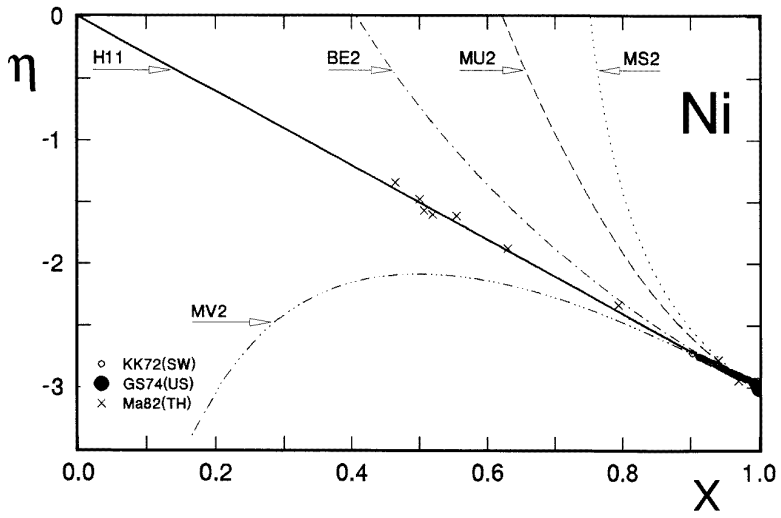

Figure 14. η-x plot for Ni with different shock wave (SW) [286], theoretical (TH) [305] and ultrasonic (US) [287] data from the literature. The same fixed values for K_0 and K_0' are used for the extrapolated isotherms H11, MV2, BE2 and MU2 as well as for the Hugoniot curve MS2.

low pressures in comparison with the one parameter interpolation H11. As illustrated by the calculated Hugoniot curve MS2 the three sets of shock wave data deviate from each other and from the linear fits probably just due to minor differences in their thermal corrections. The theoretical data show obviously very close agreement with the best fits H02 and H12 even in the TPa region. Within the experimental region, MU2 deviates already significantly, when the same values for K_0 and K_0' are used in all the second order forms, but both BE2 and MV2 diverge only at pressures much in excess of the experimental region.

While Cu, Ag and Au show the same behaviour like Pt, the result for Au deserves some special attention, since these data have been proposed especially for pressure calibrations not only at ambient temperature but also for wide temperature regions [311–313]. As illustrated in figure 16, both sets of semiempirical isotherms have been adapted to the ultrasonic values at ambient pressures, however, the H12 interpolations fit also at larger compressions with their slopes quite perfectly to the theoretical results, which deviate slightly in their initial value from the ultrasonic data, whereas the earlier isotherms show unusual curvatures due to the fact that these data had been derived from shock wave measurements in a similar way as the AIP tabulations which show similar slopes at strong compression but in addition a significant offset at ambient pressure. One may thus conclude that the original evaluation of the shock wave data introduced primarily large errors at low pressures due to the extrapolation of the shock wave data into this lower pressure region, whereas the adaptation of these data to the ultrasonic values at low pressures shifted the errors just into the high pressure region. Thus one can rationalize that the curves H12 are most compatible with all existing original data with an uncertainty of possibly 4% in pressure just in the upper experimental region of 100 GPa and 1200 K.

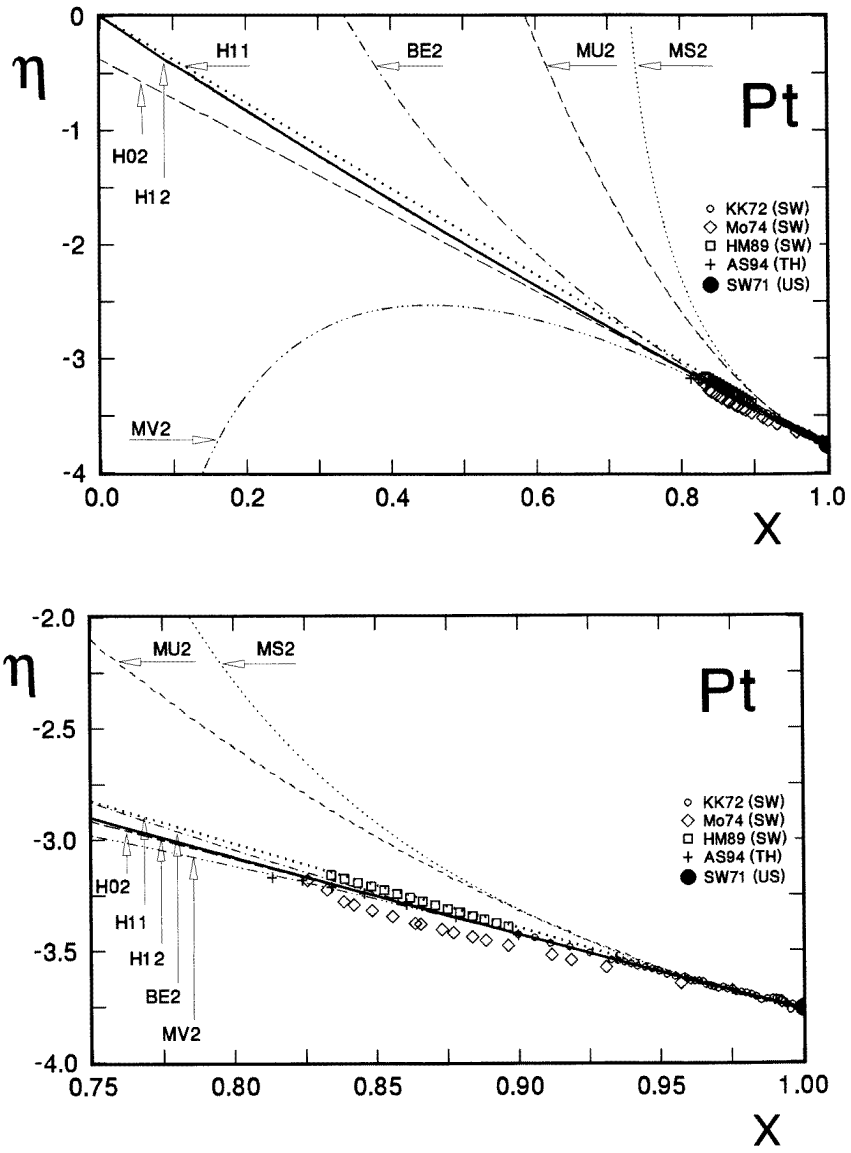

Figure 15. η-x plots for Pt with different shock wave (SW) [287, 307, 308], theoretical (TH) [309], and ultrasonic (US) [310] data from the literature. The same fixed values for K_0 and K_0' are used for the extrapolated isotherms H02, H12, BE2 and MU2 as well as for the Hugoniot curve MS2. The first order form H11 uses only K_0 and both a complete and an expanded view are presented to illustrate the differences in the forms H02, H12 and H11, respectively.

4.4. EOS data for metals with special softness

The data for Na, given in figure 17, point on the other hand to a specific anomaly of all the alkaline metals at low compression [320]. Obviously, the initial slope is rather small in comparison with the straight line interpolation H11 for the simple solids and the straight line extrapolation H02 would only fit to a Fermi-gas pressure with much lower

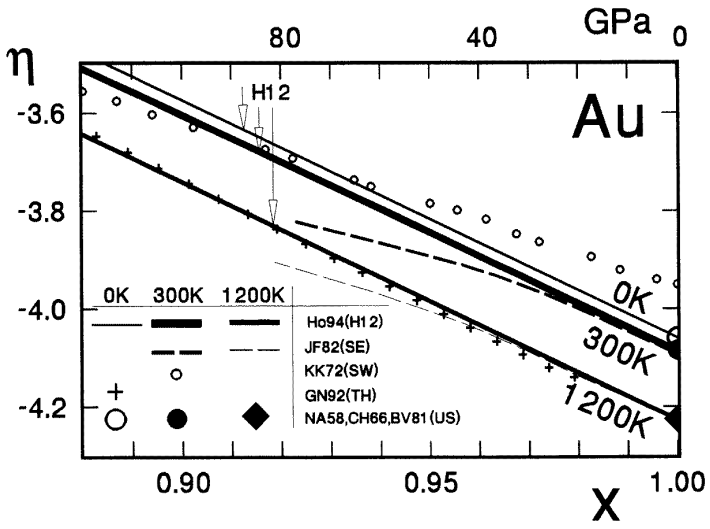

Figure 16. Expanded view of η-x plots for Au with different isotherms H12 fitted to the ultrasonic data (US) [314–316]. Previous semiempirical isotherms (SE) [311], ambient temperature data from shock wave results (SW) [287] and theoretical data for the static lattice (TH) [313] are shown for comparison.

total electron number than $Z = 11$ for Na. This observation fits to the picture that the cohesion of Na at moderate pressures is dominated just by one electron in the conduction band and core repulsion becomes dominant only under pressures much in excess of the present experimental range. The different curves for various best fitted second order EOS forms illustrate again that extrapolations using the forms MU2, BE2 or MV2 diverge quite rapidly from any reasonable behaviour while H02 deviates at the most by a factor of 5 at ultimate compression. It should be noted, however, that both the values for K_0 and K_0' were fixed in these fits to the best experimental values and different values of K_0' for the different forms give only slightly better fits within the region of experimental data.

A comparison of the EOS data for the heavier alkali metals [321] reveals in addition some special anomalies typical for s-d electron transfer as illustrated in figure 18, where the 'generalized strain coefficient' η is plotted versus the radius ratio R_{WS}/R_I using the pressure dependent Wigner–Seitz radius R_{WS} and a pressure independent individual value for the ionic radius R_I of each element. By the use of this radius ratio some correlations in the phase transitions of these elements are also revealed in figure 18, to be discussed in the section 5. At this point, attention should be paid primarily to the fact that the anomalous region seems to extend in Cs up to the phase Cs(IV) with its special tetragonal structure tI4 [324, 325]. At higher pressures, the phases Cs(V) and Cs(VI) exhibit more complicated structures, but the s-d transfer, responsible for the special softness in the intermediate region, seems to be almost completed in this range, as indicated by the more normal slopes.

Similar phenomena are well documented also for the heavier alkaline earth elements [326] as shown in figure 19. Furthermore, the 'regular' lanthanide metals [331] as well as some actinide metals [332, 333] show unusually flat initial slopes in their respective η-σ-plots, and earlier indications for an initial softness in the EOS data for the first part of the transition metals in the groups IVb to VIb had been already attributed long time ago

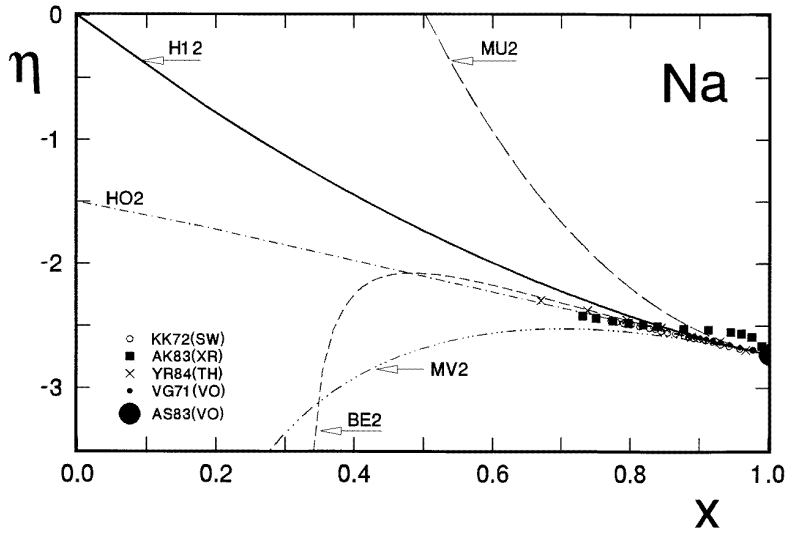

Figure 17. η-x plot for Na at ambient temperature with different shock wave (SW) [287], x-ray (XR) [317], theoretical (TH) [318], and volumetric (VO) [319, 320] results from the literature. The same fixed values for K_0 and K_0' are used for the extrapolated isotherms H02, H12, MV2, BE2 and MU2.

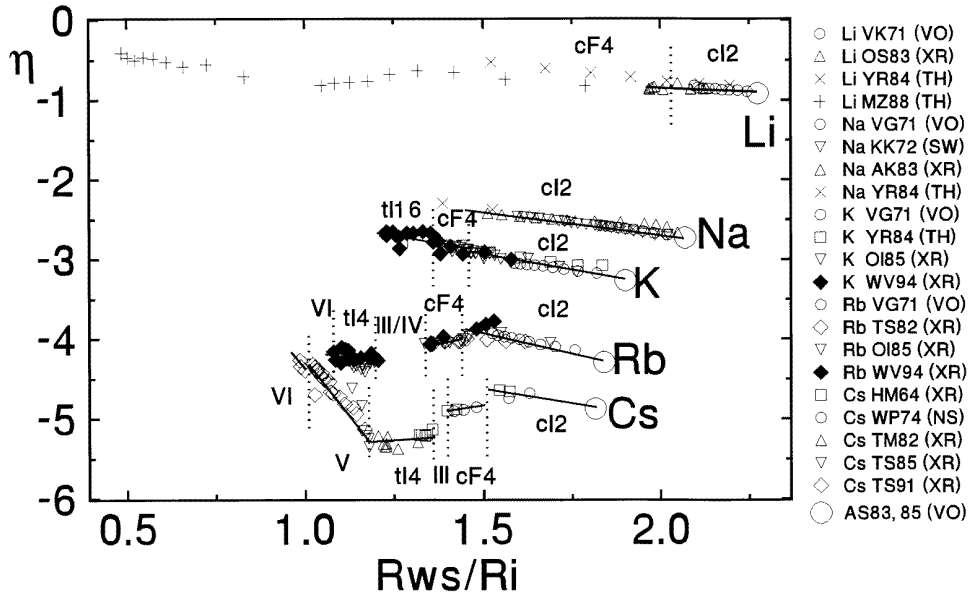

Figure 18. Variation of η versus scaled Wigner–Seitz radii R_{WS}/R_I for all the alkali metals with the use of fixed ionic radii R_I and data from various sources as given in reference 320 with additional data [302, 317, 318, 322, 323] for Li and Na.

to similar but weaker s-d-electron transfer [334]. More recently, special effects from s-d transfer were also noticed for Re and for one Mo-Re alloy under pressure.

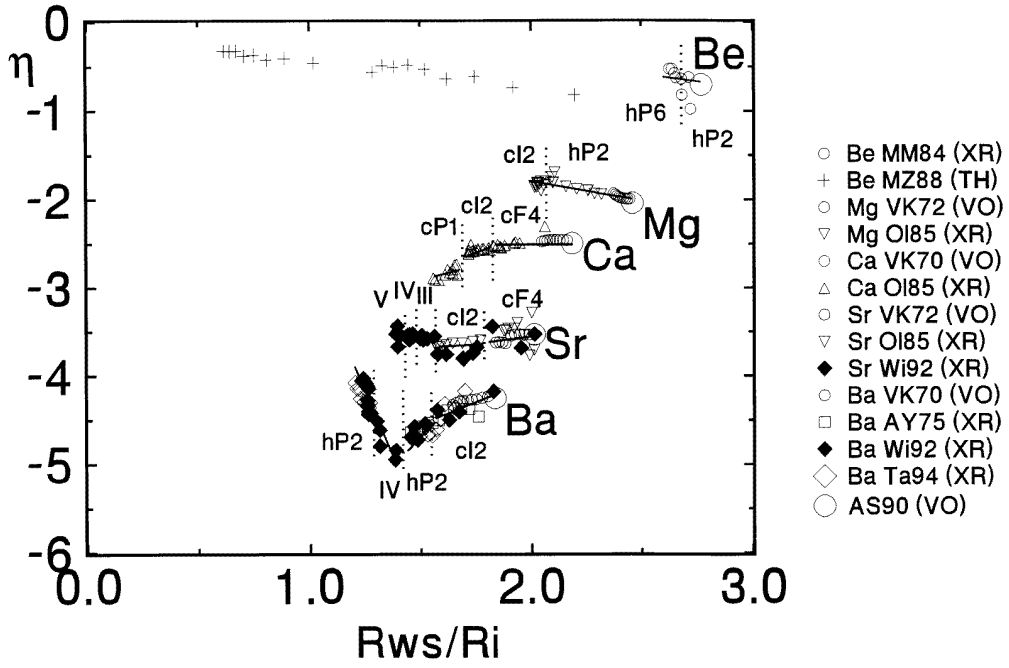

Figure 19. Variation of η versus scaled Wigner–Seitz radii R_{WS}/R_I for all the earth alkali metals with the use of fixed ionic radii R_I and data from various sources as given previously [326] with additional data [302, 327–330] for Be, Mg and Ba.

Especially for Re, a comparison of the LMTO calculations with the earlier shock wave results [335] and with recent static x-ray diffraction work [336] deserves some attention, since the shock wave results show deviations from the regular behaviour of more than 20% in pressure above 200 GPa, and therefore, these EOS data need further comparison with other calibrants before one can recommend Re itself as calibrant for other high pressure x-ray diffraction studies.

In general, first principle calculations of bulk moduli for nonmagnetic transition metals [337] show very reasonable agreement with experimental data, mostly with differences below 10% in pressure. However, the few calculations for nonmagnetic actinides exhibit still much larger differences amounting to 30% in the case of Th and 50% for Pa [338].

4.5. EOS data for carbon group elements

Experimental and theoretical studies on crystal structures, phase transitions and changes in the electronic structure for the carbon group elements under pressure revealed also some systematics in the corresponding EOS data.

Diamond itself received special attention in theoretical studies [339–342] due to its exceptional hardness and model character, and close agreement between experimental and various theoretical studies was found for the parameters $K_0 = 440(10)$ GPa and $K_0' = 3.5(3)$. With respect to the η-σ-representation of all the elements, only K_0 is unusually large, reflecting an unusual initial stiffness, which can be traced back to the special

constraints on the electronic configurations in the covalent bonds, whereas the theoretical value for K_0' fits perfectly to the simple H11 correlation presented in figure 11.

For Si, Ge and α-Sn, it may be interesting to note, that the initial extra stiffness due to the covalent bonds is lost already in the first transition to a metallic modification [343] and the 'simple' EOS form H11 describes perfectly the experimental data for all the different metallic phases, when just the (extrapolated) values for V_0 and K_0 are used as individual fit parameters for each of the phases and alloys. In fact, these extrapolated values show also quite reasonable agreement between the experimental data [344–353] and the different pseudopotential calculations [354–367] of EOS data for these high pressure phases.

In addition, β-Sn (tI4-Sn) and its first high pressure phase tI2-Sn have also been studied at elevated temperatures to derive complete EOS data with all the thermal contributions [350] with the basic result (but not explicitly started in that work) that the value of $\delta_\gamma = \mathrm{d}\ln\gamma/\mathrm{d}\ln V = 1.9 \pm 1.2$ for β-Sn falls into the range expected from general considerations.

Lead as the last member of the carbon group elements has also attracted special attention in high pressure shock wave [368] and x-ray diffraction [369–372] partly for technical reasons in the shock wave experiments but also from a more fundamental point of view in the static work. In the comparison of both types of results [372] it has been noticed that only one smooth isotherm had been derived from shock wave data whereas small, but definite breaks are noticed at the phase transitions from the low pressure cF4 phase to the hP2 phase at 13 GPa and also at the next transition at 109 GPa to the cI2 phase. However, all these isotherms are accurately described just by the simple H11 form with systematic changes in V_0, K_0 and K_0' for the different phases.

4.6. EOS data for molecular solids

Some systematics in EOS data of molecular solids were first disclosed in studies on solid halogens [373–375] where scaling of the EOS and structural data by the intramolecular bond length of Cl_2, Br_2 and I_2 revealed close structural similarities for the high pressure data as illustrated in figure 20 just for the low pressure phases of these three elements. Close similarities for the high pressure phases and phase transitions with special softness of the intermediate phases were also observed for I_2 and Br_2 and only the final close packed structure of Iodine showed 'simple' EOS behaviour.

More recently, this same idea of scaling EOS and structural data for the elemental solids of Cl_2, Br_2 and I_2 has been elaborated somewhat further [375] confirming with more data the same correlation as given in figure 20, however, without any reference to the original observation of scaling rules for molecular solids. Furthermore, these later studies [376] use the misleading terms of 'universal behaviour' and 'a universal curve' just for the observation of common scaling rules for the three heavier halogens, not taking into account that similar rules apply in different ways to other families of molecular solids.

From this point of view, it is interesting to notice, that special systematics are now emerging also for the solid chalcogens with strong homologies for Se and Te. To illustrate these systematics, new data on Se under higher pressures [377–382] are added to a previously published diagram [383] as shown in figure 21. At first, one may notice in this diagram that the initial values $\eta_0 = \ln(3K_0/p_{\mathrm{FG}_0})$ for the first phase hP3-Se show drastic differences between the ultrasonic values on the one hand and the piston cylinder data [384] on the other hand, whereby the deviation of the bulk compression data can be traced back

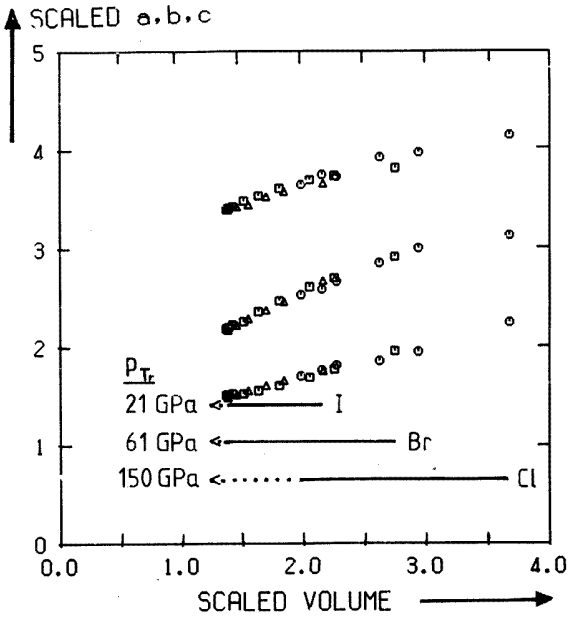

Figure 20. Homologous scaling of lattice parameters versus volume for the solid halogens Cl_2, Br_2 and I_2 under pressure. In each case, the intramolecular bond length of the free molecule is used for scaling [374].

to contributions from nonhydrostatic stresses resulting from the elastic anisotropy of the individual crystallites in the polycrystalline sample. Furthermore, one can notice a specially steep slope just for the first (molecular) phase hP3-Se, as well as a lack of accurate data for the more complex second phase mS4-Se and an apparent divergence of the experimental data at the highest pressures, where problems arise in the pressure measurements and from the influence of nonhydrostatic stresses. However, one can see that the previously adapted EOS form H10 for hR3-Se fits very well to the later theoretical data, which falls right into the middle between the two sets of the experimental data. In fact, the EOS data for all the metallic phases of Se are perfectly reproduced within the given experimental uncertainties just by the one parameter form H10 for an 'ideal' solid, where all the usual parameters, K_0, K'_0, ..., are determined by a fit of the (extrapolated) zero pressure volume V_0.

4.7. EOS data for noble gas solids

Some common features in the compressional behaviour of the noble gas solids (extrapolated to 0 K) are illustrated in figure 22, which had been presented with more details for the other nonmetallic elements previously. Evidently, Xe shows rather 'simple' behaviour in this diagram, following almost exactly the average behaviour $\bar{\eta}$ of an 'ideal' solid. As one proceeds to the lighter noble gas solids increasing deviations and nonlinearities are noticed and reasonably reproduced by the form H12.

Figure 23 represents the data for Ne in more detail. The shift of the experimental 0 K isotherm with respect to the theoretical static lattice data is well explained by the zero point

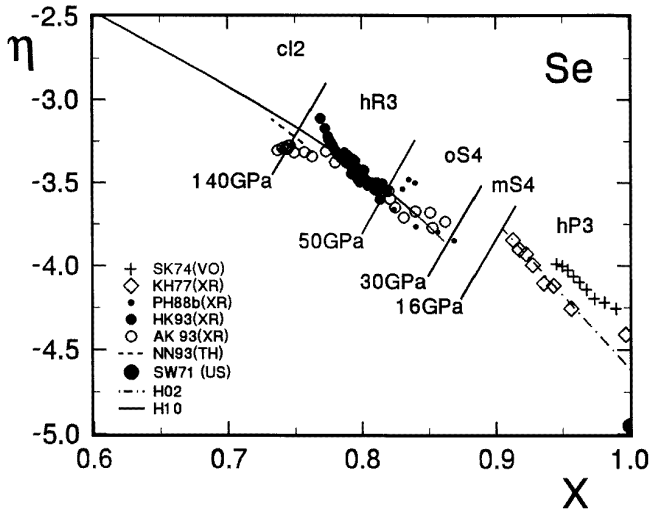

Figure 21. η-x plot for Se with linear H02-fit for the low pressure data of the hP3-Se phase and a common H10-fit for all the metallic high pressure phases. Recent experimental (XR) [377–381] and theoretical data (TH) [382] are added in the upper pressure range to the previous figure from Holzapfel *et al* [383].

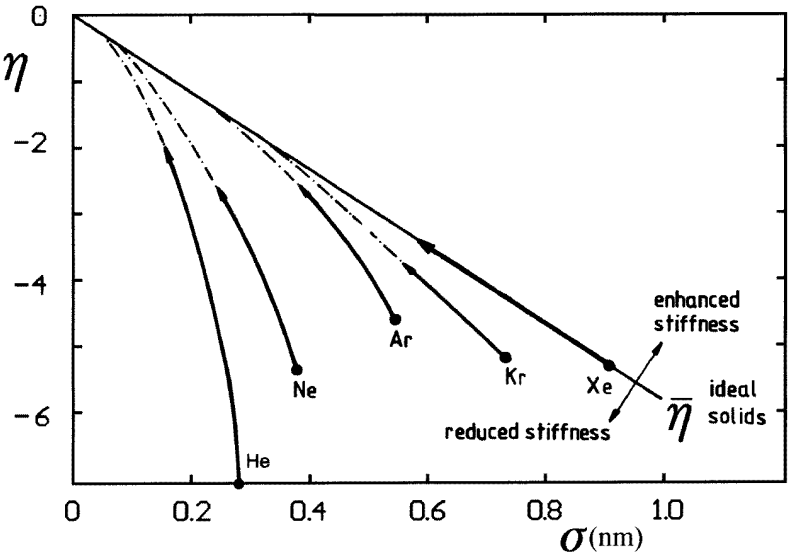

Figure 22. η-σ plot for noble gas solids with modifications from reference 227.

motion and both curves are perfectly reproduced by the form H12. Here, one can notice also that MV2 fits reasonably the experimental data, but diverges in the upper region of the theoretical data, and BE2 diverges rather rapidly even with its different value of K_0'.

Figure 24 shows a similar representation of theoretical and experimental data for He, whereby the experimental data are all reduced to 0 K and the theoretical data represent

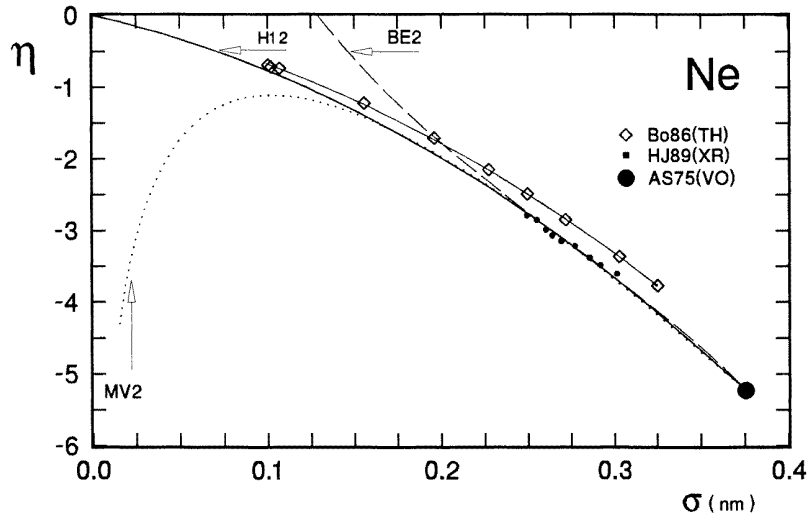

Figure 23. η-σ plot for solid Ne with experimental volumetric (VO) [288] and x-ray (XR) [385] data for 0 K and theoretical data (TH) for the static lattice [595]. The extrapolated second order forms represent best fits to the experimental data with the same value for K_0 but individual values for K_0'.

again only the static lattice part. In the fitting of the different second order EOS forms all the forms were forced to start at the well determined low pressure value of K_0, and K_0' was adapted individually to reproduce also the x-ray data. With this procedure, BE2 shows large deviations at intermediate pressures with respect to the optical data and diverges at very strong compression in its usual way, MV2 appears to fit best and the small deviations of H12 from the data at intermediate pressures do not really justify the use of a third order form H13. In any case, detailed considerations of the zero point motion together with further experimental and theoretical studies may deserve still more attention in the future to clarify the remaining uncertainties for this most basic model system.

4.8. EOS data for hydrogen

The EOS of hydrogen has been the subject of many experimental [390–400] and theoretical [401–403] studies, not only for its application in modelling the interior of the giant planets [405, 406] but primarily with respect to a better understanding of this most 'simplest' solid, which shows indeed so many unexpected properties challenging both experimentalists and theorists.

Nevertheless, if one looks just at all the data for the 0 K isotherm of H_2 presented as η-σ plot in figure 25, one finds still a surprisingly simple behaviour for this wide range of compression. Thereby, the difference between the starting points in the 0 K isotherms for H_2 and D_2 illustrates directly effects from zero point motion in figure 25, and the theoretical results for the static lattice case show rather large divergencies especially at lower pressures due to the fact that they are more appropriate for the predicted high pressure metallic phases and less accurate at moderate compression, where these calculations seem to overestimate

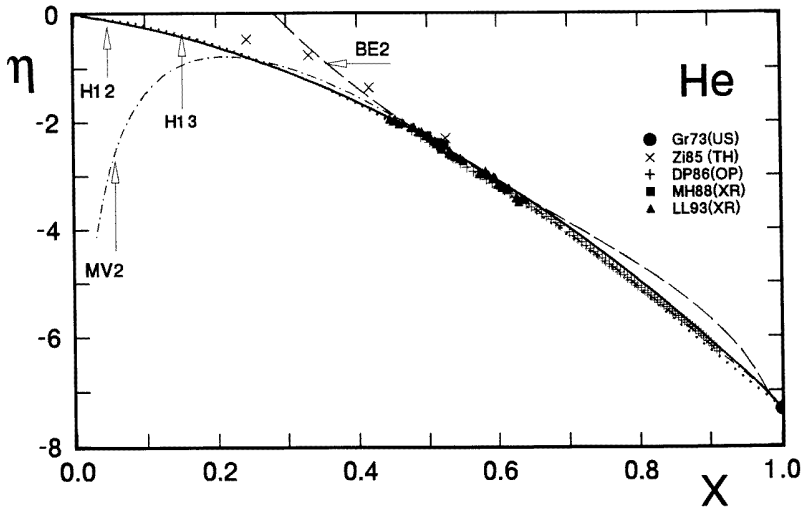

Figure 24. η-x plot for He with experimental data for 0 K from ultrasonic (US) [386], optical (OP) [290] and x-ray (XR) [387, 388] measurements. The theoretical data (TH) [389] do not include zeropoint motion. The fixed best value for K_0 was used with individual values for K_0' in the fits of the different second order forms. The marginal change in the fit with the third order form H13 is also illustrated.

the bonding forces. In contrast to He, the larger cohesion leads already at ambient pressure to much smaller deviations from regular behaviour, however, the very steep slope in this η-σ representation reflects quite clearly some unusual stiffening at lower pressures. Finally, the approach towards the straight line for 'ideal' solids seems to herald also the approach towards the insulator-metal transition, which should then be accompanied by the usual softening discussed before with respect to electronic transitions in the heavier pretransition metals.

4.9. EOS forms for compounds

Although EOS data for a large number of compounds and alloys have been collected over wide ranges in pressure, only a few rules have been derived so far and also tests of different forms have not been performed in greater extension, mostly due to the fact that the stability regions of the low pressure phases are usually very limited in pressure and compression, partly due to the differences in the individual ionic or atomic compressibilities.

Therefore, it becomes also difficult to determine curvatures of EOS data in η-x plots with any reasonable accuracy. In alkali halides, which are isoelectronic to the neighbouring noble gas elements, similar repulsive potentials and the same asymptotic behaviour in their EOS forms under strong compression can be observed. To reveal further systematics in the EOS data of compounds very detailed analysis of the available data is needed. With the use of semiempirical 'soft ion' potentials [409] some systematics seem to emerge for the alkali halides in both the NaCl-type (cF8) and also the CsCl-type (cP2) structures, when the same ionic repulsive parameters are used for each ionic species throughout the whole series.

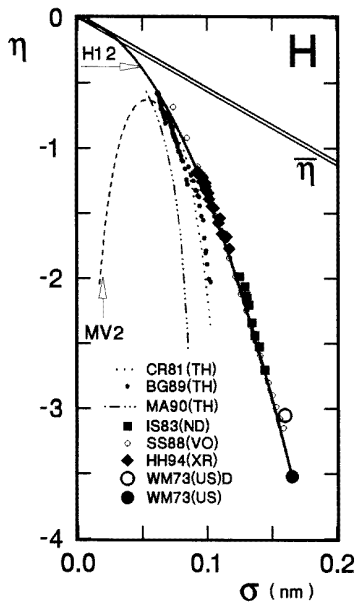

Figure 25. η-σ plot for EOS data of hydrogen at 0 K. The starting points from ultra sonic measurements (US) [407] for hydrogen and for deuterium are shown by a large closed and open circle respectively to illustrate the effects of zero-point motion. Experimental data from neutron diffraction (ND) [408], from volumetric measurements (VO) together with their semiempirical extrapolation [397], and x-ray diffraction data (XR) [398–400] are compared with theoretical predictions (TH) [401–404] and with both the H12 and MV2 extrapolations of the low pressure data. The behaviour of 'ideal' metallic solids is represented by the straight line labelled $\bar{\eta}$. References are given in the text.

If one uses the 'best' data for V_0, K_0 and K_0' for all the alkali halides and plots K_0' versus the parameter $c_0 = -\ln(3K_0/p_{\mathrm{FG}_0})$, where $p_{\mathrm{FG}_0} = a_{\mathrm{FG}} \cdot (Z_{\mathrm{eff}}/v_{\mathrm{eff}})^{5/3}$ is just determined by the total average electron density $Z_{\mathrm{eff}}/v_{\mathrm{eff}} = (Z_+ + Z_-)/(v_+ + v_-)$, one finds that the data for the fluorides follow very closely the correlation implied by the first order EOS form H11 but the heavier halogenides seem to show weakly reduced stiffening ($c_2 < 0$), which would correspond to slightly concave H12 forms in η-x plots.

More systematic rules may be derived also for other compounds by the use of η-σ representations with effective values for Z and v, where the comparison with Thomas–Fermi scaling [410] requires that

$$Z = (\Sigma n_i Z_i^{5/3}/\Sigma n_i Z_i)^{3/2} \qquad \text{and} \qquad v = Z \cdot (\Sigma n_i v_i/\Sigma n_i Z_i) \tag{14}$$

when $\Sigma n_i v_i$ represents thereby the unit cell volume of a compound consisting of n_i atoms of type i with the atomic numbers Z_i.

5. Phase transitions and structural systematics

One of the major goals of high pressure physics concerns structural stabilities of solids and their relations to changes in electronic structures, whereby a strong mutual stimulation between experimental studies and theoretical modelling can be noticed. An excellent monograph [12] on ' Phase Diagrams of the Elements' reviewed all the experimental facts and especially also all the relations between experiments and theory in this wide field with all its richness in rules and exceptions. A topical review [411] on 'High Pressure Phase Transformations' described more recent experimental observations on Ti, Zr, Hf as well as some systematics in III-V, II-VI and I-VII compounds which were evolving at that time, and short notes on the molecular solids I_2, O_2, N_2 and H_2 were included also in this work. Furthermore, progress in theoretical modelling was also surveyed in two more recent studies [412]. In comparison with these extended reviews, the present short contribution can only point out some predominant rules with a few remarks on recent results.

Before entering into a detailed discussion of structural systematics under pressure, the situation at ambient conditions must be recalled. As illustrated for the elements in figure 26, the metallic elements exhibit clear systematics within their groups and also as one proceeds from left to right. For the nonmagnetic transition metals, these trends are well described with different approaches just by the filling of the d-bands [416], and the irregularities of Mn and Fe are traced back to magnetic interactions. For the sp-bonded metals, effective pair potentials with strong Friedel-type oscillations from the 'free electron' contributions allowed to derive some 'structure maps' [417] which describe the trends at ambient conditions as well as changes under pressure.

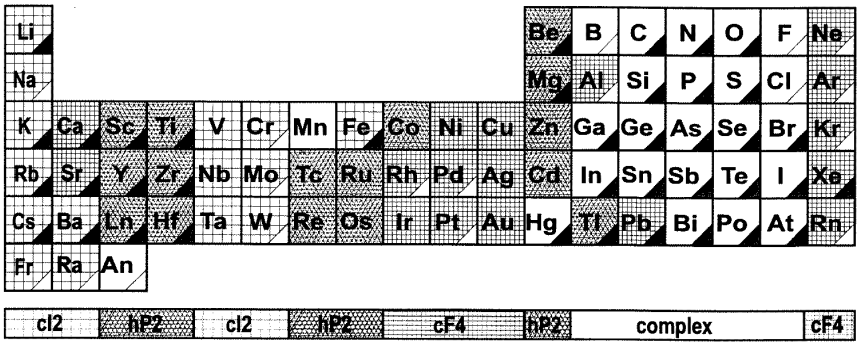

Figure 26. Structural systematics of the solid elements at ambient condition with data for the solidified gases and liquids at 0 K. Elements with one or more high pressure phases are labelled by a triangle in the lower right hand corner. Dark and white corners mark experimental observations and theoretical predictions, respectively. Recent theoretical [239, 309, 413, 414] and experimental [415] results are added to the earlier compilation [12] of structural data.

When one looks, however, at the upper right hand corner of the periodic table, where one finds the semimetals, semiconductors and molecular solids or molecular gases, the systematics are not very evident at ambient conditions, and all these elements exhibit a very rich variety of structural phase transitions under pressure, as pointed out in figure 26 just by the black triangles in the lower right hand corner for each of these elements. In the few cases, where only theoretical considerations predict high pressure phase transitions (mostly much above the range of present structural studies) open triangles mark these elements, and

from these studies one can notice that the structural stability for the central portion of the nonmagnetic transition metals even breaks down at very strong compression not only at the border between the cI2 and the hP2 type metals with corresponding transitions for Cr at 700 GPa, for Mo at 420 GPa and for W at 1.25 TPa but apparently also for the most central elements, where transformations to the cI2 structure are predicted for Rh, Pd and Pt at compressions of $V/V_0 = 0.29$, 0.39 and 0.40, respectively [418] corresponding to pressures of 4.7 TPa, 2.0 TPa and 2.6 TPa.

In contrast to this high stability of the central transition metals, a very rich variety of phase transitions is typical for the 'pretransition metals' with their incipient d-band occupation.

5.1. Alkali and alkaline-earth metals

As pointed out already in section 4.2 with figure 18, the EOS data for the heavier alkali metals, K, Rb and Cs, exhibit a special softness due to s-d electron transfer, and characteristic sequences of phase transitions are noticed in these materials under strong compression. At first, there is only the tendency to closer packing from cI2 to cF4, however, all the following phases have lower symmetry [419–423] and some systematics and similarities can be noticed for the individual phase transitions, when not the transition pressures but rather some critical radius ratios are compared as illustrated in figure 18, where the pressure dependent Wigner–Seitz radius R_{WS} is scaled for each of the elements by its ionic radius at ambient condition R_I. The selection of a pseudopotential core radius for R_I may result in similar systematics of critical radius ratios for these phase transitions, since it is primarily this radius ratio, which determines the band structure and corresponding phase transitions. It should be noted, however, that the lighter alkali metals, Na and Li, follow their own sequences as illustrated also in figure 18, where one should take into account that both Na and Li seem to transform from their cI2 structure at low temperatures to an hR9 or oS4 (α-U) type structure [424]. At ambient temperature Li transforms to cF4 at 6.9 GPa as discussed before and GPT calculations for Na [425] predict a phase transition at 100 GPa to the hP2 structure, but none of these transitions fit from structure type or radius ratio to the sequence of the heavier alkali metals.

Very similar structural behaviour is observed also for the alkaline-earth metals as illustrated in section 4.2 by figure 19 with respect to the s-d-electron transfer noticed in the EOS curves. Again, simple systematics are lost in the region of the s-d-transfer and Mg as well as Be show their separate behaviour.

5.2. Rare earth and actinide metals

The rare earth metals Sc, Y and Ln, with Ln representing the lanthanide metals from La to Lu, are dominated in their structural behaviour by three effects. First of all, theoretical studies [426, 427] pointed out, that s-d-electron transfer dominates the structural sequence from hP2 $\rightarrow$ hR9 $\rightarrow$ hP4 $\rightarrow$ cF4 in regular trivalent Ln metals under pressure or with decreasing atomic number. Critical radius ratios were revealed [428, 429] to explain both these trends and x-ray studies on Y under pressure are considered as experimental proof, for minor contributions of f-electrons to this structural sequence which is illustrated in figure

27 in the form of a generalized alloy phase diagram [431]. It should be noted that Sc, the 'divalent' Ln metals Eu and Yb, as well as the irregular f-band metal Ce show different structural behaviour. Much theoretical [432] and experimental [433–434] attention has been devoted to the transition of Eu and Yb from 'divalent' to 'trivalent' behaviour, however, regular trivalent behaviour is not observed for these two elements under pressure within the present experimental region. The third anomaly concerns the f-electron delocalization observed at first by a volume collapse between the isostructural cF4 phases γ and α of Ce on cooling at ambient pressure. An intermediate β phase, with hP4 structure, fits thereby still to the regular sequence with localized f-electrons, and further details of the unusual phase diagram for Ce under pressure are discussed at various places in the literature. At this point, it may be sufficient to notice that Ce is just the first of the Ln metals with effects from f-electron delocalization, but similar anomalies have been observed also for Pr, Nd and Sm [436] as illustrated in figure 27 by the heavily drawn columns with the special shading for unusual structures, and it appears, that Eu and Yb as well as the other Ln metals at much higher pressures are finally affected by similar phenomena.

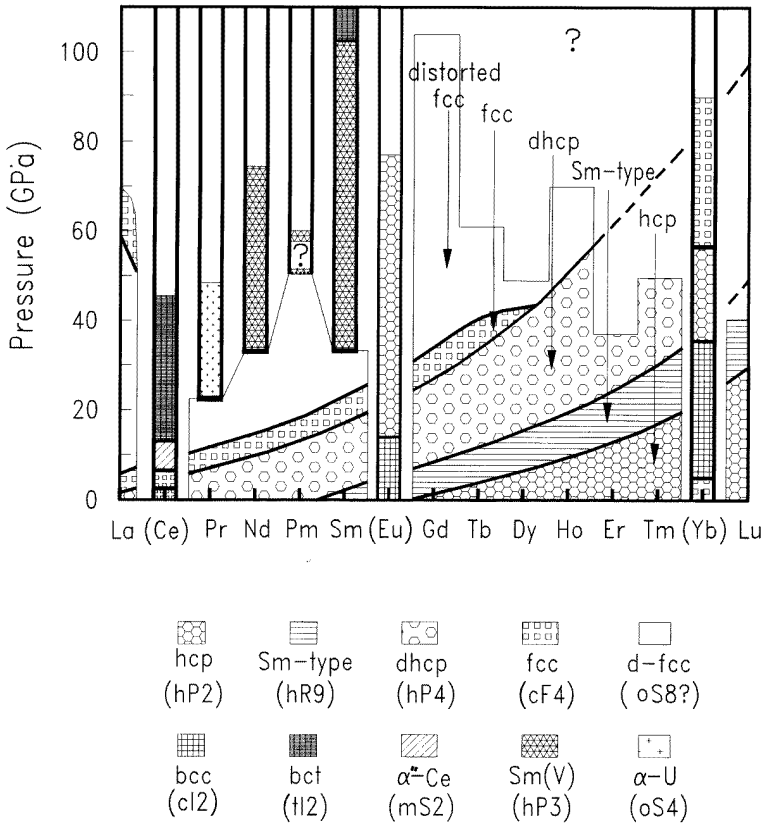

Figure 27. Generalized phase diagram for lanthanide metals and interlanthanide alloys under pressure at ambient temperature [430].

These conclusions are also supported by comparisons between lanthanide and actinide metals under pressure [437], where the lighter actinides show f-delocalization or f-bonding already at ambient pressure and the heavier actinides change over from regular Ln-

type behaviour with localized f-electrons to Ce-type with delocalized f-electrons already under moderate pressures. In addition, new theoretical results [438–445] elucidate the contributions of delocalized f-electrons on various structural properties concerning Ce, Sm, Th, and heavier actinide metals under pressure, for instance, with the prediction of *back transitions* from the tI2 to the cF4 structure in Ce at about 3TPa and in Th at 1.6 TPa.

5.3. Ti, Zr and Hf

Already at moderate pressures these elements change into the special ω-phase, which could be denoted as hP1+2 due to the special hexagonal arrangement with two inequivalent sites, 1a and 2d in the space group P6/mmm. Theoretical calculations [446–448] as well as experimental studies [450, 451] have clearly shown, that this special structure is stable only over a limited range in pressures with subsequent transformations to cI2 in Zr at 35(3) GPa and in Hf at 71(11) GPa at ambient temperature and with a negative slope in the transition pressure versus temperature, indicating that hP1+2 is stable only at low temperatures. Therefore, the low pressure, high temperature cI2 phase is just the same phase as high pressure cI2.

5.4. sp-bonded metals

sp-bonded metals had been of special interest for theorists due to their simple electronic structures with early predictions about structural systematics, a later prediction of a cF4 $\rightarrow$ cI2 transition at 330 GPa for Al, and detailed considerations on the phase diagram of Mg with respect to its hP2 $\rightarrow$ cI2 transition under pressure [452]. Recent experimental studies elucidated the phase diagram of Hg up to 67 GPa and 500 K [453], and revealed an intermediate oS4 structure from about 12 to 40 GPa at moderate temperatures before the expected hP2 structure is stabilized. In addition, a direct transition from α-Hg (hR3) to the hP2 phase has been predicted for temperatures above 600 K and pressures around 29 GPa.

Furthermore, a new transition from tI2 to oF4 was also disclosed for In around 45 GPa [454].

5.5. Carbon group elements

The structural systematics for the group IV elements are summarized in figure 28, which includes in addition to the results of the latest review new theoretical data for carbon, concerning a predicted cI8 structure [345] and further cI16 and hP1 structures at even higher pressures [455] new experimental data for Si, concerning an intermediate phase between the tI4 and hP1 phases in the range from 13 to 15 GPa with oI4 structure [456], the assignment of an oP4 structure to the phases Si(VI) (at 39 GPa) and Ge(IV) (at 113 GPa), and new theoretical results on the stability of cI2-Sn up to 200 GPa. While earlier calculations had indicated a marginal stability of the hP2 structure at pressures above 61 GPa for 0 K, where no experimental studies were available, the stability of the cI2 structure was attributed to entropy terms in the later study.

C	hP4	$\xrightarrow{0}$	cF8	$\xrightarrow{(1100)}$	(cI16)		$\xrightarrow{(1700)}$	(hP1)							
Si			cF8	$\xrightarrow{10}$	tI4	$\xrightarrow{13}$	oI4	$\xrightarrow{15}$	hP1	$\xrightarrow{36}$	oP4	$\xrightarrow{42}$	hP2	$\xrightarrow{79}$	cF4 $\rightarrow$ 248 GPa $<$?
Ge			cF8	$\xrightarrow{11}$	tI4		$\xrightarrow{75}$		hP1	$\xrightarrow{102}$	oP4 $\rightarrow$ 130 GPa $<$?				
Sn			[cF8]	$\xrightarrow{0}$	tI4		$\xrightarrow{8}$		tI2		$\xrightarrow{44}$				cI2 $\rightarrow$ 120 GPa $<$?
Pb									cF4	$\xrightarrow{13}$	hP2	$\xrightarrow{109}$			cI2 $\rightarrow$ 272 GPa $<$?
rules	$s^2p^2 \longrightarrow$		sp^3	$\longrightarrow$	spd		s $\rightarrow$ d transfer								

Figure 28. Structural systematics for the carbon group elements at ambient temperature with forward transition pressures in GPa. Theoretical results are presented in rounded brackets and the low temperature phase α-Sn is included as [cF8]. References are given in the text.

With these new data figure 28 shows then clearly, that the structural homologies in the carbon group are very limited. The diamond structure, cF8, occurs in C, Si, Ge and Sn (at low temperatures) and the β-Sn structure, tI4, is also a common high pressure phase for Ge and Si. The intermediate hP1 and oP4 phases occur as common structures for the elements Si and Ge, but the predicted cI8 structure of C has been observed only as metastable structure for Si. Beyond these similarities, the behaviour at higher pressure seems not to show more systematics. Therefore, one may conclude, that the difference of C with respect to Si and Ge can be explained by increasing d-electron admixture in the heavier elements under pressure, and the distinctly different behaviour of Pb has to be attributed to relativistic effects.

5.6. Nitrogen group elements

With respect to the previous discussion of structural systematics for the nitrogen group elements, some progress has been made in recent years as illustrated in figure 29. X-ray diffraction measurements at ambient temperature to 44 GPa [457, 458] supported the assignment of the same space group $R\bar{3}c$ with the short notation hR48 to the new phase after the phase transition at 16.3 GPa which had been assigned before to the low temperature ϵ-phase. However, no drastic changes are seen in the x-ray pattern at the transition to the η-phase at 20 GPa. Since definite gradual changes in the Raman spectra for both external and internal modes are noticed, it was concluded, that minor changes in the molecular positions or orientations must be involved in this transition [459]. Raman studies at temperatures between 100 and 350 K in the stability range of the δ-phase (cP16) revealed a new second order phase transition roughly 50 K above the ϵ-δ transition corresponding to a transition pressure of 10.5 GPa at ambient temperature [460]. Since the δ-phase (cP16) is characterized by orientational disorder of the molecules, some orientational localization is attributed to this phase transition, and later Monte Carlo simulations [461] suggested, that quadrupole–quadrupole interactions have to be taken into account in addition to the non-sphericity of the molecules in structural calculations for these phases.

Furthermore, new theoretical studies came to the conclusion [462], that polymeric nitrogen should be the stable form at pressures in excess of 50(15) GPa. The previous observation in Raman studies to 130 and 180 GPa, respectively [463, 464], were thereby considered to indicate only, that there is a large barrier for the formation of a polymeric

N	fluid	$\xrightarrow{2.3}$ hP4	$\xrightarrow{4.7}$ cP16	$\xrightarrow{16.3}$ hR48	$\rightarrow$ 180 GPa $<$?	
P	oS8	$\xrightarrow{3}$ hR6	$\xrightarrow{10}$ cP1	$\rightarrow$ 58 GPa $<$?		
As		hR6	$\xrightarrow{24}$ cP1	$\xrightarrow{48}$ oP8 ?	$\xrightarrow{97}$ cI2 $\rightarrow$ 122 GPa $<$?	
Sb		hR6	$\xrightarrow{8.6}$ [cP1]	$\xrightarrow{8.6}$ tP10	$\xrightarrow{28}$ cI2 $\rightarrow$ 43 GPa $<$?	
Bi		hR6	$\xrightarrow{2.5}$ mS4	$\xrightarrow{2.8}$ tP10	$\xrightarrow{7.7}$ cI2 $\rightarrow$ 40 GPa $<$?	
rules		hR6	$\longrightarrow$ complex	$\longrightarrow$ tP10	$\longrightarrow$ cI2	

Figure 29. Structural systematics for the nitrogen group elements at ambient temperature with forward transition pressures in GPa. References are given in the text.

form. In contrast to the previously proposed hR6 structure for polymeric nitrogen [461] a 'cubic gauche' (cg) structure was found to be more stable. In a note added in proof, possible large 'LSD-errors' were taken into consideration, which could possibly shift the pressure for polymerization to significantly larger values. Simulations on the behaviour of shock compressed liquid nitrogen support also the view [466], that extremely high temperatures might be needed to induce the transition to the polymeric state at pressures below 100 GPa. Thus, it might be interesting to see, whether photochemical reactions under strong compression might possibly induce this polymerization at lower pressures and moderate temperatures.

Structural stability calculations for hypothetical semimetallic phases of solid nitrogen indicated again that the hR6 structure, typical for the other nitrogen group elements, should be the stable phase with respect to cP1 or tP1 structures, at least up to 1 TPa, where all these three structures merge to a common behaviour of their total energy [467].

Finally, also the structure of Sb(II) and Bi(III), stable at ambient temperature in the pressure range from 8.6 to 28 GPa, and 2.8 to 7.7 GPa, respectively, were solved by powder x-ray diffraction [468–471], and Rietveld refinements resulted in a tP10 structure. A recent x-ray diffraction study on As to 122 GPa reported the first observation of a cI2 phase above 97 GPa now also for As however, the diffraction pattern for the intermediate phase As(III) was tentatively assigned to an oP8 structure, in contrast to the common tP10 structure for Sb(II) and Bi(III), but better spectra are required to support these first conclusions on the structure of As(III).

Inspection of figure 29 shows now a somewhat stronger structural homology for the nitrogen group than for the carbon group. Nitrogen as the lightest element starts out again with special structures, however, the recent calculations give some evidence for a structural sequence from hR6 to cP1 when N has entered into a metallic state, and this same sequence is noticed just for the next two heavier elements P and As, whereas the cP1 structure may exist for Sb only under uniaxial stress as a metastable configuration, and both the tP10 and cI2 structures are found as common structures at present for both Sb and Bi. But here again, Bi, at intermediate temperatures, shows its own rich sequence of unusual structures, which may be caused by strong relativistic effects offering still interesting challenges for further theoretical modelling.

5.7. Chalcogens

Progress on structural systematics for the chalcogens is illustrated in figure 30, which includes in addition to the previously discussed data many new results on S [472–478], on Se [479–482], and on Te [483, 484]. While the model calculations show some ambiguity with respect to the question whether generalized gradient corrections do indeed improve the agreement between experiment and theory for the structural properties of the semiconducting low pressure phases of Se and Te, the agreement between theory and experiment seems to improve as one approaches the simpler metallic high pressure phases for Te as well as for Se as illustrated already in figure 21 with the comparison of experimental and theoretical EOS data for Se under strong compression.

On the other hand, high temperature studies on melting and phase transitions in Te under pressures up to 11 GPa have now located the triple point between the phases III-IV and the melt at 820 K and 8.0 GPa which had been estimated about 3 GPa higher from measurements at lower temperatures. With all the data shown in figure 30, one finds a limited homology in the structural behaviour of the chalcogens, again with special structures for the lighter elements, some close homology for Se and Te, but so far with only one common phase with Po. Some common d-band contributions for S, Se and Te under pressure and relativistic effects for Po may then account for these similarities and differences.

O	fluid $\xrightarrow{5.4}$ hR6 $\xrightarrow{9.3}$ oF8 $\xrightarrow{9.8}$ mS4 $\rightarrow$ 62 GPa $<$?
S	oF128 $\xrightarrow{5}$ mP128 ? $\xrightarrow{\sim 20}$ amorph. $\xrightarrow{37}$? $\xrightarrow{83}$ oS4 $\xrightarrow{162}$ hR3 $\rightarrow$ 212 GPa $<$?
Se	hP3 $\xrightarrow{14}$ mS4 $\xrightarrow{35}$ oS4 $\xrightarrow{60}$ hR3 $\xrightarrow{140}$ cI2 $\rightarrow$ 150 GPa $<$?
Te	hP3 $\xrightarrow{4.5}$ mS4 $\xrightarrow{6.6}$ oS4 $\xrightarrow{11}$ hR3 $\xrightarrow{27}$ cI2 $\rightarrow$ 75 GPa $<$?
Po	cP1 $\longrightarrow$ hR3 $\rightarrow$?
rules	rings $\longrightarrow$ amorph. $\longrightarrow$ hP3 chains $\longrightarrow$ layers $\longrightarrow$ hR3 $\longrightarrow$ cI2 $\rightarrow$?

Figure 30. Structural systematics of the chalcogens at ambient temperature with forward transition pressures in GPa. References are given in the text.

5.8. Halogens

Structural studies on halogens under pressure revealed already many years ago some structural homologies, which could be well described by scaling all the structural parameters with respect to the intramolecular bond length [485, 486]. With respect to the observation of phase transitions under pressure, the results are, however, still rather limited as illustrated in figure 31, which is based on the data of previous reviews and few additional results. Since these molecular solids were also considered as model substances for the approach of solid H_2 into a metallic state, studies on I_2 indicated at least, that this process might go in steps, first from a molecular semiconductor to a diatomic semimetal with oI2 structure, and through the intermediate structure, tI2, finally into a close packed structure, cF4, with superconductivity at low temperatures [483].

F	fluid $\xrightarrow{2.4}$ mS8 $\rightarrow$ 5 GPa $<$?
Cl	fluid $\xrightarrow{1.0}$ oS8 $\rightarrow$ 45 GPa $<$?
Br	fluid $\xrightarrow{0.2}$ oS8 $\xrightarrow{82}$ oI2 $\rightarrow$ 88 GPa $<$?
I	oS8 $\xrightarrow{21}$ oI2 $\xrightarrow{43}$ tI2 $\xrightarrow{55}$ cF4 $\rightarrow$ 278 GPa $<$?
rules	fluid $\longrightarrow$ oS8 $\longrightarrow$ oI2 $\longrightarrow$ tI2 $\longrightarrow$ cF4
	mol. semicond. $\longrightarrow$ layered metal $\longrightarrow$ simple metal

Figure 31. Structural systematics of the halogens at ambient temperature with forward transition pressures in GPa. References are given in the text.

However, the actual studies on hydrogen showed that the halogens have their own systematics which can be attributed to a large extent also to s-d electron transfer under strong compression in the elements Cl, Br and I, and, therefore, distinctly different behaviour should also be expected for F under strong compression.

5.9. Compounds

Structural studies on compounds under pressure cover another wide field of experimental activities [488–491], where many exceptions to simple rules are noticed in recent years [492–512] which call then also for theoretical interpretations.

If one considers just the simple rule that (negative) anions are usually more compressible than (positive) cations, one can use packing arguments to rationalized a tendency for I-VII and II-VI compounds to transform under pressure from the 6-fold coordinated cF8 (NaCl-type) structure to the 8-fold coordinated cP2 (CsCl-type) structure. However, when one looks at the actual data for the cF8 $\rightarrow$ cP2 transitions pressures of I-VII and II-VI compounds one finds that smaller radius ratios lead to higher transition pressures only within the MX series with fixed anion X, whereas the series with fixed cation would contradict this simple rule. Thus one can see [513] that the interplay between covalency (or electronic band gaps) and ionicity leads to more detailed balances, which seem to effort still individual band structure and structural stability calculations for each case [514–521]. Further complications can arise even in the simple MX compounds, when changes in magnetic moments or f-electron delocalizations are encountered, and similar features related to formations of new electronic ground states have attracted strong attention in various fields of high pressure studies.

6. Semiconductor-metal transitions

The almost classical semiconductor-metal transitions of the elements, Si (12 GPa), Ge (11 GPa), Se (20 GPa), Te (4 GPa), Br (100 GPa), I (17 GPa) and Xe ($\sim$ 160 GPa), which

were discussed in detail in a recent review by [13], pose naturally the question, whether all the other elements from the upper right hand corner of the periodic table, figure 26, can be transformed into a metallic state within the presently accessible range of pressures. Theoretical estimates for semiconductor-metal transition pressures give values of 210 GPa for boron [522], 1.1 TPa for carbon, about 100 GPa for nitrogen [523], 33 GPa for Br and 67 GPa for Cl, respectively [524], and from a comparison with the experimental information, one can see, that diamond should be strong enough to reach some more of these transitions. The fact that experimental studies on N_2 to 180 GPa show no transition to a metallic phase has led to the conclusion, that large ranges of metastability may be encountered, especially in cases with very strong intramolecular bonding, and this situation may be encountered also with boron.

Reflectivity measurements on Br under pressures up to 170 GPa [525] give evidence for metallic behaviour only above 100 GPa where Br is already in the oI2 phase, and by the scaling rules for halogens the metallization for Cl should then occur only much above 150 GPa in contrast to the theoretical predictions [526].

It should be noticed also, that most of the semiconductor-metal transitions, as for instance in Si, Ge, Se and Te, as well as for the III-V compounds, are linked to strongly first order structural changes. Detailed studies on black phosphorus under pressure indicate, however, that in this case the band gap closure occurs continuously at 1.7 GPa [527] without a structural transition [528]. Marginal discontinuities in the pressure dependence of the structural parameters at the band gap closure appear to be compatible with a truly second order phase transition, however, an ultimate proof of perfect continuity imposes serious experimental problems. Similarly the band gap closures in Br at 100 GPa, in I at 17 GPa as well as in Xe around 160 GPa with in its hP2 structure [529, 530] are presently still considered as good candidates for second order phase transitions, at least at ambient temperature, where most of the experiments were performed. This observation leads also to the intriguing question, whether a continuous band gap closure in the solid state would be compatible with the prediction of a first order insulator-metal transition in the fluid state, ending in a second critical point, predicted for Xe to occur around 5000 K and 50 GPa [531, 532]. However, various recent studies cast also some doubt on the second order character of the semiconductor-metal transition in I around 17.5 GPa [215, 533–535].

With all this information in mind, metallization of hydrogen poses a special challenge to both experimentalists and theorists.

7. Hydrogen

With the increasing number of studies on hydrogen under pressure in recent years as pointed out for instance in three recent reviews [536, 537] with about 300, 43 and 103 references each, it becomes clear that hydrogen under pressure is one of the most intriguing solids not only for experimentalists but also for theorists.

If one takes into account, that the intramolecular H-H-distance, $d_0 = 74.1$ pm, is very small compared with $d_{\min} \approx 340$ pm, the position of the minimum for the effective isotropic molecular pair potential, it becomes obvious that hydrogen at low pressures can be treated in a good first order approximation as a molecular solid with freely rotating H_2 modules with only small perturbations on the intramolecular properties [538].

The distinction between para- and ortho-H_2 and, correspondingly, ortho- and para-D_2 with even total nuclear spin I_{mol} for the molecules and even rotational quantum number J in the first cases and odd values for the second cases, leads to a series of special phenomena, which are most pronounced at low pressures and low temperatures. Since the energy difference between the even and odd configurations corresponds to only 170.5 K, and the conversion rate from the odd to the even state is only of the order of 2% per hour at normal density and only 2.5 times more rapid at 1.7 times higher density, many studies have been performed on pure o- or p-H_2 and D_2, respectively, in addition to studies on both H_2 and D_2 in their temperature dependent equilibrium composition designated as n-H_2 and n-D_2. However, at low temperature and strong compression, J is no longer a good quantum number and an orientally ordered phase can be expected in each case. However, the transition pressures (and temperatures) for the formation of this ordered phase depend thereby on the specially prepared ortho-para ratio, if one does not wait for the formation of the equilibrium concentration. As illustrated in figure 32 just for the case of H_2, one find for any of the hydrogen molecules with pure or mixed species containing the different isotopes H, D and T at first the phase I at least at high temperature, with hexagonal close packing of 'spherical' molecules. In short this structure is designed hP2$\times$2 due to the occupation of each site with two equivalent atoms, since the molecules are treated as 'spherical' either due to the spherical symmetry of the $J = 0$ wave function for p-H_2, o-D_4 and p-T_2 or due to the thermal disorder in the other cases. For the non-spherical species, an ordered phase II occurs at low temperatures with Pa3 space group and cP8 structure, where the molecular centres rest on a cubic close packed lattice and the quadrupole interaction leads to a lowering of the symmetry due to the ordering of the molecular axis. At low pressures, this structural transition between the phase I and II occurs at about 2.8 K in pure o-H_2 and at about 3.8 K in pure p-D_2 with significant hysteresis in both cases, and in both cases the transition temperature increases strongly with pressure as indicated by the shaded area in figure 32, where one must keep in mind that these 'phase boundaries' correspond to transitions between two metastable phases and the precise phase lines for the thermodynamic equilibrium mixtures, n-H_2 and n-D_2, have not yet been studied in detail. For pure o-D_2, the corresponding 'broken symmetry phase', BSP or phase II, is found at pressures above 2.2 GPa (at 4 K) [539] with steep increase in the transition temperature with pressure up to 150 GPa, where a triple point is observed with respect to the next high pressure phase III at about 130 K in the case of pure o-D_2. Similar behaviour of pure p-H_2 with a transition to a BSP-phase II at about 120 GPa has also been noticed at low temperatures [540, 544] and from corresponding studies on 1:1 o:p-H_2 mixtures, one can estimate the location of the 'equilibrium' triple point for n-H_2 near 50(20) K and 150 GPa. For n-D_2 the I-II-III-triple point has been located at 167(8) GPa and 129(3) K and similar values were found also for o-D_2. In any case, it should be noted that the structure for phase II is only known for the low pressure (metastable) species o-H_2 and p-D_2, but it is very likely, that the same ordering occurs also for the other species and for the equilibrium mixture at high pressures.

Most interestingly, the first order transition between phase I and III ends in a critical point located near 170 GPa and 150 K for hydrogen [545, 546] and at much higher values (above 190 GPa and 270 K) also for n-D_2 [547]. Thus, the structure of phase III is obviously closely related to the hP2$\times$2 structure of phase I, however, with a lowering of the symmetry due to at least some partial ordering of the molecular species [548, 549].

Optical studies give evidence for a weak (indirect) band overlap in phase III at low temperatures [550–554], and a strong increase in the IR-vibron absorption with further increase in pressure indicates that the mixing of odd and even rotational wave functions for the molecules may be responsible for a strong increase in electronic charge transfer

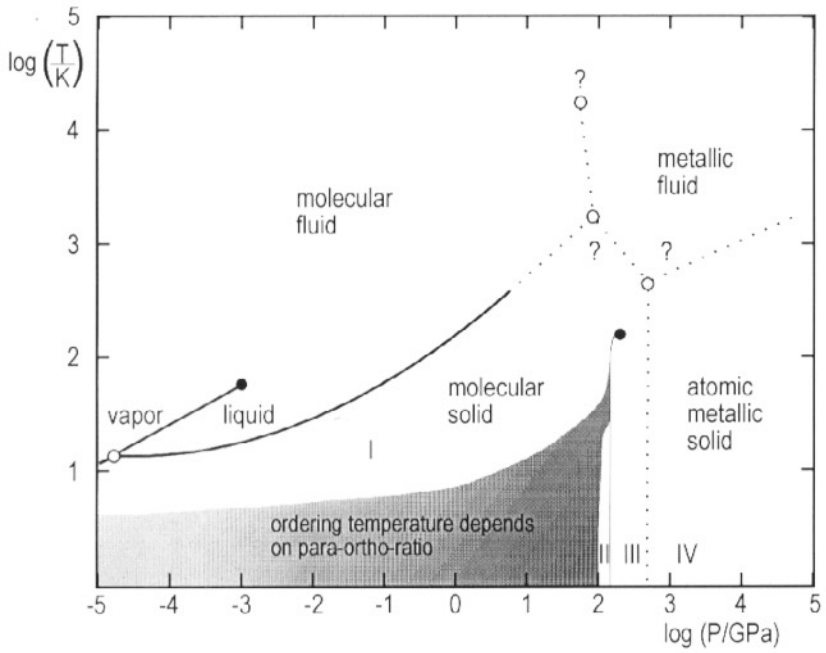

Figure 32. p-T-phase diagram of hydrogen. References are given in the text.

transitions between the molecules, especially, when the molecules turn toward head-on orientations.

Above 250 GPa a new phase IV seems to occur as evidenced by a strong increase in visible absorption and by the disappearance of the molecular Raman vibron bands. Both observations are considered as first indications that the long expected monoatomic metallic phase has been found, but more experimental evidences are required for a definite proof.

While the first theoretical prediction of a metallic high pressure phase for hydrogen [555] proposed a transition pressure of only 25 GPa, more recent estimates for the metallization within the molecular phase cluster around 200(50) GPa [556–561] and for the transition to the monoatomic metallic phase around 300 GPa. Most recent quantum Monte Carlo calculations predict for metallic atomic hydrogen a sequence of structural transitions from cF8 (diamond) $\rightarrow$ tI4 (β-Sn) $\rightarrow$ cP1 $\rightarrow$ cI2 in the range from 200–900 GPa [562] and for the molecular phases below $\sim$ 200 GPa a hcp lattice with tilted molecules seems to be favoured [563]. With respect to earlier predictions about a metallic quantum liquid phase for monatomic hydrogen [564], recent calculations indicate, that such a phase should be observed at 0 K only at much higher compressing $P \geqslant 5$ TPa [565]. It may be interesting to note also, that a superconducting state has been predicted for the monatomic structures [566] with recent estimates for the transition temperatures ranging between 145 and 300 K [567, 568].

In addition to the known melting data for H_2 [568], figure 32 includes also some speculations about the possible extension of the melting curve to higher pressures. While early studies [569] proposed regular melting with positive $\mathrm{d}T_m/\mathrm{d}p$ for all the solid phases, a section with negative slopes and rather low melting temperatures for the metallic solid together with the possibility of a (second) critical point as end point for a first order insulator-

metal transition in the fluid phase have later been proposed [570, 571]. However, these stimulating predictions have not yet been confirmed by any experimental studies due to the rather difficult experimental conditions of combined high pressure and high temperature together with the possibility of very high chemical reactivity of hydrogen under these extreme conditions.

Finally, the EOS data for hydrogen at 0 K given already in figure 25 illustrate that only minor volume discontinuities may occur at the phase transitions between the phases I, II, III and IV at low temperatures. Zero point motion effects the EOS curve at low pressures by extra curvature and an extension of this curve to larger values of σ_0 with smaller values of the starting point η_0 in comparison with the hypothetical static lattice cases as indicated by the different starting point for deuterium with its much weaker contributions from zero point motion. Corrections for elevated temperatures would also introduce a significant lowering with respect to the 0 K curve in figure 25 but only at its lower end without much change of the asymptotic variation at strong compression. In fact, at the transition to the monatomic metallic phase, hydrogen has entered into a region where the EOS data come close to the Thomas–Fermi limit and to the regular behaviour of simple metallic solids illustrated for comparison in figure 25 by the linear double line.

8. Melting

Melting of 'simple' solids under pressure may be considered as a phase transition, which follows simple scaling rules. The most successful scaling rule for melting is obviously Lindemann's (1910) melting law which relates in modern terms the melting temperature $T_m = c_L \cdot \Theta_D^2 \cdot v^{2/3} \cdot M$ for monatomic solids with atomic mass number M and atomic volume v to the Debye Temperature Θ_D by the use of an almost constant Lindemann parameter $c_L \approx 2.7 \cdot 10^{-3}$ K^{-1} nm^{-2}. If one assumes that the pressure dependence of c_L can be neglected, and that the Debye–Grüneisen parameter $\gamma_D = -\ln\Theta_D/\mathrm{d}\ln v$ is reasonably represented by $\gamma_D \approx K'/2 - 1/3$, one obtains $\gamma_m = -\mathrm{d}\ln T_m/\mathrm{d}\ln v \approx K' - 4/3$, which indicates that small values of K' and correspondingly small slopes in η-σ plots should usually be related to small slopes in the respective melting curves. Deviations from this simple rule are certainly expected for solids with shear mode softening and also in the neighbourhood of liquid-solid triple points, where extra contributions from the entropy of mixing lead to additional depressions. However, with these reservations in mind, this rough correlation between γ_m and K' appears to be the only rule for melting under strong compressions, and comparisons of the well known melting minima for Cs, Ba and Ce with the corresponding η-σ plots given for Cs and Ba in figures 18 and 19 and for Ce in previous reviews can substantiate this rule. More recently [572] melting anomalies were documented also for Pr under pressure, where 4f-electron delocalization plays a similar role as in the case for Ce, lending additional support to this specific melting rule.

From the point of view of direct applications, one may note, that many experimental studies with laser heated DACs were recently devoted just to the melting of iron and some Fe-O-S alloys under pressures comparable to the Earth's core-mantle boundary for modelling the temperature profile of the Earth with many controversial and unexpected results [573, 574].

9. Transitions to new ground states

Structural transitions of metals as well as insulator-metal transitions under pressure provide an excellent testing ground also for theoretical models on superconductivity. While the simple BCS formula for the superconducting transition temperature $T_c \sim \theta_D \exp(-1/(V_{ep} \cdot D(E_F)))$ predicts as a rule a decrease of T_c under pressure due to the dominant decrease in the electronic density of states $D(E_F)$ at the Fermi energy E_F as the bands are broadening with minor contributions from changes in the Debye temperature θ_D and in the electron–phonon coupling parameter V_{ep}. However, a complete appearance or disappearance of superconductivity under pressure needs for its understanding an additional competing term from Coulomb repulsion, which is in fact incorporated in McMillan's relation [575]. Thus, one can rationalize, that usually $\mathrm{d}\,T_c/\mathrm{d}\,p$ is negative for the metallic elements, however, positive slopes can be observed just for the first metallic phase after an insulator metal transition under pressure as evidenced by the recent tabulation of the experimental data for the elements. From the low mass of hydrogen and an expected strong electron–phonon coupling together with a high density of states at the Fermi surface for the narrow bands of an incipient semimetal, one can then understand that detailed calculations for metallic hydrogen predict extremely high values of $T_c \sim 230$ K, offering a strong challenge to experimentalist to verify this value.

For high T_c superconductors, on the other hand, a tuning of T_c with pressure, typically passing over a maximum in T_c if the initial slope is not already negative, provides some further insight into the nature of the relevant interactions [43, 576, 577].

Similarity, high pressure is expected to destroy magnetic ground states, when bands are broadening and localized electronic moments get quenched by stronger hybridization of the 'atomic' wave functions under pressure, as evidenced also by many recent high pressure studies on magnetic ordering and moment instabilities [578–586]. In fact, local high-spin to low-spin transitions, spin fluctuations and electron delocalization can be considered as common high pressure phenomena not only for Ln and Ac elements and compounds, but also for transition metals, their invar alloys and many of their compounds with unusual valencies which offer still a wide field of open questions for the future.

10. Conclusions

With the developments of the diamond anvil technique and the extension of the range for optical and x-ray measurements under static pressures to 400 GPa and above, a new domain has been opened for solid state physics and crystallography, a domain, which was previously only accessible in part to shock-wave studies with all their problems with heating and residual stresses. Present comparisons of ultrasonic low pressure measurements with static, dynamic and theoretical results on EOS data for solids under strong compression start to establish an absolute pressure scale with an accuracy of a few percent in pressure even for the range above 100 GPa. Rules on 'regular' behaviour of 'simple' solids are emerging together with the possibility to trace back some anomalies in EOS behaviour to special changes in the electronic structure, whereby s-d-transfer in pretransition and early transition metals show their fingerprints and effects from f-electron delocalization are clearly noticed in Ln and An elements and compounds together with some corresponding changes in the crystal structure.

The partial systematics in the structural sequences for the elements under pressure provide an excellent test ground for theoretical total energy and structural stability calculations and a 'hierarchy of symmetries' seems to provide a new approach for the unification of structural phase transitions [587–594] whereby Landau-theory is applied not only to continuous (second order) phase transitions but also to discontinuous cases together with an analysis of the respective unit cell distortions in terms of Γ point phonons (Bain mechanisms) or with respect to layer displacements corresponding to zone boundary or other high-symmetry phonons (Burgers mechanisms).

Wide ranges in compression seem to provide in this case an even wider variety of phase transitions than all the earlier studies at ambient pressure and variable temperature. With all the structural studies just on the seemingly simple MX compounds, another new dimension is added to this field.

In addition, questions concerning insulator-metal transitions, electron delocalization, quenching of magnetic moments, rise and fall of superconducting transition temperatures, all offer opportunities to gain a deeper understanding of the relevant physical parameters by studies on solids under strong compression.

Thus, one can envisage that further developments of the various high pressure techniques involving also new analytical tools will affect many fields of solid state physics and, with their results, also the modelling in geo- and planetary sciences.

References

[1] Mao H K and Hemley R J 1994 *Rev. Mod. Phys.* **66** 671–92
[2] Bridgman P W 1931 *The Physics of High Pressure* (London: Bell) reprinted 1970 (New York: Dover)
[3] Bridgman P W 1964 *Collected Experimental Papers* (Cambridge, MA: Harvard University Press)
[4] Spain I L and Paauwe J (eds) 1977 *High Pressure Technology* (New York: Dekker) vol I+II
[5] Peggs G N 1983 *High Pressure Measurement Techniques* (London: Applied Science)
[6] Ulmer G C and Barnes H L (eds) 1987 *Hydrothermal Experimental Techniques* (New York: Wiley)
[7] Sherman W F and Stadtmuller A A 1987 *Experimental Techniques in High Pressure Research* (New York: Wiley)
[8] Isaacs N S and Holzapfel W B (eds) 1995 *High Pressure Techniques in Chemistry and Physics: A Practical Approach* (Oxford: Oxford University Press)
[9] Zharkov V N and Kalinin V A 1971 *Equations of State for Solids at High Pressure and Temperatures* (New York: Consultants Bureau)
[10] Eliezer S, Ghatak A, Hora H and Teller E 1986 *An Introduction to Equations of State: Theory and Applications* (Cambridge: Cambridge University Press)
[11] Eliezer S and Ricci R A (eds) 1991 *High-Pressure Equations of State: Theory and Applications* (New York: North-Holland)
[12] Young D A 1991 *Phase Diagrams of the Elements* (Berkeley, CA: University of California Press)
[13] Timmerhaus K D and Barber M S (eds) 1979 *High-Pressure Science and Technology* (New York: Plenum)
[14] Vodar B and Marteau Ph (eds) 1980 *High Pressure Science and Technology* (Oxford: Pergamon) vol I, II
[15] Backman C M, Johanison T and Tegner L (eds) 1982 *High Pressure in Research and Industry* (Uppsala: Arkitkopia)
[16] Homan C, McCrone R K and Whalley E (eds) 1984 *High Pressure in Science and Technology* (Amsterdam: North-Holland)
[17] Trappeniers N J, Biswas S N, van den Berg H R, Prins C, Prins K O and Schouten J A (eds) 1986 *Proceedings of the Xth AIRAPT International High Pressure Conference* (Amsterdam: North-Holland) special volume of Physica **139/140B**
[18] Novikov N V (ed) 1989 *High Pressure Science and Technology* (Kiev: Naukova Dumka)
[19] Holzapfel W B and Johannsen P G (eds) 1990 *High Pressure Science Technology* (New York: Gordon and Breach)

[20] Singh A K (ed) 1992 *Recent Trends in High Pressure Research* (New Delhi: Oxford)
[21] Schmidt S C, Shaner J W, Samara G A and Ross M (eds) 1994 *High-Pressure Science and Technology* (New York: American Institute of Physics)
[22] Manghnani M H and Akimoto S (eds) 1977 *High-Pressure Research Application in Geophysics* (New York: Academic)
[23] Chu C W and Woollam J A (eds) 1978 *High Pressure and Low Temperature Physics* (New York: Plenum)
[24] Kelm H (ed) 1978 *High Pressure Chemistry* (Holland: Reidel)
[25] Schilling J S and Shelton R M (eds) 1981 *Physics of Solids under High Pressure* (Amsterdam: North-Holland)
[26] Akimoto S and Manghnani M H (eds) 1982 *High Pressure Research in Geophysics* (Tokyo: Center for Acad. Public.)
[27] Minomura S (ed) 1985 *Solid State Physics under Pressure* (Tokyo: KTK)
[28] Gupta Y M (ed) 1986 *Proc. 4th Amer. Phys. Soc. (APS) Topical Conf. on Shock Waves in Condensed Matter* (New York: Plenum)
[29] Manghnani M H and Syono Y (eds) 1987 *High-Pressure Research in Mineral Physics* (Washington, DC: American Geophysical Union)
[30] Vollstädt H (ed) 1988 *High Pressure Geosciences and Material Synthesis* (Berlin: Academie)
[31] Polian A, Loubeyre P and Boccara N (eds) 1989 *Simple Molecular Systems at Very High Density, NATO ASI Series, Series B: Physics vol 186* (New York: Plenum)
[32] Schmidt S C, Jonson J N and Davidson L W (eds) 1990 *Shock Compression of Condensed Matter—;1989* (Amsterdam: North-Holland)
[33] Pucci R, Piccitto T G (eds) 1991 *Molecular Solids under Pressure* (Amsterdam: North-Holland)
[34] Syono Y and Manghnani M H (eds) 1992 *High Pressure Research: Application to Earth and Planetary Sciences* (Tokyo: Terra)
[35] Ross M 1985 *Rep. Prog. Phys.* **48** 1–52
[36] Liu Lin-Gun and Bassett W A 1986 *Elements, Oxides, and Silicates High-Pressure Phases with Implications for the Earth's Interior* (New York: Oxford University Press)
[37] Williams Q and Jeanloz R 1991 *Molten Salt Techniques* ed R J Gale and D G Lovering (New York: Plenum) vol 4, pp 193–227
[38] Sikka S K 1992 *Bulletin of Materials Science* **15** 35–46
[39] Schilling J S and Klotz S 1992 *Physical Properties of High Temperature Superconductors* ed D M Ginsberg (Singapore: World Scientific) vol III, p 59
[40] Wijngaarden R J and Griessen R 1992 *Concise Encyclopedia of Magnetic and Superconducting Materials* ed J E Evetts (Oxford: Pergamon) p 583
[41] Wijngaarden R J and Griessen R 1989 *Studies of High Temperature Superconductors* ed A V Narlikar (New York: Nova) pp 1–51
[42] Ross M and Young D A 1993 *Annu. Rev. Phys. Chem.* **44** 61–87
[43] Gathers G R 1994 *Selected Topics in Shock Wave Physics and Equation of State Modeling* (Singapore: World Scientific)
[44] Hall H T 1962 *Rev. Sci. Instrum.* **33** 1278
[45] Bundy F P 1963 *J. Chem. Phys.* **38** 631
[46] Holzapfel W B and Franck E U 1966 *Ber. d. Bunsenges. f. phys. Chem.* **70** 1105–12
[47] Holzapfel W B 1973 *Umschau* **73** 517–21
[48] Drickamer H G, Clendenon R L, Lynch R W and Perez-Albuerne E A 1966 *Solid State Physics* ed F Seitz and D Turnbull (New York: Academic) vol 19
[49] Drickamer H G and Frank C W (eds) 1973 *Electronic Tranisitions and the High Pressure Chemistry and Physics of Solids* (London: Chapman and Hall)
[50] Khvostantsev L G 1984 *High Temp.-High Press.* **16** 165
[51] Ramaseshan S, Parthasarathy G and Gopal E S R 1987 *Pramana—J. Phys.* **28** 435–69
[52] Ruoff A L pp 13–33 in [22]
[53] Zerr A and Boehler R 1993 *Science* **262** 553–5
[54] Boehler R 1993 *Nature* **363** 534–6
[55] Jeanloz R 1989 *Annu. Rev. Phys. Chem.* **40** 237–59
[56] Jeanloz R 1990 *Annu. Rev. Earth Planet. Sci.* **18** 357–86
[57] Hawke R S, Duerre D E, Huebel J G, Keeler R N and Klapper H 1972 *J. Appl. Phys.* **43** 2734
[58] Besson J M, Nelmes R J, Loveday J S, Hamel G, Pruzan Ph and Hull S 1992 *High Pressure Res.* **9** 179–93
[59] Goncharenko I N, Glazkov V P, Irodova A V, Lavrova O A and Somenkov V A 1992 *J. Alloys Compounds* **179** 253–7

[60] Holzapfel W B 1970 *High Temp.-High Press.* **2** 241–58
[61] Bartunik H D, Holzapfel W B and Mössbauer R L 1970 *Phys. Lett.* **33A** 469–70
[62] Holzapfel W B 1975 *Crit. Rev. Solid State Sci.* **5** 89–123
[63] Holzapfel W B pp 159–75 in [25]
[64] Moser J, Wortmann G, Bykovetz N and Kalvius G M 1979 *J. Magn. Magn. Mater.* **12** 77–82
[65] Potzel W, Moser J, Potzel U, Gleiáner A, Litterst F J, Kalvius G M, Gal J, Boge M, Chappert J and Spirlet J 1987 *Hyperfine Interact.* **34** 391
[66] Adlassnig W, Potzel W, Schiessl J W, Schäfer C and Kalvius G M 1988 *Hyperfine Interact.* **41** 531–4
[67] Adlassnig W, Potzel W, Moser J, Schäfer C, Steiner M and Kalvius G M 1989 *Nucl. Instrum. Methods* A **277** 485–90
[68] Potzel W, Adlassnig W, Moser J, Schäfer C, Steiner M and Kalvius G M 1989 *Phys. Rev.* B **12** 8236–41
[69] Potzel W 1992 *Hyperfine Interact.* **71** 1515–22
[70] Abd-Elmeguid M M, Pattyn H and Bukshpan S 1994 *Phys. Rev. Lett.* **72** 502–5
[71] Hafner S S, Kojima N, Stanek J and Zhang L 1994 *Phys. Lett.* **192A** 385–8
[72] Raghavan P, Raghavan R S and Holzapfel W B 1972 *Phys. Rev. Lett.* **28** 903–6
[73] Butz T, Wortmann G, Kalvius G M and Holzapfel W B 1974 *Phys. Lett.* **50A** 127–8
[74] Butz T, Kalvius G M, Göbel H and Holzapfel W B 1975 *Hyperfine Interact.* **1** 1–14
[75] Oomi G and Itho F 1993 *Jpn. J. Appl. Phys.* **32** Suppl. 1, 352–4
[76] Onodera A 1987 *High Temp.-High Press.* **19** 579–609
[77] Onodera A, Sumiya H, Higashi K, Takahashi N, Oshima R, Saka H, Nobugai K and Kanamaru F 1992 *High Temp.-High Press.* **24** 45–54
[78] Yagi T pp 1621–4 in [22]
[79] Wortmann G 1989 *Hyperfine Interact.* **47** 179–202
[80] Weir S 1959 *J. Res. Nat. Bur. Stand.* A**63** 55–62
[81] Jayaraman A 1983 *Rev. Mod. Phys.* **55** 65–108
[82] Jayaraman A 1986 *Rev. Sci. Instrum.* **57** 1013
[83] Taylor R D and Pasternak M P 1990 *Hyperfine Interact.* **53** 159–74
[84] Besson J M and Pinceaux J P 1979 *Science* **206** 1073–4
[85] Mills R L, Liebenberg D H, Bronson J C and Schmidt L C 1980 *Rev. Sci. Instrum.* **51** 891–5
[86] Jephcoat A P and Bell P M p 38 in [6]
[87] Hazen R M and Finger L W 1982 *Comparative Crystal Chemistry* (New York: Wiley)
[88] Nicol M F, Hirsch K R and Holzapfel W B 1979 *Chem. Phys. Lett.* **68** 49–52
[89] Syassen K and Sonnenschein R 1982 *Rev. Sci. Instrum.* **53** 644–50
[90] Hanfland M, Hemley R J and Mao H K 1991 *Phys. Rev.* B **43** 8767–70
[91] Hanfland M, Hemley R J, Mao H K and Williams G P 1992 *Phys. Rev. Lett.* **69** 1129–32
[92] Reichlin R, McMahon A K, Ross M, Martin S, Hemley R J, Mao H K and Hu J 1994 *Phys. Rev.* B **49** 3725
[93] Reichlin R, Ross M, Martin S M and Goettel K A 1986 *Phys. Rev. Lett.* **56** 2858–60
[94] Holzapfel W B, Seiler B and Nicol M F 1984 *J. Geophys. Res.* B **89** 707–10
[95] Johannsen P G, Wefringhaus C and Holzapfel W B 1987 *J. Phys. C: Solid State Phys.* **20** 151–3
[96] Johannsen P G, Krobok M P and Holzapfel W B 1988 *Brucker Report* **1** 39–43
[97] Hanfland M, Hemley R J and Mao H K 1993 *Phys. Rev. Lett.* **70** 3760–3
[98] Barnett J D, Block S and Piermarini G J 1973 *Rev. Sci. Instrum.* **44** 1
[99] Bettini M and Holzapfel W B 1975 *Solid State Commun.* **16** 27–30
[100] Bäuerle D, Holzapfel W B, Pinczuk A and Yacoby Y 1977 *Phys. Status. Solidi* b **83** 99–107
[101] Heyns A M, Hirsch K R and Holzapfel W B 1979 *Solid State Commun.* **29** 351–3
[102] Sharma S K, Mao H K and Bell P M 1980 *Phys. Rev. Lett.* **44** 886
[103] Hirsch K R and Holzapfel W B 1981 *Rev. Sci. Instrum.* **52** 52–5
[104] Dil J G and Brody E M 1976 *Phys. Rev.* B **14** 5218
[105] Whitfield C H, Brody E M and Bassett W A 1976 *Rev. Sci. Instrum.* **47** 942
[106] Shimizu H, Mao H K, Bassett W A, Bell P M and Brody E M 1981 *J. Appl. Phys.* **52** 3583
[107] Brody E M, Shimizu H and Bell P M 1981 *Phys. Rev. Lett.* **47** 128
[108] Shimizu H, Kumazawa M, Mao H K, Bell P M and Brody E M, 1983 *Jpn. J. Appl. Phys.* **22** 52
[109] Polian A and Grimsditch M 1984 *Phys. Rev. Lett.* **52** 1312
[110] Hemley R J and Bell P M 1987 *Science* **237** 605–12
[111] Shimizu H and Sasaki S 1992 *Science* **257** 514–16
[112] Shimizu H and Sasaki S 1993 *Jpn. J. Appl. Phys.* **32** Suppl. 2, 355–7
[113] Shimizu H and Sasaki S pp 89–92 in [22]

[114] Zha Ch, Duffy T S, Mao H K and Hemley R J pp 873–6 in [22]
[115] Ingalls R, Garcia G A and Stern E A 1978 *Phys. Rev. Lett.* **40** 334
[116] Syassen K, Wortmann G, Feldhaus J, Frank K H and Kaindl G 1982 *Phys. Rev.* B **26** 4745–8
[117] Itié J P 1991 *High Pressure Res.* **7** 354–7
[118] Itié J P 1992 *Phase Transition* **39** 81
[119] Herber R and Spijkerman J 1965 *J. Chem. Phys.* **42** 4312
[120] Huggins F E and Virgo D 1975 *Carnegie Institute of Washington Year Book 74* (Washington) p 405
[121] Cort G, Taylor R D and Willis J O 1982 *J. Appl. Phys.* **53** 2064
[122] Taylor R D, Cort G and Willis J O 1982 *J. Appl. Phys.* **53** 8199
[123] Syono Y, Ito A, Moromoto S, Suzuki T, Yagi T and Akimoto S 1984 *Solid State Commun.* **50** 97
[124] Nasu S, Kurimoto K, Nagatomo S, Endo S and Fujita F E 1983 *Hyperfine Interact.* **29** 1583
[125] Nasu S, Kurimoto K, Nagatomo S, Endo S and Fujita F E 1986 *Hyperfine Interact.* **29** 1583–6
[126] Kurimoto K, Nasu S, Nagatomo S, Endo S and Fujita F E 1986 *Physica* **139B/140** 495
[127] Chow L, Deane P A, Farrell J M, Magill P M, Roberts L D 1986 *Phys. Rev.* B **33** 3039
[128] Takano M, Nasu S, Abe T, Yamamoto K, Endo S, Takeda Y and Goodenough J B 1991 *Phys. Rev. Lett.* **67** 3267–70
[129] Hesse H-J and Wortmann G 1994 *Hyperfine Interact.* **93** 1499–504
[130] Wortmann G, Goodwin H A, Rüffer R, Chumakov A I, Grünsteudel H, Leupold O and Metge J 1994 *ESRF Newsletter* **22** 1–24
[131] Holzapfel W B 1984 *Rev. Phys. Appl.* **19** 705–13
[132] Holzapfel W B pp 257–76 in [32]
[133] Nelmes R J, Hatton P D, McMahon M I, Piltz R O, Crain J, Cernik R J and Bushnell-Wye G 1992 *Rev. Sci. Instrum.* **63** 1039–42
[134] Shimomura O, Takemura K, Fujihisa H, Fujii Y, Ohishi Y, Kikegawa T, Amemiya Y and Matsushita T 1992 *Rev. Sci. Instrum.* **63** 967–73
[135] Holzapfel W B 1993 *Physica* **190B** 21–30
[136] Nelmes R J and McMahon M I 1994 *Advances in X-Ray Analysis* ed J V Gilfrich *et al* (New York: Plenum) vol 37, pp 419–32
[137] Nelmes R J and McMahon M I 1994 *J. Synchrotron Rad.* **1** 69–73
[138] Glazkov V P, Besedin S P, Goncharenko I N, Irodova A V, Makarenko I N, Somenkov V A, Stishov S M and Shil'shtein S Sh 1988 *JETP Lett.* **47** 661
[139] Glazkov V P, Goncharenko I N, Irodova V A, Somenkov V A, Shil'shtein S Sh and Besedin S P 1989 *Z. f. phys. Chemie N.F.* **163** 509
[140] Besedin S P, Makarenko I N, Stishov S M, Glazkov V P, Goncharenko I N, Irodova A V, Somenkov V A and Shil'shtein S Sh 1990 *High Pressure Res.* **4** 447–9
[141] Lee S-H, Luszczynski K, Norberg R E and Conradi M S, 1987 *Rev. Sci. Instrum.* **58** 415
[142] Lee S-H, Conradi M S and Norberg R E 1989 *Phys. Rev.* B **40** 12492 –8
[143] Radousky H B, Howell R H and Reichlin R L 1984 *J. Phys. C: Solid State Phys.* **8** 369–72
[144] Block S and Piermarini G J 1976 *Physics Today* **29** 44–52
[145] Mao H K and Bell P M 1981 *Rev. Sci. Instrum.* **52** 615
[146] Sakai N, Kajiwara T, Tsuji K and Minomura S 1982 *Rev. Sci. Instrum.* **53(4)** 499–502
[147] Reichlin R 1983 *Rev. Sci. Instrum.* **54** 1674–7
[148] Reichlin R 1984 *J. Physique* C **8** 399–402
[149] Boehler R 1986 *Geophys. Res. Lett.* **13** 1153–6
[150] Samuel T and Ruoff A L 1988 *Scr. Metall.* **22** 151–6
[151] van Bargen N and Boehler R 1990 *High Pressure Res.* **6** 133–40
[152] Bodea S and Jeanloz R 1989 *J. Appl. Phys.* **65** 4688–92
[153] Williams Q and Knittle E 1991 *J. Geophys. Res.* **96** 2171–84
[154] Boehler R 1992 *Earth Planet. Sci. Lett.* **111** 217–27
[155] Radousky H B, Mitchell A C and Nellis W J 1990 *J. Chem. Phys.* **93** 8235–9
[156] Boehler R, von Bargen N and Chopelas A 1990 *J. Geophys. Res.* **95** 21731 –6
[157] Kerley G I pp 903–9 in [22]
[158] Anderson O L pp 907–10 in [22]
[159] Stixrude L and Cohen R E pp 911–14 in [22]
[160] Bassett W A and Weathers M S pp 915–18 in [22]
[161] Boehler R pp 919–22 in [22]
[162] Duba A G pp 923–6 in [22]
[163] Schiferl D, Katz A I, Mills R L, Schmidt L C, Vanderborgh C A, Skelton E F, Elam W T, Weber A W,

Qadri S B and Schaffer M 1986 *Physica* **139B/140** 897–900
[164] Schiferl D, Fritz J N, Katz A I, Schaefer M, Skelton E F, Qadri S B, Ming L C and Manghnani M H pp 75–83 in [30]
[165] Fei Y, Mao H K, Shu J, Bassett W A, Parthasarathy G and Ko J 1992 *J. Geophys. Res.* **97** 4489–95
[166] Holzapfel W B 1973 *Gerät für Röntgenbeugung*, Deutsches Patent 2312507.7
[167] Thorwarth E and Dietrich M 1979 *Rev. Sci. Instrum.* **50** 768–71
[168] Bellussi G, Benedict U and Holzapfel W B 1981 *J. Less-Common Met.* **78** 147
[169] Vohra Y K, Holzapfel W B, Olijnyk W and Grosshans W A 1981 *Phys. Rev. Lett.* **47** 1065–7
[170] Holzapfel W B and May W pp 73–80 in [27]
[171] Yagi T and Akimoto S pp 81–90 in [27]
[172] Benedict U and Dufour C 1984 *High Temp.-High Press.* **16** 501–5
[173] Sikka S K, Sankaran H, Sharma S M, Vijayakumar V, Godwal B K and Chidambaram R 1989 *Indian J. Pure Appl. Phys.* **27** 472–8
[174] Neuling H W, Schulte O, Krüger Th and Holzapfel W B 1992 *Meas. Sci. Technol.* **3** 170–3
[175] Häusermann D and Itié J P 1992 *Rev. Sci. Instrum.* **63** 1080–2
[176] Cooper K P, Finger L W, Mao H K, Hu Z, Skelton E F, Ayers J D, Qadri S B and Moulton N E 1991 *Science* **253** 1123–5
[177] Winzenick M and Holzapfel W B 1995 *HASYLAB, Jahresbericht 1994* (Hamburg: DESY) pp 689–90
[178] Shen Y R, Gregorian T and Holzapfel W B 1991 *High Pressure Res.* **7** 73–5
[179] Holzapfel W B, Lorenz B and Shen Y R 1994 *High Pressure Res.* **12** 91–9
[180] Neuling H W and Holzapfel W B 1992 *High Pressure Res.* **8** 655–60
[181] Weber S, Porsch F and Holzapfel W B 1995 *HASYLAB Jahrbuch 1994* (Hamburg: DESY) pp 963–4
[182] Piltz R O, McMahon M I, Crain J, Hatton P D, Nelmes R J, Cernik R J and Bushnell-Wye G 1992 *Rev. Sci. Instrum.* **63** 700–3
[183] Cromer D T, Mills R L, Schiferl D and Schwalbe L A 1981 *Acta Crystallogr.* B **37** 8
[184] d'Amour H, Holzapfel W B and Nicol M F 1981 *J. Phys. Chem.* **85** 130–1
[185] Schiferl D, Cromer D T and Mills R L 1981 *Acta Crystallogr.* B **37** 1329
[186] Schiferl D, Cromer D T, Ryan R R, Larson A C, LeSar R and Mills R L 1983 *Acta Crystallogr.* C **39** 1151
[187] Cromer D T, Schiferl D, LeSar R and Mills R L 1983 *Acta Crystallogr.* C **39** 1146
[188] Hemley R J, Hazen R M, Mao H K and Finger L W 1987 *Phys. Rev.* B **360** 3944–7
[189] Mao H K, Jephcoat A P, Hemley R J, Finger L W, Zha C S, Hazen R M and Cox D E 1988 *Science* **239** 1131–4
[190] Hemley R J, Mao H K, Finger L W, Jephcoat A P, Hazen R M, Zha C S 1990 *Phys. Rev.* B **42** 6458–70
[191] Hu J, Mao H K, Shu J and Hemley R J pp 441–4 in [22]
[192] Besson J M, Nelmes R J, Hamel G, Loveday J S, Weill G and Hull S 1992 *Physica* **180B/181** 907–10
[193] Besson J M, Weill G, Hamel G, Nelmes R J, Loveday J S and Hull S 1992 *Phys. Rev.* B **45** 2613–19
[194] Nelmes R J, Loveday J S, Allan D R, Besson J M, Hamel G, Grima P and Hull S 1993 *Phys. Rev.* B **47** 7668–73
[195] Nelmes R J, Loveday J S, Wilson R M, Besson J M, Klotz S and Hamel G 1993 *PCA Transactions Symposium* pp 1–11
[196] Röhler J, Kappler J P and Krill G 1983 *Nuclear Instruments and Methods* **208** 647–50
[197] Itié J P, Polian A, Jauberthie-Carillon C, Dartyge E, Fontaine A, Tolentino H and Tourillon G 1989 *Phys. Rev.* B **40** 9709–14
[198] Itié J P, San-Miguel A F and Polian A 1992 *Jpn. J. Appl. Phys.* **32** 711–15
[199] San-Miguel A, Polian A, Gauthier M and Itié J P 1993 *Phys. Rev.* B **48** 8683–93
[200] Itié J P, Polian A, Grimsditch M and Susman S 1992 *Jpn. J. Appl. Phys.* **32** 719–21
[201] Meade Ch, Jeanloz R, Pasternak M P, Taylor R D, Chen A, GieFalicow L M and Yu P Y 1990 *Phys. Rev. Lett.* **65** 790–3
[202] Potzel W, Gleissner A, Litterst F J, Moser J, Zwirner S, Boge M, Potzel U, Gal J and Kalvius G M 1993 *Physica* **190B** 98–106
[203] Gleissner A, Potzel W, Moser J, Kalvius G M 1993 *Phys. Rev. Lett.* **70** 2032–5
[204] Butz T, Göbel H, Kalvius G M and Holzapfel W B 1975 *Hyperfine Interact.* **1** 1–14
[205] Chow L, Zhao X and Collins G S 1992 *Phys. Rev.* B **45** 4672
[206] Hemley R J, Mao H K and Shu J F 1990 *Phys. Rev. Lett.* **65** 2670–3
[207] Olijnyk H 1992 *High Pressure Res.* **10** 461–4
[208] Olijnyk H 1992 *Phys. Rev. Lett.* **68** 2232–4
[209] Olijnyk H 1992 *Phys. Rev.* B **46** 6589–91
[210] Olijnyk H 1994 *High Pressure Res.* **13** 99–102

[211] Endo S, Yamamoto K, Yamagishi A, Mikami H, Hori H and Date M 1991 *Rev. Sci. Instrum.* **62** 2988–90
[212] Seigel A E pp 481–520 in [4]
[213] Fernando E and Renero C 1994 *Phys. Rev.* B **49** 15498 –504
[214] Ragan C E 1984 *Phys. Rev.* A **29** 1391
[215] Vladimirov A S, Voloshin N P, Nogin V N, Petrovtsev A V and Simonenko V A 1984 *JETP Lett.* **39** 82
[216] Avrorin E N, Vodolaga B K, Volkov L P, Vladimirov A S, Simonenko V A and Chernovolyuk B T 1980 *JETP Lett.* **31** 687
[217] Volkov A P, Voloshin N P, Vladimirov A S, Nogin V N and Simonenko V A 1980 *JETP Lett.* **31** 588
[218] Mitchell A C and Nellis W J 1981 *J. Appl. Phys.* **52** 3363–74
[219] Al'tshuler L V, Kalitkin N N, Kuzmina L V and Chekin B S 1977 *Sov. Phys. JETP* **45** 167
[220] Trunin R F, Produrets M A, Moiseev B N, Simakov G V and Popov L V 1969 *Sov. Phys. JETP* **29** 630
[221] Trunin R F, Produrets M A, Simakov G V, Popov L V and Moiseev B N 1972 *Sov. Phys. JETP* **35** 550
[222] van Thiel M 1966 *X-Ray Diffraction of Electronic Transition in Cesium under High Pressure* (Lawrence Radiation Laboratory, University of California, Livermore)
[223] Vereschagin L F, Zubova E V and Stupnikov V A 1973 *High Temp.-High Press.* **5** 401
[224] Smith A H and Lawson A W 1954 *J. Chem. Phys.* **22** 351
[225] Holzapfel W B 1991 *Landoldt-Börnstein 'Units and Fundamental Constants in Physics and Chemistry'* ed J Bortfeld and B Kramer (Berlin: Springer Verlag) pp 2.177–84
[226] Yoneda A, Spetzler H and Getting I pp 1609–12 in [22]
[227] Holzapfel W B 1991 *High Pressure Res.* **7** 290–3
[228] Holzapfel W B 1994 *J. Phys. Chem. Solids* **55** 711–19
[229] Godwal B K and Jeanloz R 1989 *Phys. Rev.* B **40** 7501–7
[230] Decker D L 1965 *J. Appl. Phys.* **36** 157–61
[231] Decker D L 1966 *J. Appl. Phys.* **38** 5012–14
[232] Decker D L 1971 *J. Appl. Phys.* **42** 3239–44
[233] Decker D L, Bassett W A, Merrill L, Hall H T and Barnett J D 1972 *J. Phys. Chem.* **1** 773
[234] Cox D E, Chen L C, Shu J F, Hemley R J, Mao H K, Wu Y and Finger L W 1989 *Phys. Rev. Lett.* **64** 1749
[235] Mao H K, Hemley R J and Chen L C 1989 *Science* **246** 649–51
[236] Mao H K, Wu Y, Chen L C, Shu J F and Hemley R J 1990 *High Pressure Res.* **5** 773–5
[237] Mao H K, Bell P M, Shaner J W and Steinberg D J 1978 *J. Appl. Phys.* **49** 3276–83
[238] Godwal B K and Jeanloz R 1990 *Phys. Rev.* B **41** 7440–45
[239] Moriarty J A 1992 *Phys. Rev.* B **45** 2004–14
[240] Moriarty J A 1994 *Phys. Rev.* B **49** 12431 –5
[241] Sikka S K and Vijayakumar V 1988 *Phys. Rev.* B **38** 10926 –8
[242] Liu L G, Liu H, Verbeek H, Höffner Ch and Will G 1990 *J. Phys. Chem. Solids* **5** 435–8
[243] Forman R A, Piermarini G J, Barnett J D and Block S 1972 *Science* **176** 284
[244] Piermarini G J, Block S, Barnett J D, Forman R A 1975 *J. Appl. Phys.* **46** 2774
[245] Bean V E 1986 *Physica* **139/140** 739–42
[246] Bell P M and Xu J pp 125–30 in [29]
[247] Mao H K pp 221–36 in [32]
[248] McCumber D E and Sturge M D 1963 *J. Appl. Phys.* **34** 1682
[249] Lorenz B, Shen Y R and Holzapfel W B 1994 *High Pressure Res.* **12** 91–9
[250] Shen Y R and Holzapfel W B 1993 *J. Alloys Compounds* **192** 53–4
[251] Liu J and Vohra Y K 1993 *Solid State Commun.* **88** 417–19
[252] Liu J and Vohra Y K 1994 *Appl. Phys. Lett.* **64** 3386–8
[253] Liu J and Vohra Y K pp 1681–4 in [22]
[254] Yusa H, Yagi T and Arashi H 1994 *J. Appl. Phys.* **75** 1463–6
[255] Jahren A H, Kruger M B and Jeanloz R 1992 *J. Appl. Phys.* **71** 1579–82
[256] Noack R A and Holzapfel W B pp 748–53 in [14]
[257] Hemley R J, Hanfland M and Mao H K 1992 *Phys. Rev.* B **45** 8108–11
[258] Ershine D Yu and Martinez G 1987 *Rev. Sci. Instrum.* **59** 406
[259] Bireckoven B and Wittig J 1988 *J. Phys. E: Sci. Instrum.* **21** 841
[260] Friedl C and Ashcroft N W 1975 *Phys. Rev.* B **12** 5552
[261] Godwal B K, Sikka S K and Chidambaram R 1983 *Phys. Rep.* **102** 121–97
[262] Westphal W H (ed) 1952 *'Physikalisches Wörterbuch'* (Berlin: Springer)
[263] Kiefer S W 1979 *Rev. Geophys. Space Phys.* **17** 1–59
[264] Grüneisen E 1926 *Handbuch der Physik* **10** 1–59
[265] Aziz R A 1975 *Inert Gas Solids* ed M I Klein (Berlin: Springer) p 117

[266] Barker J A 1976 *Rare Gas Solids* ed M I Klein and J A Venable (New York: Academic) vol 1, Chap 4
[267] Maitland G C, Rigby M, Smith E B and Wakeham W A 1981 *Intermolecular Forces, Their Origin and Determination* (Oxford: Clarendon)
[268] Barker J A pp 331–51 in [32]
[269] Bulski M pp 353–88 in [32]
[270] Ree F H pp 33–60 in [34]
[271] LeSar R pp 389–410 in [32]
[272] Hafner J and Heine V 1986 *J. Phys. F: Met. Phys.* **16** 1429–58
[273] Hafner J 1987 *Solid-State Science* ed M Cardona, P Fulde, K von Klitzing and H-J Queisser (Berlin: Springer) vol 70, pp 1–404
[274] Pettifor D G 1987 *Solid State Physics* ed H Ehrenreich and D Turnbull (New York: Academic) vol 40, pp 43–92
[275] Ree T and Choi Y 1991 *J. Chem. Phys.* **95** 7548–51
[276] Hafner J 1994 *Statics and Dynamics of Alloy Phase Transformations* ed P E A Turchi and A Gonis (New York: Plenum) pp 269–304
[277] Moriarty J A 1988 *Phys. Rev.* B **38** 3199
[278] Murnaghan F D 1967 *Finite Deformation of an Elastic Solid* (New York: Dover)
[279] Birch F 1978 *J. Geophys. Res.* **83** 1257
[280] Holzapfel W B 1991 *Europhys. Lett.* **16** 67–72
[281] Smith G S 1989 *Phys. Lett.* **140A** 431
[282] Grüneisen E 1912 *Ann. Phys. (Leipzig)* **IV(39)** 257–306
[283] McQueen R G pp 101–216 in [12]
[284] Young D A 1991 *Comments Condens. Matter Phys.* **15** 175–99
[285] Gschneidner K A Jr 1964 *Solid State Phys.* **16** 275–446
[286] Keeler R N and Kennedy G C 1972 *American Institute of Physics Handbook 3. Edition* ed D E Gray (New York: McGraw Hill) pp 4938–5104
[287] Guinan M W and Steinberg D J 1974 *J. Phys. Chem. Solids* **35** 1501–12
[288] Anderson M S and Swenson C A 1975 *J. Phys. Chem. Solids* **36** 145–62
[289] Finger L W, Hazen R M, Zou G, Mao H K and Bell P M 1981 *Appl. Phys. Lett.* **39** 892–4
[290] Driessen A and Silvera I F 1986 *Phys. Rev.* B **33** 3269
[291] Vinet P, Ferrante J, Smith J R and Rose J H 1986 *J. Phys. C: Solid State Phys.* **19** 1467
[292] Banerjea A and Smith J R 1988 *Phys. Rev.* B **37** 6632
[293] Rodean H C 1968 *J. Chem. Phys.* **49** 4117
[294] Holzapfel W B pp 61–88 in [34]
[295] Ho-Kim I, Jeanloz R, Soo Jhung K, Ho Bae Y and Choi Ch-K 1992 *Phys. Rev.* B **46** 3095–7
[296] Leigh G J 1990 (Oxford: Blackwell)
[297] Friedli C and Ashcroft N W 1975 *Phys. Rev.* B **12** 5552
[298] Nellis W J, Moriarty J A, Mitchell A C, Ross M, Dandrea R G, Ashcroft N W, Holmes N C and Gathers R G 1988 *Phys. Rev. Lett.* **60** 1414
[299] Mitchell A C, Nellis W J, Moriarty J A, Heinle R A, Holmes N C and Tipton R E 1991 *J. Appl. Phys.* **69** 2981–6
[300] Godwal B K, Sikka S K and Chidambaram R 1981 *Phys. Rev. Lett.* **47** 1144–7
[301] Boettger J C and Trickey S B 1984 *Phys. Rev.* B **29** 6434–42
[302] Meyer-ter-Vehn J and Zittel W 1988 *Phys. Rev.* B **37** 8647–88
[303] Ruoff A L, Luo H and Greene R G 1995 *Phys. Rev.* B **73** 2075–8
[304] Ruoff A L and Lincoln R C 1973 *Phys. Rev.* **44** 1239
[305] McMahan A K and Albers R C 1982 *Phys. Rev. Lett.* **49** 1198
[306] Schulte O and Holzapfel W B 1993 *Phys. Rev.* B **48** 767–73
[307] Morgan J A 1974 *High Temp.-High Press.* **6** 195
[308] Holmes N C, Moriarty J A, Gathers G R and Nellis W J 1989 *J. Appl. Phys.* **66** 2966
[309] Ahuja R, Eriksson O, Söderling P, Willis J M and Johansson B 1994 *High Pressure Res.* **12** 161–70
[310] Simmon G and Wang H 1971 *Single Crystal Elastic Constants and Calculated Aggregate Properties: A Handbook* (Cambridge, MA: MIT)
[311] Jamieson J C, Fritz J N and Manghnani M H p 27 in [27]
[312] Ming L C, Manghnani M H, Balogh J, Qadri S B, Skelton E F and Jamieson J C 1983 *J. Appl. Phys.* **54** 4390
[313] Godwal B K, Ng A and Jeanloz R 1992 *High Press. Res.* **10** 687
[314] Neighbours J R and Alers G A 1958 *Phys. Rev.* **III** 707

[315] Chang Y A and Himmel L 1966 *J. Appl. Phys.* **37** 3567
[316] Biswas S N, Van't Klooster P and Trappeniers N 1981 *Physica* **103B** 235
[317] Aleksandrov I V, Kachinski V N, Makarenko I N and Stishov S M 1983 *JETP Lett.* **36** 411
[318] Young D A and Ross M 1984 *Phys. Rev.* B **29** 682
[319] Vaidya S N 1971 *J. Phys. Chem. Solids* **32** 2545
[320] Anderson M S and Swenson C A 1983 *Phys. Rev.* B **28** 5395
[321] Winzenick M, Vijayakumar V and Holzapfel W B 1994 *Phys. Rev.* B **50** 12381 –5
[322] Vaidya S N, Getting I C and Kennedy G C 1971 *J. Phys. Chem. Solids* **32** 2545
[323] Olinger B and Shaner J W 1983 *Science* **291** 1071
[324] Takemura K, Minomura S, Shimomura O, Fujii Y and Axe J D 1982 *Phys. Rev.* B **49** 1172
[325] Badding J V, Mao H K and Hemley R J 1991 *Solid State Commun.* **77** 801–5
[326] Winzenick M 1994 *Thesis* Paderborn
[327] Vaidya S N and Kennedy G C 1972 *J. Phys. Chem. Solids* **33** 1381
[328] Ming L C and Manghnani M H 1984 *J. Phys. F: Met. Phys.* **14** L1–8
[329] Olijnyk H and Holzapfel W B 1985 *Phys. Rev.* B **31** 4782
[330] Takemura K 1994 *Phys. Rev.* B **50** 16238 –46
[331] Grosshans W A and Holzapfel W B 1992 *Phys. Rev.* B **45** 5171–8
[332] Vohra Y K and Holzapfel W B 1993 *High Pressure Res.* **11** 223–37
[333] Benedict U and Holzapfel W B 1993 *Lanthanide/Actinide: Physics-I* ed K A Gschneidner Jr, L Eyring, G H Lander and G R Choppin (Amsterdam: North-Holland) pp 245–300
[334] Vohra Y K, Sikka S K and Holzapfel W B 1983 *J. Phys. F: Met. Phys.* **13** L107–10
[335] McQueen R G, Marsh S P, Taylor W J, Fitz J N and Carter W J 1970 *High Velocity Impact Phenomenon* ed R Kinslow (New York: Academic) p 293
[336] Jeanloz R, Godwal B K and Meade C 1991 *Nature* **349** 687–9
[337] Söderlind P, Eriksson O, Wills J M and Boring A M 1993 *Phys. Rev.* B **48** 9306–12
[338] Wills J M and Eriksson O 1992 *Phys. Rev.* B **45** 13879
[339] Chelikowsky J R and Louie S G 1984 *Phys. Rev.* B **29** 3470–81
[340] Fahy S and Louie S G 1987 *Phys. Rev.* B **36** 3373–85
[341] Furthmüller J, Hafner J and Kresse G 1994 *Phys. Rev.* B **50** 15606 –22
[342] Liu A Y and Cohen M L 1992 *Phys. Rev.* B **45** 4579–81
[343] Queisser G and Holzapfel W B 1991 *Appl. Phys.* A **53** 114–17
[344] Olijnyk H and Holzapfel W B 1984 *J. Physique Colloq.* **8** 153–5
[345] Olijnyk H, Sikka S K and Holzapfel W B 1984 *Phys. Lett.* **103A** 137–40
[346] Liu M and Liu L 1986 *High Temp.-High Press.* **18** 79
[347] Hu J Z, Merkle L D, Menoni C S and Spain I L 1986 *Phys. Rev.* B **34** 4679
[348] Vohra Y K, Brister K E, Desgreniers S, Ruoff A L, Chang K J and Cohen M L 1986 *Phys. Rev. Lett.* **56** 1944
[349] Duclos S J, Vohra Y K and Ruoff A L 1987 *Phys. Rev. Lett.* **58** 775
[350] Cavalerie M E, Plymate T G and Stout J H 1988 *J. Phys. Chem. Solids* **49** 945–56
[351] Desgreniers S, Vohra Y K and Ruoff A L 1989 *Phys. Rev.* B **39** 10359 –61
[352] Duclos S J, Vohra Y K and Ruoff A L 1990 *Phys. Rev.* B **41** 12021
[353] McMahon M I and Nelmes R J 1993 *Phys. Rev.* B **47** 8337–40
[354] Yin M T and Cohen M L 1980 *Solid State Commun.* **45** 1004
[355] Ihm J and Cohen M L 1981 *Phys. Rev.* B **23** 1576
[356] Yin M T and Cohen M L 1981 *Solid State Commun.* **38** 625
[357] Yin M T and Cohen M L 1982 *Phys. Rev.* B **26** 5668
[358] Yin M T and Cohen M L 1982 *Phys. Rev.* B **26** 3259
[359] Yin M T and Cohen M L 1983 *Phys. Rev. Lett.* **50** 2006
[360] Yin M T and Cohen M L 1984 *Phys. Rev.* B **29** 6996
[361] Chang K J and Cohen M L 1984 *Phys. Rev.* B **30** 5376
[362] Chang K J and Cohen M L 1985 *Phys. Rev.* B **31** 7819
[363] Chang K J and Cohen J L 1986 *Phys. Rev.* B **34** 8581
[364] Cheong B H and Chang K J 1991 *Phys. Rev.* B **44** 4103–8
[365] Neethiulagarajan A and Balasubramanian S 1991 *Phys. Rev.* B **43** 13525 –7
[366] Neethiulagarajan A and Vijayakumar V 1993 *Phys. Rev.* B **47** 487–9
[367] Christensen N E and Methfessel M 1993 *Phys. Rev.* B **48** 5797–807
[368] Avrorin E N, Vodolaga B K, Voloshin N P, Kovalenko G V, Kuropatenko V F, Simonenko V A and Chernovolyuk B T 1987 *Sov. Phys. JETP* **66** 347–54

[369] Queisser G 1986 Paderborn
[370] Vanderborgh C A, Vohra Y K, Xia H and Ruoff A L 1990 *Phys. Rev.* B **41** 7338
[371] Vohra Y K and Ruoff A L 1990 *Phys. Rev.* B **42** 8651–4
[372] Schulte O and Holzapfel W B 1995 *Phys. Rev.* B **52**
[373] Holzapfel W B, Johannsen P G and Grosshans W A 1987 *Dynamics of Molecular Crystals* ed J Lascombe (Amsterdam: Elsevier) pp 133–40
[374] Holzapfel W B pp 120–36 in [19]
[375] Fujii Y, Hase K, Ohishi Y, Fujihisa H, Hamaya N, Takemura K, Shimomura O, Kikegawa T, Amemiya Y and Matsushita T 1989 *Phys. Rev. Lett.* **63** 536–9
[376] Fujihisa H, Fujii Y, Takemura K and Shimomura O 1995 *J. Phys. Chem. Solids* in press
[377] Akahama Y, Kobayashi M and Kawamura H 1992 *Solid State Commun.* **83** 269–72
[378] Akahama Y, Kobayashi M and Kawamura H 1992 *Jpn. J. Appl. Phys.* **31** L1621–4
[379] Akahama Y, Kobayashi M and Kawamura H 1992 *Solid State Commun.* **83** 273–6
[380] Akahama Y, Kobayashi M and Kawamura H 1993 *Jpn. J. Appl. Phys.* **32** Suppl. 1, 22–5
[381] Akahama Y, Kobayashi M and Kawamura H 1993 *Phys. Rev.* B **47** 20–6
[382] Nishikawa A, Niizeki K and Shindo K 1992 *Jpn. J. Appl. Phys.* **32** Suppl. 1, 48–50
[383] Holzapfel W B, Krüger Th, Sievers W and Vijayakumar V 1993 *Jpn. J. Appl. Phys.* **32** Suppl. 1, 16–21
[384] Singh A K and Kennedy G C 1974 *J. Phys. Chem. Solids* **35** 1545
[385] Hemley R J, Jephcoat A P, Zha C S, Mao H K, Finger L W and Cox D E pp 211–17 in vol 3 [18]
[386] Grilly E R 1973 *J. Low Temp. Phys.* **11** 33
[387] Mao H K, Hemley R J, Wu Y, Jephcoat A P, Finger L W, Zha C S and Bassett W A 1988 *Phys. Rev. Lett.* **60** 2649–52
[388] Pinceaux J P, LeToullec R, Mao H K, Hemley R J and Loubeyre P 1993 *Phys. Rev. Lett.* **71** 2272–5
[389] Zittel W 1985 *Thesis* Darmstadt
[390] Anderson M S and Swenson C A 1974 *Phys. Rev.* B **10** 5184
[391] Silvera I F and Goldman V V 1978 *J. Chem. Phys.* **69** 4209
[392] Driessen A, deWaal J A and Silvera I F 1979 *J. Low Temp. Phys.* **34** 255
[393] Krause J K and Swenson C A 1980 *Phys. Rev.* B **21** 2533
[394] Straaten J v, Wijngaarden R J and Silvera I F 1982 *Phys. Rev. Lett.* **48** 97–100
[395] Sokol P E, Simmons R O, Jørgensen J D and Jørgensen J E 1985 *Phys. Rev.* B **31** 620–2
[396] Hemmes H, Driessen A and Griessen R 1986 *Physica* **139/140B** 116–18
[397] Straaten J v and Silvera I F 1988 *Phys. Rev.* B **37** 1989
[398] Hanfland M, Mao H K and Hemley R J 1991 *Nature* **350** 488–91
[399] Loubeyre P 1994 High pressure experiments for Astrophysics *The Equation of State in Astrophysics* ed G Chabrier and E Schatzmann (Cambridge: Cambridge Press)
[400] Häusermann D, Hanfland M, Loubeyre P, LeToullec R, Mao H K, Hemley R J, Finger L W, Jephcoat A P, Häusermann D, Hanfland M, Loubeyre P and LeToullec R 1994 *ESRF Newsletter* **21** 8–9
[401] Chakravarty S, Rose J H, Wood D and Ashcroft N W 1981 *Phys. Rev.* B **24** 1624–35
[402] Young D A and Ross M 1981 *J. Chem. Phys.* **74** 6950–5
[403] Moulopoulos K and Ashcroft N W 1990 *Phys. Rev.* B **41** 6500–19
[404] Barbee T W, Garcia A, Cohen M L and Martin J L 1989 *Phys. Rev. Lett.* **62** 1150
[405] Gautier D 1987 *Europhys. News* **18** 116–19
[406] Duffy Th S, Voss W L, Zha Ch, Hemley R J and Mao H 1994 *Science* **263** 1590–3
[407] Wanner R and Meyer H 1973 *J. Low Temp. Phys.* **11** 715
[408] Ishmev S N, Sadikev I P, Chernyslov A A, Vindryaerskii B A, Sukhoparov V A, Telepnev A S and Kobelev G V 1983 *Sov. Phys. JETP* **57** 228–33
[409] Johannsen P G (private communication)
[410] Knopoff L 1965 *Phys. Rev.* A **138** 1445–7
[411] Ruoff A L 1991 *Materials Science and Technology* ed R W Cahn, P Haasen and E J Kramer (Weinheim: VCH) vol 5, pp 474–95
[412] Pettifor D G 1993 *Material Science and Technology* ed R W Cahn, P Haasen and E J Kramer (Weinheim: VCH) vol I, pp 61–122
[413] Söderlind P, Ahuja R, Eriksson O, Johansson B and Wills J M 1994 *Phys. Rev.* B **49** 9365–71
[414] Ahuja R, Söderlind P, Wills J M, Johansson B and Eriksson O 1994 *High Pressure Res.* **12** 161
[415] Takemura K and Fujihisa H 1993 *Phys. Rev.* B **47** 8465–70
[416] Pettifor D G 1977 *J. Phys. F: Met. Phys.* **7** 613
[417] Hafner S and Heine V 1983 *J. Phys. F: Met. Phys.* **13** 2479
[418] Ahuja R, Söderlind P, Trygg J, Eriksson O, Wills J M and Johansson B O *Phys. Rev.* B at press

[419] Takemura K and Syassen K 1985 *Phys. Rev.* B **32** 2213
[420] Olijnyk H 1985 *Thesis* Paderborn
[421] Olijnyk H and Holzapfel W B pp 75–9 in [31]
[422] Takemura K, Syassen L and Fujihiso H 1991 *Phys. Rev. Lett.* **66** 2014
[423] Vijayakumar V, Sikka S K and Olijnyk H 1991 *Phys. Lett.* **152A** 353–5
[424] Sankaran H, Sharma S M and Sikka S K 1992 *J. Phys.: Condens. Matter* **4** L61–6
[425] McMahan A K and Moriarty J A 1983 *Phys. Rev.* B **27** 3235
[426] Johansson B and Rosengren A 1975 *Phys. Rev.* B **11** 2836
[427] Duthie J C and Pettifor D G 1977 *Phys. Rev. Lett.* **38** 564
[428] Holzapfel W B 1980 *Metall* **34** 138–43
[429] Benedict U, Grosshans W A and Holzapfel W B 1986 *Physica* **144B** 14–18
[430] Holzapfel W B 1995 *J. Alloys Compounds* **223** 170–3
[431] Gschneidner K A Jr and Calderwood F W 1986 *Handbook on the Physics and Chemsitry of Rare Earths* ed K A Gschneidner Jr and LeDog Eyring (Amsterdam: North-Holland) vol 8, p 1
[432] Skriver H L 1985 *Phys. Rev.* B **31** 1909
[433] Syassen K and Holzapfel W B pp 223–6 in [14]
[434] Zhao Y C, Porsch F and Holzapfel W B 1994 *Phys. Rev.* B **49** 815–17
[435] Holzapfel W B and Grosshans W A 1984 *J. Physique Coll.* **8** 141–3
[436] Zhao Y C, Porsch F and Holzapfel W B 1994 *Phys. Rev.* B **50** 6603–8
[437] Grosshans W A, Vohra Y K and Holzapfel W B 1982 *J. Magn. Magn. Mater.* **29** 282–6
[438] Eriksson O, Söderlind P and Wills J M 1992 *Phys. Rev.* B **45** 12588
[439] Eriksson O, Söderlin P, Wills J M and Boring A M 1993 *Physica* **190B** 5–11
[440] Johansson B, Fast L, Söderlind P and Eriksson O 1993 *Physica* **190B** 12–20
[441] Eriksson O, Wills J M, Söderlind P, Melsen J, Ahuja R, Boring A M and Johansson B *J. Alloys Compounds* in press
[442] Wills J M, Eriksson O, Söderlind P and Boring A M in press
[443] Söderlind P, Eriksson O, Wills J M and Johansson B *Phys. Rev. Lett.* in press
[444] Söderlind P, Eriksson O, Wills J M and Johansson B *Phys. Rev.* B in press
[445] Söderlind P, Wills J M, Boring A M, Johansson B and Eriksson O 1994 *J. Phys. C: Solid State Phys.* **6** 6573–80
[446] Gyanchandani J S, Gupta S C, Sikka S K and Chidambaram R 1990 *High Pressure Res.* **4** 472–4
[447] Gyanchandani J S, Sikka S K and Chidambaram R pp 331–4 in [21]
[448] Gupta S C 1992 *Structure Calculation to Predict Phase Transformation at High Pressure* ed S C Schmidt, R D Dick, J W Forbes and D G Tasker (Amsterdam: Elsevier) pp 157–63
[449] Ahuja R, Wills J M, Johansson B and Eriksson O 1993 *Phys. Rev.* B **48** 16269 –79.
[450] Xia H, Parthasarathy G, Luo H, Vohra Y K and Ruoff A L 1990 *Phys. Rev.* B **42** 6736–8
[451] Xia H, Ruoff A L and Vohra Y K 1991 *Phys. Rev.* B **44** 10374 –6
[452] Althoff J D, Allen P B, Wentzcovitch R M, Moriarty J A 1993 *Phys. Rev.* B **48** 13253
[453] Schulte O and Holzapfel W B 1993 *Phys. Rev.* B **48** 14009
[454] Takemura K and Fujikisa H 1993 *Phys. Rev.* B **47** 8465
[455] Rao R S, Godwal B K and Sikka S K pp 167–9 in [22]
[456] Vijayakumar V and Sikka S K 1990 *High Pressure Res.* **4** 306–8
[457] Olijnyk H 1990 *J. Chem. Phys.* **93** 8968–72
[458] Olijnyk W 1991 *High Pressure Res.* **7** 313–15
[459] Schneider H, Häfner W, Wokaun A and Olijnyk H 1992 *J. Chem. Phys.* **96** 8046–53
[460] Scheerboom M I M and Schouten J A 1993 *Phys. Rev. Lett.* **71** 2252–5
[461] Mulder A, Michels J P J and Schouten J A pp 225–8 in [22]
[462] Mailhiot C, Yang L H and McMahan A K 1992 *Phys. Rev.* B **46** 14419
[463] Reichlin R, Schiferl D, Martin S, Vanderborgh C and Mills R L 1985 *Phys. Rev. Lett.* **55** 1464–7
[464] Bell P M, Mao H K and Hemley R J 1986 *Physica B+C* **139/140B** 16
[465] Martin R M and Needs R J 1986 *Phys. Rev.* B **34** 5082
[466] Douglas C, Ree H and Ree F H 1989 *J. Chem. Phys.* **90** 4972–81
[467] Lewis S P and Cohen M L 1992 *Phys. Rev.* B **46** 11117
[468] Kikegawa T pp 61–8 in [30]
[469] Iwasaki H and Kikegawa T 1990 *High Pressure Res.* **6** 121–32
[470] Iwasaki H, Chen J H, Kikegawa T, Yaoita K and Tsuji K 1993 *Bull. Am. Phys. Soc.* **38** 1574
[471] Chen J H, Iwasaki H, Kikegawa T, Yaoita K and Tsuji K pp 421–4 in [22]
[472] Häfner W, Kritzenberger J, Olijnyk H and Wokaun A 1990 *High Pressure Res.* **6** 57–75

[473] Häfner W, Olijnyk H and Wokaun A 1990 *High Pressure Res.* **3** 248–50
[474] Luo H, Desgreniers S, Vohra Y K and Ruoff A L 1991 *Phys. Rev. Lett.* **67** 2998–3001
[475] Rossmanith P, Häfner W, Wokaun A and Olijnyk H 1993 *High Pressure Res.* **11** 183–94
[476] Luo H, Greene R G and Ruoff A L 1993 *Phys. Rev. Lett.* **71** 2943–6
[477] Luo H and Ruoff A L 1993 *Phys. Rev.* B **48** 569–72
[478] Akahama Y, Kobayashi M and Kawamura H pp 425–8 in [22]
[479] Krüger Th and Holzapfel W B 1992 *HASYLAB Jahresbericht 1991* (Hamburg: DESY) pp 305–6
[480] Krüger Th and Holzapfel W B 1992 *Phys. Rev. Lett.* **69** 305–7
[481] Akahama Y, Kobayashi M and Kawamura H 1992 *Solid State Commun.* **84** 803–6
[482] Kresse G, Furthmüller J and Hafner J 1994 *Phys. Rev.* B **50**
[483] Brazhkin V V, Voloshin R N, Popova S V and Umnov A G 1992 *J. Phys.: Condens. Matter* **4** 1419–25
[484] Kirchhoff F, Binggeli N, Galli G and Massidda S 1994 *Phys. Rev.* B **13** 9063–71
[485] Düsing E F, Grosshans W A and Holzapfel W B 1984 *J. Physique Coll.* **8** 203
[486] Johannsen P G, Düsing E F and Holzapfel W B pp 105–8 in [28]
[487] Shimizu K, Tamitani N, Takeshita N, Ishizuka M, Amaya K and Endo S 1992 *J. Phys. Soc. Jpn.* **61** 3853–5
[488] Pistorius C W F T 1976 *Solid State Chemistry* **11** 1–151
[489] Merrill L 1977 *J. Phys. Chem. Ref. Data* **6** 1205–52
[490] Zimmer H G, Winzen H and Syassen K 1985 *Phys. Rev.* B **32** 4066–70
[491] Benedict U 1987 *J. Less-Common Met.* **128** 7–45
[492] Syassen K 1985 *Phys. Stat. Sol. a* **91** 11–15
[493] Weir S T, Vohra Y K and Ruoff A L 1986 *Phys. Rev.* B **33** 4221–6
[494] Weir S T, Vohra Y K and Ruoff A L 1987 *Phys. Rev.* B **36** 4543–6
[495] Mao H K, Wu Y, Shu J F, Hu J Z, Hemley R J and Cox D E 1990 *Solid State Commun.* **74** 1927
[496] Ves S, Schwarz U, Christensen N E, Syassenk and Cardona M 1990 *Phys. Rev.* B **42** 9113–18
[497] Ueno M, Onodera A, Shimomura O and Takemura K 1992 *Phys. Rev.* B **45** 10123 –6
[498] Ueno M, Yoshida M, Onodera A, Shimomura O and Takemura K 1992 *Jpn. J. Appl. Phys.* **32** 42–4
[499] Xia Q, Xia H and Ruoff A L 1993 *J. Appl. Phys.* **73** 8198–200
[500] Nelmes R J, McMahon M I, Hatton P D, Piltz R O and Crain J 1993 *Jpn. J. Appl. Phys.* **32** Suppl. 1, 1–5
[501] Nelmes R J, McMahon M I, Hatton P D, Crain J and Piltz R O 1993 *Phys. Rev.* B **47** 35–54
[502] Nelmes R J, McMahon M I, Wright N G and Allan D R 1993 *Phys. Rev.* B **48** 1314–17
[503] Nelmes R J, McMahon M I, Wright N G and Allan D R 1993 *Phys. Rev.* B **48** 16246 –51
[504] McMahon M I, Nelmes R J, Wright N G and Allan D R 1994 *Phys. Rev.* B **50** 13047 –50
[505] Nelmes R J, McMahon M I, Wright N G and Allan D R 1994 *Phys. Rev. Lett.* **73** 1805–8
[506] Nelmes R J and McMahon M I 1995 *Phys. Rev. Lett.* **74** 106–9
[507] Xia Q, Xia H and Ruoff A L pp 307–10 in [22]
[508] Greene R G, Luo H, Ruoff A L, Trail S S, DiSalvo F J Jr 1994 *Phys. Rev. Lett.* **73** 2476–9
[509] Greene R G, Luo H, Li T and Ruoff A L 1994 *Phys. Rev. Lett.* **13** 2045–8
[510] Greene R G, Luo H and Ruoff A L 1994 *J. Appl. Phys.* **76** 7296–9
[511] Luo H, Greene R G and Ruoff A L 1994 *Phys. Rev.* B **49** 15341 –3
[512] Luo H, Greene R G, Ghandehari K, Li T and Ruoff A L 1994 *Phys. Rev.* B **50** 16232 –7
[513] Chelikowsky J R and Burdett J K 1986 *Phys. Rev. Lett.* **56** 961
[514] Gorczyca I and Christensen N E 1991 *Solid State Commun.* **79** 1033
[515] Gorczyca I and Christensen N E 1991 *Solid State Commun.* **80** 335
[516] Singh R K and Singh S 1992 *Phys. Rev.* B **45** 1019–22
[517] Perlin P, Gorczyca I, Porowsky S, Suski T, Christensen N E and Polian A 1993 *Jpn. J. Appl. Phys.* **32** 334
[518] Christensen N E and Gorczyca I 1993 *Phys. Rev.* B **47** 4307–14
[519] Gorczyca I and Christensen N E 1993 *Physica* **185B** 410–14
[520] Jaffe J E, Pandey R and Seel M J 1993 *Phys. Rev.* B **47** 6299–303
[521] Christensen N E and Gorczyca I 1994 *Phys. Rev.* B **50** 4397
[522] Mailhiot C, Grant J B and McMahan A K 1990 *Phys. Rev.* B **42** 9033–9
[523] McMahan A K and LeSar R 1985 *Phys. Rev. Lett.* **54** 1929
[524] Siringo F, Pucci R and March N H 1990 *High Pressure Res.* **2** 109–34
[525] Reichlin R, private communication, cited on p 148 in [13]
[526] Siringo F, Piccitto G and Pucci R 1990 *High Pressure Res.* **3** 162–4
[527] Akahama Y, Endo S and Narita S 1986 *Physica* **139B/140** 397–400
[528] Akai T, Endo S, Akahama Y, Koto K and Maruyama Y 1989 *High Pressure Res.* **1** 115–30
[529] Jephcoat A P, Mao H K, Finger L W, Hemley R J, Cox D E and Zha C S 1987 *Phys. Rev. Lett.* **59** 2670–3
[530] Reichlin R, Brister K, Ross M, Martin S, Ruoff A L, McMahan A K and Vohra Y 1989 *Phys. Rev. Lett.* **62**

669
[531] Ebeling W, Förster A, Richert W and Hess H 1988 *Physica* **150A** 159
[532] Ebeling W, Förster A, Fortov V E, Gryaznov V K and Polishchuk A Y 1991 (Stuttgart: Teubner)
[533] Pasternak M, Farell N J and Taylor R D 1987 *Phys. Rev. Lett.* **58** 575
[534] Pasternak M, Farell J N and Taylor R D 1987 *Phys. Rev. Lett.* **59** 945
[535] Olijnyk H, Li W and Wokaun A 1994 *High Pressure Res.* **13** 103–8
[536] Singh A K 1980 *High Temp.-High Press.* **12** 47
[537] Mao H K and Hemley R J 1992 *Am. Sci.* 233–47
[538] Silvera I F 1982 *Europhys. News* **13** 4
[539] Cui L, Chen N H, Jeon S J and Silvera I F 1994 *Phys. Rev. Lett.* **72** 3048–51
[540] Hemley R J and Mao H K 1988 *Phys. Rev. Lett.* **61** 857–60
[541] Lorenzana H E, Silvera I F and Goettel K A 1989 *Phys. Rev. Lett.* **63** 2080–3
[542] Lorenzana H E, Silvera I F and Goettel K A 1990 *Phys. Rev. Lett.* **64** 1939–42
[543] Lorenzana H E, Silvera I F and Goettel K A 1990 *Phys. Rev. Lett.* **65** 1901–4
[544] Hemley R J and Mao H K 1990 *Science* **249** 391–3
[545] Lorenzana H E and Jeanloz R 1991 *J. Chem. Phys.* **95** 3838–40
[546] Silvera I F 1993 *Fiz. Nizk. Temp.* **19** 628–30
[547] Hemley R J and Mao H K 1989 *Phys. Rev. Lett.* **63** 1393–5
[548] Hemley R J, Soos Z G, Hanfland M and Mao H K 1994 *Nature* **369** 384–7
[549] Surh M P and Runge K J pp 853–6 in [22]
[550] Mao H K and Hemley R J 1989 *Science* **244** 1462–5
[551] Hemley R J, Hanfland M and Mao H K 1990 *Phys. Rev. Lett.* **65** 484–7
[552] Eggert J H, Goettel K A and Silvera I F 1990 *Europhys. Lett.* **11** 775–81
[553] Garcia A, Barbee T W, Cohen M L and Silvera I F 1990 *Europhys. Lett.* **13** 355–60
[554] Eggert J H, Moshary F, Evans W J, Lorenzana H E, Goettel K A, Silvera I F and Moss W C 1991 *Phys. Rev. Lett.* **66** 193–6
[555] Wigner E and Huntington H B 1935 *J. Chem. Phys.* **3** 764
[556] Ramaker D E, Kumar L and Harris F E 1975 *Phys. Rev. Lett.* **34** 812–14
[557] Min B I, Jansen H J F and Freeman A J 1984 *Phys. Rev.* B **30** 5076
[558] Min B I, Jansen H J F and Freeman A J 1986 *Phys. Rev.* B **33** 6383
[559] Ceperley D M and Alder B J 1987 *Phys. Rev.* B **36** 2092
[560] Chacham H and Louie S G 1991 *Phys. Rev. Lett.* **66** 64–71
[561] Barbee T W and Cohen M L 1991 *Phys. Rev.* B **43** 5269–75
[562] Natoli V, Martin R M and Ceperley D M 1993 *Phys. Rev. Lett.* **70** 1952–5
[563] Natoli V, Martin R M and Ceperley D M 1995 *Phys. Rev. Lett.* **74** 1601–4
[564] MacDonald A H and Burgess C P 1982 *Phys. Rev.* B **26** 2849
[565] Giavoni M and Ferraz A 1991 *Phys. Lett.* **161A** 71–3
[566] Ashcroft N W 1968 *Phys. Rev. Lett.* **21** 1748
[567] Barbee T W, Garcia A and Cohen M L 1989 *Nature* **340** 369–71
[568] Diatschenko V, Chu C W, Liebenberg D H, Young D A, Ross M and Mills R L 1985 *Phys. Rev.* B **32** 381–9
[569] Kerley G I 1972 Equation of State and Phase Diagram of Dense Hydrogen *Phys. Earth Planet. Int.* **l6** 78–82
[570] Ebeling W and Richert W 1985 *Phys. Lett.* **108A** 80–2
[571] Ebeling W and Kraeft W D and Kremp D 1986 *Europhys. News* **17** 52–5
[572] Zhao Y C, Porsch F and Holzapfel W B 1995 *Phys. Rev.* B **52** 687–8
[573] Ross M, Young D A and Grover R 1990 *J. Geophys. Res.* **95** 21713 –16
[574] Knittle E and Jeanloz R 1991 *J. Geophys. Res.* **96** 16169
[575] McMillan W L 1968 *Phys. Rev.* **168** 605
[576] Wijngaarden R J, Scholtz J J, van Eenige E N, Heeck K and Griessen R 1992 *High Pressure Res.* **9/10** 479–85
[577] Wijngaarden R J, van Eenige E N, Scholtz J J, Jover D T and Griessen R *High Pressure Chemistry, Biochemistry and Materials-Science* ed R Winter and J Jonas (Kluwer: Academic) pp 1–26
[578] Moruzzi V L, Markus P M, Schwarz K and Mohn P 1986 *Phys. Rev.* B **34** 1784
[579] Abd-Elmeguid M M and Micklitz H 1989 *Phys. Rev.* B **40** 7395
[580] Wassermann E F, Acet M and Pepperhoff W 1990 *J. Magn. Magn. Mater.* **90/91** 126–9
[581] Kakeshita T, Shimizu K, Tanaka R, Nakamichi S, Endo S and Ono F 1991 *Materials Transactions* **32** 1115–19
[582] Hochheimer H D and Münch R 1991 *Phil. Mag. B* **63** 979–92

[583] Podgorny M 1991 *Phys. Rev.* B **43** 11300
[584] Kawano S, Achiwa N, Onodera A and Nakai Y 1992 *Physica B* 104–6
[585] Kakeshita T, Mizoguchi K, Shimizu K, Nakamichi S, Endo S and Ono F 1992 *Materials Transactions* **33** 1035–9
[586] Wassermann E F 1993 *Ferienkurs 'Magnetismus'* IFF Jülich
[587] Ben Ghozlen M H and Mlik Y 1983 *J. Phys. C: Solid State Phys.* **16** 4365–81
[588] Dmitriev V P and Rochal S B 1989 *Phys. Rev. Lett.* **21** 2495–8
[589] Krumhansl J A and Gooding R J 1989 *Phys. Rev.* B **39** 3047–53
[590] Dimitriev V P, Toledano P and Gufan Y M 1991 *Phys. Rev.* B **44** 7248–55
[591] Wentzcovitch R M 1991 *Phys. Rev.* B **44** 9155–8
[592] Mettout B, Dmitriev V P, Jaber M B and Toledano P 1993 *Phys. Rev.* B **48** 6908–13
[593] Toledano P 1993 *Condensed Matter News* **2** 9–15
[594] Gupta S C and Chidambaram R 1994 *High Pressure Res.* **12** 51–70
[595] Boettger J C 1986 *Phys. Rev.* B **33** 6788